451

POLYMER NANOCOMPOSITES

FUNDAMENTALS AND POSSIBLE APPLICATIONS TO POWER SECTORS

Working Group

D1. 24

February 2011

WG D1.24

POLYMER NANOCOMPOSITES

- FUNDAMENTALS AND POSSIBLE APPLICATIONS TO POWER SECTORS -

Members and Contributors

T. Tanaka, Convenor (JP), J. Kindersberger (DE), M. Fréchette Secretary (CA), S. Gubanski (SE)
A. S. Vaughan (UK), S. Sutton (GB), P. Morshuis (NL), J - P. Mattmann (CH), G. C. Montanari (IT)
C. Reed (US), A. Krivda (CH), J. Castellon (FR), T. Shimizu (JP), S. Pélissou (CA), M. Nagao (JP)

ISBN 978-2-85873-140-4

TABLE OF CONTENTS

Chapter 1 Introduction – Overview

1.1. Nanotechnology

1.1.1. Nanotechnology as the 21st Century Technologies

Nanotechnology is emerging as one of the 21st century technologies. More than half century has passed since a famous physicist Richard P. Feynman (1959) predicted its possibility by his talk on “There is Plenty of Room at the Bottom” on December 29th 1959 at the annual meeting of the American Physical Society at the California Institute of Technology. What is the modern meaning of nanotechnology? It is a general term covering a wide range of many fields ranging over such as electronics, photonics, mechanics, micro-machines, and biomaterials. We may recognize that it is not as yet a science that is theoretically arranged, nor an engineering that is systematically structured, such as physics and electrical engineering (Iijima 1991). It deals with characteristics in nanometer size and/or mesoscopic regions on materials and functional devices. It should be stressed that macroscopic performances must appear as collective behaviors of individual performances at the nanometric level. Therefore, it is a key issue for us to control mesoscopic characteristics. Then, it is expected that such a nanotechnology will bring about enormous innovation in various fields such as structural materials, resources and energy, communication and electronics, biotechnology, environmental safety, medicine, and health.

US National Nanotechnology Initiative (NNI) defines nanotechnology as follows (US Office of STP 1999). Nanotechnology is the understanding and control of matter at dimensions of roughly 1 to 200 nanometers, where unique phenomena enable novel applications. A nanometer is one-billionth of a meter: a sheet of paper is about 100,000 nanometers thick. Encompassing nanoscale science, engineering and technology, nanotechnology involves imaging, measuring, modeling, and manipulating matter at this length scale. It is rather biased to applications than fundamentals.

1.1.2. Top-down and Bottom-up Nanotechnologies

Nanotechnology		
Concept	Bottom-up	Top-down
Target	Nanomaterials	Micromachines
Method	Self-Assembly Function Nanoscale and Mesoscopic Level	Lithography by Photo and Electron Beam
Examples	Nanocomposites Polymer-Inorganic Polymer-Polymer Inorganic-Inorganic	TFT, TF Solar Cells, MEMS etc

Figure 1.1.1 Two streams for nanotechnology

There are two methodological streams in nanotechnology, i.e. the top-down method and the bottom-up method. The former is an evolutional technology originating from conventional processing techniques. This method is based on the concept that a small machine manufactures a smaller machine tool, which fabricates a further smaller machine. Such a repeated process will create an infinitely tiny device. But in reality, a different approach has been made. Nano-scale devices are fabricated by a fine processing technology that is made highly advanced. This is actually a main stream. What is really a motive force to drive has been reached by the development of various technologies for computer control, fine processing, laser processing, lithography, electron microscopes and atomic force microscopes. In this case, man should control by man-made or artificial computer programs whatever small a target device might be. There might be a limitation. On the contrary, the bottom-up method is no doubt a more advanced trial to manufacture target nanomaterials and/or nanodevices by utilizing self-assembly mechanisms based on natural programs.

1.2. Nanomaterials

1.2.1. Nanomaterials-Definition and Kinds

Mesoscopic substances in between bulks and molecules or atoms can be considered to represent nanomaterials. They tend to manifest unique surface properties in addition to bulk performances due to the limited number of constituent atoms and molecules, and enable to exhibit even quantum effects in their mesoscopic regions. Such nanomaterials draw much attention because they will potentially create not only a brand new academic arena but also strongly lead their foreseeable applications. Nanomaterials can be made for wide range of substances such as inorganic, organic and bio materials. It is a kind of surprise that many kinds of nanomaterials can be fabricated only by carbons, as shown in Fig. 1.2.1 for example. Graphite is electrically conductive, while diamond is either semi-conducting or insulating. What are called carbon nanomaterials now includes fullerene, nanotube, nanocone, nanowire, nanosheet, nanobelt and the like. Even if we take only nanotube for instance, we can recognize that it is tinged with properties of metals and semiconductors depending on its size and structure. Nanotube can emit electrons form its tip, when it is subjected to high electric field, and can store hydrogen inside.

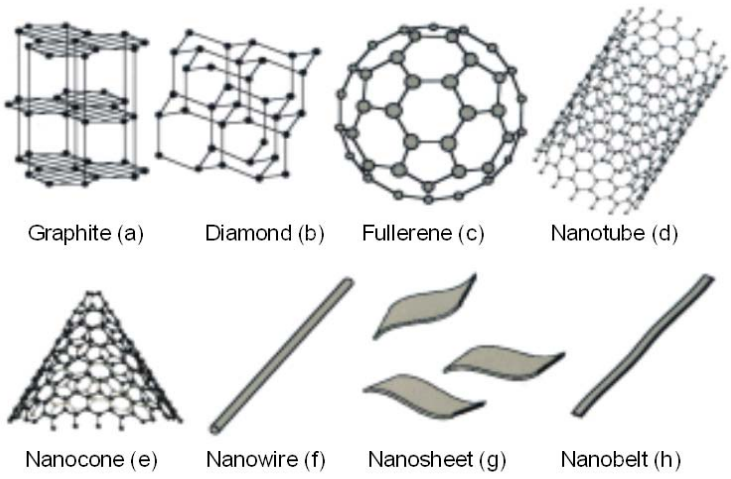

Figure 1.2.1. Examples of carbon nanomaterials

1.2.2. Mesoscopic Performances

Nanomaterials are characterized by the fact that they are endowed with mesoscopic features. When the matters are in mesoscopic size, they exhibit prominent surface effects and possibly size-quantum effects, because constituent atoms and molecules are limited in number. As a result, it is generally considered that they are quite different in properties from macroscopic substances and atoms and molecules, and are called mesoscopic particles or mesoscopic substances. Intensive investigation has been continued on various materials such as metals, semiconductors, ionic crystals, carbons, fullerene, and nanotube to find out how such physical and chemical characteristics emerge in mesoscopic regions.

1.2.3. Self-Assembly

Self-assembly functions are needed by nature to create nanomaterials (Self-assembly and Nanotechnology). Self-assembly should proceed autonomously under a certain defined condition to produce a target nanomaterial. For example, a silicone crystal can be grown from its seed under certain temperature and vacuum conditions without artificial manipulation, and various types of carbon materials can be derived depending on processing conditions. Organisms or living bodies are a typical substance created by self-assembly functions, and are achieved through DNA information transfer. This process can be utilized to regenerate living tissues.

1.3. Nanocomposites

1.3.1. Expectation to Nanocomposites

Nanocomposites are composed of host and guest materials in general. They should be fabricated so that they may be endowed with superb performances of the guest materials, while keeping original performances of the host materials. Such a technology would lead to the development of materials with hard and, at the same time, soft (elastic) performances that appear to be mutually contradictory. In general, inorganic materials are excellent in optical, electrical, mechanical and thermal properties, while organic materials are superb in light weight, flexibility, and processability. Such performances for both materials can be transferred, complementally, to nanocomposites. Furthermore, novel performances that neither of them holds by nature will possibly appear in newly fabricated nanocomposites (Lewis 1994, Fréchette 2001, Tanaka 2004).

1.3.2. Kinds of Nanocomposites

There are three kinds of combination as for hosts and guests, i.e. inorganic-inorganic, inorganic-organic, and organic-organic composite systems. The materials that attract most attention lately are nanocomposites that consist of organic polymers as host and inorganic substances as guest. This field was pioneered by the successful invention of polyamide/organic clay nanocomposites in 1990’s. Much attention was directed toward mechanical and optical properties in the beginning. Furthermore, recent investigation is oriented also to gas barrier, lubrication, thermal endurance, heat radiation, electrical conductivity, electrical insulation and the like, aiming at drastic change in such performances that are expected to appear by controlling material structures in nanometer scale in self-assembly mode.

1.4. Polymer Nanocomposites

1.4.1. Interfaces and Interaction Zones

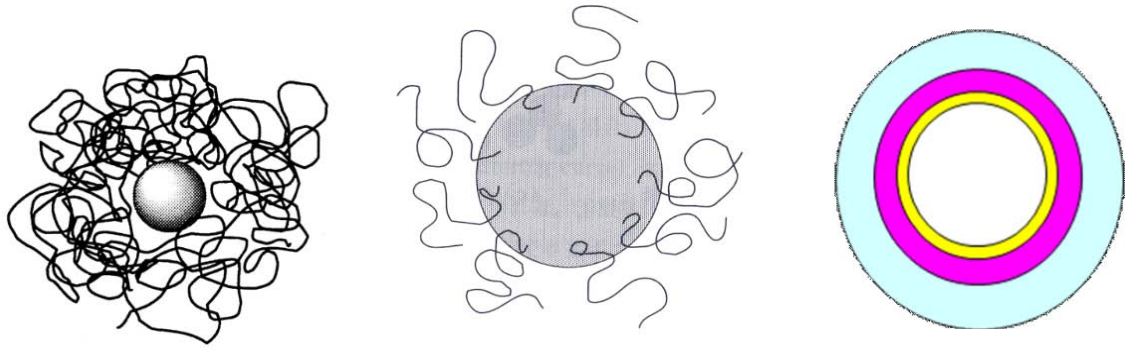

Figure 1.4.1. States of interfaces between nano fillers and polymers

Polymer nanocomposites are a composite of organic polymers and inorganic nano fillers. Since they have enormous total areas of interfaces around the nano fillers that contact the polymer matrices, it is widely recognized that they are significantly affected in their performances by the properties of such interfaces. Figure 1.4.1 shows three representative models for interfacial states (Tanaka 2005). Sub-figures (a) and (b) show two kinds of directed polymer chains; (a) random or parallel direction to the surface of a nano particle, and (b) more or less perpendicular to the surface of a nano particle. The sub-figure (b) represents a spherulite in part. Interfaces are expanded in radial direction outside the surface of a nano particle, and have their thickness that is usually called an interaction zone. Such interfaces are different in their performances from both nano particles and polymer matrices. They are now considered to consist of distinctive several layers with respective different characteristics. Two-layer model is generally accepted, but multi or three-core model is also proposed as show in Sub-figure (c) in order to interpret more properly various characteristics that nanocomposites possess in nature. Mesoscopic properties are expected to appear at the interfaces as described above. In order to clarify interfacial characteristics, we need to investigate material structures such as morphology by using modern physico-chemical analysis methods.

1.4.2. Dielectric and Electrical Insulating Characteristics

Dielectric and electrical insulation properties are a main topic of this technical brochure. Details are described in the text. Investigation of various polymer nanocomposites has been intensively made on permittivity, loss tangent, electrical conductivity, space charge, TSC, dielectric breakdown, treeing breakdown (short time breakdown and treeing V-t characteristics), partial discharge (PD) resistance, electroluminescence, and the like. It is now recognized that the improvement of PD resistance, the prolongation of treeing lifetime, and the suppression of space charge formation are most prominent among them as nanocomposites. Even only these characteristics will certainly encourage potential application in reality. However, nanocomposites are still under development stage, and then should be explored in their material preparation methods above all in order to obtain good and reliable nanocomposites, although it is important to promote the study of characterization.

1.4.3. Performances as Engineering Materials

For practical applications, mechanical properties such as tensile strength and flexural rigidity, weathering resistance, water resistance, flame retardant properties and the like need to be investigated. In other words, an engineering material must satisfy a matrix of properties required by a particular application. It is also necessary to grasp performances specific to each of the applications. Such data have been continuously collected.

1.4.4. Application Fields

Enamel nanocomposites with improved PD resistance are already in practical use in some countries. Application of nanocomposites is expected in the field of UHV (ac and dc) extruded power cables, switch gears, transformers, electric rotating machines, and power capacitors in the power sector. Study of nanocomposites has been initiated for use under high density assembly and high temperatures in the electronics sector. Safety issue for nano fillers is important, when nanocomposites are in practical use.

1.5. Safety Issue

Four areas of human exposure to nanoparticles have to be addressed when adopting safety measures in power engineering industry (Dreher 2004):

• production of power equipment. It is preferred to work with liquid suspensions, pastes or granules rather than dry powders, and closed rather than open manufacturing systems should be used.

• storage and transportation. The most common danger present spills, vapor leaks and fire during accidents.

• operation of equipment. Nanoparticles can be released into environment via mechanical abrasion, ablation (surface discharges, flashovers) or from equipment fires.

• end of equipment lifetime. Ecotoxicity of nanoparticles and sudden catalytic reaction with risk of explosion in incinerators have to be considered during recycling and waste disposal of power equipment. Preparation of ionic solutions instead of solid nanoparticles and creation of microagglomerates may address these challenges.

References

Dreher KL (2004) Toxicological highlight - Health and environmental impact of nanotechnology: Toxicological assessment of manufactured nanoparticles, Toxicological Sciences 77: 3-5

Feynman R (1959) There's plenty of room at the bottom, The Annual Meeting of the American Physical Society http://www.zyvex.com/nanotech/feynman.html

Frechette MF, Trudeau M, Alamdari HD, Boily S (2001) Introductory remarks on anodielectrics, Annual Rept. IEEE-CEIDP:92-99

Ijima S, Ichihashi T (1991) Single-shell carbon nanotubes of 1-nm diameter, Nature 1993;363: 603–605.

Lewis TJ (1994) Nanometric dielectrics, IEEE Trans DEI-1:821-825

Self-assembly and nanotechnology: http://www.edinformatics.com/nanotechnology/self_assembly.htm

Tanaka T, Montanari GC, Muelhaupt R (2004) Polymer nanocomposites as dielectrics and electrical Insulation—perspectives for processing technologies, material characterization and future application, IEEE Trans DEI-11:763-784

Tanaka T, Kozako M, Fuse N, Ohki Y (2005) Proposal of a multi-core model for polymer nanocomposites, IEEE Trans DEI-12:668-681

US Office of Science and Technology Policy (1999) US National Nanotechnology Initiative http://www.nano.gov/html/about/history.html

Chapter 2 Materials—Synthesis and Characterization

2.1. Preparation

Techniques from the production of nanocomposites can be divided into four categories.

(i) A filler that is already nanoscopic is dispersed within an existing polymeric system.

(ii) A filler than has the potential to become nanoscopic is introduced into an existing polymeric material in such a way that it is both dispersed and dimensionally altered to exhibit nanoscopic character.

(iii) Approaches where a polymerisation reaction is performed in the presence of a material that will ultimately behave as a nanofiller.

(iv) Approaches where the synthesis of nanoparticles occurs within a polymeric material.

The primary scientific literature contains a very large number of papers that describe various approaches; in addition there are also a number of excellent review articles and the account that follows is largely derived from these. For more detail the reader is therefore referred to “Polymer nanotechnology: Nanocomposites” (Paul and Robeson, 2008), “Processing of nanographene platelets (NGPs) and NGP nanocomposites: a review” (Jang and Zhamu, 2008), “Polymer-Nanoparticle Composites: Preparative Methods and Electronically Active Materials” (Sudeep and Emrick, 2007), “Nanocomposites based on polyolefins and functional thermoplastic materials” (Ciardelli et al, 2008) and “The search of a homogeneously dispersed material—the art of handling the organic polymer/metal oxide interface” (Kickelbick 2008). Other relevant reviews that have been published recently include those by Varsha et al, 2008, Liu, 2007, and Raquez et al, 2008.

2.1.1. Dispersion of Nanofillers within an Existing Polymeric System

This is the most direct approach and has been used successfully to prepare many different nanocomposites. For example, many nanofillers can be readily introduced into a polymeric system using batch mixing approaches or, of more industrial validity, some form of continuous process such as extrusion. A less direct strategy involves the use of a solution phase to mix nanoparticles and a polymer. An example of this concerns the production of polymer/oxidised graphite nanocomposites. Graphite oxide nanoplatelets can possess active surfaces containing carboxyl, carbonyl, epoxide, and hydroxyl functionalities, which facilitate their ready dispersal in polar solvents, notably water, and subsequent mixing with water soluble polymers; poly(ethylene oxide) (PEO) poly(allylamine hydrochloride) (PAH), poly(diallyldimethylammoniumchloride) (PDDA) and poly(vinyl alcohol) (PVA) have all been investigated. After subsequent reduction of the graphite oxide back to graphene, a polystyrene–graphene nanocomposite was found to exhibit a percolation threshold for electrical conductivity percolation of just 0.1% by volume at room temperature, indicating an extremely high degree of dispersion. However, with the exception of polymers like epoxy resins that are supplied in a liquid state, this approach is not well suited to industrial-scale mass processing, due to the need to separate the final product from the solvent and dispose of large quantities of waste. In the laboratory, where small scale batch production is all that is required, solution processing has been employed successfully with many different polymers. As described above, epoxies are fluid at room temperature and therefore liquid processing routes constitute potentially viable means of introducing nanoparticles, prior to curing. However, many epoxies are highly viscous and therefore solvents can be used as viscosity modifiers, together with sonication, in order to attempt to improve dispersion.

2.1.2. Combined Dispersion and Disaggregation of Fillers within an Existing Polymer

The classic example of this strategy concerns the wide range of nanocomposite systems that have been prepared using layered materials, such as clays, as fillers. In this case, the role of processing is both to distribute and break up the initially macroscopic aggregates of layers, such that the final material contains a uniform

dispersion of nanoscopic (in one-dimension) filler particles. Organoclays, as supplied, exist in the form of particles, ~10 μm in size, which are formed from an assembly of smaller units (tactoids) that are made up of the primary layers. Dispersion of such a structure can be thought of in terms of the break of the particles into tactoids, diffusion of polymer molecules into the galleries that separate the primary layers (intercalation) and, finally, separation of individual layers (exfoliation). Literature reports have suggested that this final step occurs in a stepwise manner, in which individual layers are sequentially stripped from tactoids, rather than through increasing amounts of intercalation leading to wholesale tactoid breakdown. Nevertheless, whatever the precise mechanisms, detailed studies have shown that the conditions pertaining during mixing are critical in achieving optimum results. In the case of extrusion, the nature of the extruder, the screw configuration, the residence time, the melt viscosity and the point at which the organoclay is introduced are all reported to affect the dispersion that is ultimately achieved. Nevertheless, whatever state is reached during shear, this will not be thermodynamically stable; it has been shown that polyolefins nanocomposites prepared by melt mixing undergo a degree of re-agglomeration if subsequently held in the melt.

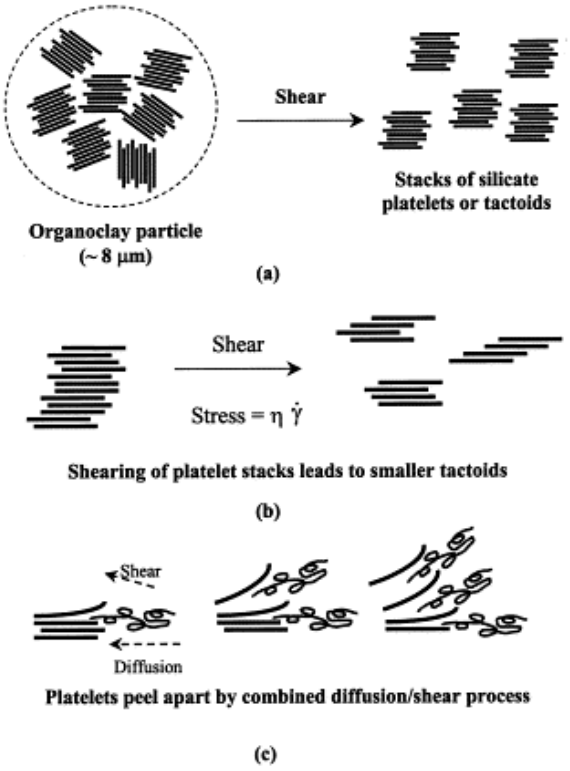

Figure 2.1.1 Schematic diagram showing the layered structure of MMT in various aggregation states and the processes by which these are broken up. Reprinted from *Polymer* 2001, 42(25), Fornes, T. D., Yoon, P. J., Keskkula, H., and Paul, D. R., Nylon 6 nanocomposites: the effect of matrix molecular weight, pp.09929-09940, with permission from Elsevier.

While mechanical forces are effective in breaking up larger particles, there is a limit to how fine a dispersion mechanical forces alone can produce. For example, the clay montmorillonite (MMT) (see Figure 2.1.1) is a member of the smectite family and contains layers that are made up of 2 tetrahedral silica sheets sandwiching a central octahedral sheet of alumina. However, due to substitution of aluminium or silicon with elements of a lower valency, these platelets are charged, and attract ions of the opposite polarity into the galleries. If aluminium ions (Al^{3+}) are replaced by iron (Fe^{2+}), this leads to the layers acquiring a net negative charge and the inclusion of cations, such as sodium, within the galleries. That is, the layers are charged, hydrophilic and, can be

readily dispersed in water. In thermodynamic terms, for dispersion to occur, the change in the Gibbs function must be negative, and since the magnitude of the change in the entropy will only be small, dispersion will be driven by enthalpic effects. That is, good dispersion requires the existence of attractive forces between the polymer and the nanoclay. Many early studies of organoclay-based nanocomposites focused on systems based upon polyamides; in view of the hydrophilic nature of these polymers, the reason for this is clear from the above discussion. However, even for these systems, where intrinsically favourable interactions already exist, studies have shown that replacement of the counterions with moieties that favour mixing is essential in achieving good dispersion and high levels of exfoliation. These compatibilising species need to be ionic and contain both polar (to associate with the clay) and organic (to associate with the matrix polymer) elements and, as such, can be thought of as surfactants, in which the polar heads are tethered to the polar clay surfaces with the alkyl chains arrange in layered trans/gauche conformations. The effect of the molecular form of the surfactant on the interactions that occur between nylon-6 and MMT has been investigated; this work showed that surfactant molecules with a single long alkyl tail gave higher levels of exfoliation than those with additional alkyl chains and suggested that, while alkyl tails serve to reduce platelet/platelet cohesion, an excess tends to block favourable polar interactions between the nylon chains and the clay platelet surfaces. For polymers such as the bulk commodity polyolefins, polyethylene (PE) and polypropylene (PP), which are extremely hydrophobic, careful optimization of parameters such as the average charge carried by each platelet (the so-called charge exchange capacity – CEC) and the structure of the surfactant used to compatibilize the organoclay and the polymer is essential if good dispersion is o be achieved. Nevertheless, even using optimal surfactants, exfoliation in such polymers is never as successful as in systems where the polymer chains exhibit some polar character and, therefore, alternative approaches towards enhancing compatibility have been devised which involve introducing polar groups into the macromolecular structure, either through grafting or through copolymerisation. In the former case, grafting maleic anhydride at a level of about 1% has been found to be a highly successful strategy towards enhanced dispersion. A consequence of adopting this methodology for the production of the nanocomposites from non-polar polymers concerns the aspect ratio of the filler particles that form. When the extent of dispersion is low, the filler particles are, as expected, much thicker than an individual single clay platelets, but also much longer. As the polymer–organoclay affinity increases, the clay particles not only become thinner but also shorter; it is reported that the former process dominates, such that the aspect ratio increases, with beneficial consequences for certain macroscopic properties.

The effect of copolymerization with polar monomers on the interactions that occur between organoclays and polymers have been studied using systems based on ethylene and polar co-monomers such as vinyl acetate, vinyl alcohol, methacrylic acid etc. As a means of studying the effect of polymer polarity on interaction with layered nanofillers, the ethylene/(vinyl acetate) copolymers have much to recommend them, since they are readily available in a wide range of different compositions, from 100% ethylene (i.e., polyethylene) to 100% vinyl acetate {i.e. poly(vinyl acetate)}. As such, these systems have been studied extensively. An alternative to such random copolymers as a route to compatibilisation is the use of endchain, block or graft copolymers. Improved dispersion has been reported for polyethylenes in the case of systems modified with side chains containing ammonium group and for poly[ethylene-*block*-(methacrylic acid)].

While the above discussion has focused on clay-type systems, it would be incorrect to assume that disaggregation/dispersion issues are only relevant for such materials. Rather, whenever nanoparticles are introduced into a polymeric matrix, there is a tendency for phase separation to occur, such that aggregation results. Since the explanation for this is, primarily thermodynamic (i.e. enthalpic), similar strategies can be developed to

those describe above, by which the surface chemistry of the nanoparticles is modified to improve compatibility with the matrix of interest. For example, polymers can be grafted onto the surface of the nanoparticle through the initial decoration of the surface by some ligands, from which, the polymerization chemistry can subsequently be initiated. Alternatively, some pendent functionality can be introduced into the macromolecular chain whereby it reacts with the nanoparticle surface directly, or via some ligand groups introduced separately to facilitate grafting. Such approaches have been used extensively in the area of functional materials. Gold nanoparticles have been exploited since Roman times but interest in these systems has grown progressively since Faraday's pioneering work on colloidal gold in the mid 19th century. Several studies have employed thiol chemistry to produce stable gold/polymer systems in connection with possible applications as novel light emitting diodes (LEDs), where the nanoparticles enhance the luminescent stability of the polymer. Gold nanoparticles have been grown within polyaniline (PANi) nanofibres to produce materials that exhibit bistable electrical behavior and which, consequently, could find applications as memory devices; in this case switching behaviour and dispersion are strongly linked. Equivalent approaches have been used to control the dispersion of active nanoparticles, such as cadmium selenide and cadmium telluride quantum dots and nanorods, within function polymers such as poly(phenylene vinylene) (PPV) and polythiophene (PT) with a view to developing novel LEDs and solar cells. For example, the photovoltaic behaviour of polythiophene/ cadmium selenide nanorod devices has been reported, in which the nanorods were functionalized with amine-terminated polythiophene. This, it was suggested, led to materials with improved dispersion, increased interfacial area, more efficient exciton charge separation and enhanced power conversion efficiencies. However, alternative studies of such systems have indicated that while the motivation behind the modification of surface functionality may well be dispersion-related, the consequences of changing the polymer/nanoparticle interface chemistry may be more wide ranging. Studies of the behaviour of hybrid solar cells based upon polythiophene and nanoparticles or nanorods of cadmium selenide have demonstrated that both the geometry of the nanoparticles themselves and their surface chemistry influence device characteristics; the performance of such devices is related to electron transfer via rapid charge separation at the nanoparticle-polymer interface which, itself, is affected by the local chemistry.

2.1.3. In-situ Polymerisation Techniques

In-situ polymerisation has most widely been used in connection with layered fillers, such as clays. The reason for this is that the diffusion of monomer molecules into interlayer galleries, followed by polymerisation, is a far easier route to intercalation/exfoliation than introducing fully formed macromolecules. However, the approach suffers from two problems in that (a) the facilities for polymerization of the required quantity of material must exist and (b) the effect of the filler on the polymerization process must be carefully considered. For example, naturally occurring silicate materials are incompatible with many catalyst systems and therefore, just as in the case of melt processing discussed above, pre-treatment of the filler is essential both, chemically, to increase compatibility between the filler and the catalyst and, physically, to ease the insertion of the relatively bulky catalyst particles into the narrow galleries. Also, since catalysts are sensitive to their chemical environments, inclusion of a large excess of an appropriate co-catalyst is commonly required to neutralize the effect of traces of water or of acidic groups on the silicate surfaces.

Despite these potential difficulties, the above strategy has been used successfully. For example, a titanium-based Ziegler–Natta catalyst intercalated within ammonium modified MMT was used to prepare ethylene-based nanocomposites. In this case, the ammonium salt contained hydroxyl functionality, which provides facile reactive sites for anchoring the catalyst between silicate layers. PP/synthetic hectorite nanocomposites were generated through the use of a synthetic hectorite with intercalated zirconocene catalyst,

after treatment of the silicate with an excess of methylaluminoxane (MAO). The resulting PP was, however, found to be of rather low molar mass, suggesting that polymerization within inter-layer galleries is affected by local chemical or physical constraints. Further polymerization approaches that have been demonstrated to produce nanocomposites in a similar way include metallocene and Brookart type catalysts and the so-called polymerization filling technique, in which the pristine filler is first treated in order to attach the polymerization catalyst to the exterior and interlayer surfaces. Although such approaches can be used (a) successfully to generate polymer and (b) to do this in such a way that intercalation/exfoliation/dispersion results even in non-polar polymers such as PP and PE, the fact that the resulting macromolecules and filler are not thermodynamically compatible, necessarily means that re-aggregation of the filler occurs, subject to kinetic constraints.

2.1.4. In-situ Production of Nanofillers

The preceding sections have considered various means by which the thermodynamic driving forces for aggregation can be overcome. However, an alternative has been hinted at and that is to rely upon kinetic factors rather than attempting to overcome inherent thermodynamic ones; that is, generate isolated nanoparticles in situ under conditions where they are subsequently unable to aggregate. Sol–gel chemistry presents the possibility of achieving this and has been exploited widely, in particular, as a means of preparing metal oxide structures with different shapes, sizes and compositions.

The mechanism by which metal oxide networks are produced by the sol–gel process is a conventional polymerization reaction, but starting with monomers that take the form of metal alkoxides. Depending on the functionality of these, networks, linear polymers or dimers can be formed, but the result is commonly a crosslinked inorganic network that can be thought of as a highly porous gel. However, within the context of the topic considered here, the key feature of the sol–gel process is its compatibility with polymers, which facilitates the formation of ceramic strictures in the presence of organic molecules. Thus inorganic nanostructures can evolve in the presence of pre-existing polymer or, alternatively, both the polymeric and inorganic components can be formed in situ, although for this to be viable, the two reactions need to be non-interacting. Another important factor to consider is the extent to which macroscopic phase separation can occur in the duration of the reactions. In short, while the sol-gel philosophy has much to recommend it, it is not an all encompassing solution to problem of producing optimally structured nanocomposites.

A commonly studied class of sol-gel composites is based upon silica and compatible polymers. The in-situ production of silica involves the reaction of tetraalkoxysilane precursors and, therefore, one way to promote interactions with the surrounding polymer is to employ polymers that can undergo hydrogen bonding. PEO is one such material and, consequently, such systems have been studied extensively, notably in connection with the influence of the polymer on structural evolution in the silica phase. Other hydrogen bonding polymers that have been used in the same way include poly(ε-caprolactone) (PCL), poly(methyl methacrylate) (PMMA) and its more strongly hydrogen bonding relative poly(2-hydroxethyl methacrylate) (PHEMA) and poly(acrylic acid) (PAA). However, PAA, has been found to interact with evolving silica in numerous ways, such that the formation of homogenous sol-gel PAA/silica composite is difficult to achieve.

As stated above, compatibility between the polymer and the evolving silica system is important in generating a homogenous product and a number of strategies can be exploited to facilitate this. One approach involves the use of a solvent with an amphiphilic character; N,N-dimethylformamide (DMF) and N,N-dimethylacetamide (DMAc) are examples of solvents that have a high compatibility with many organic polymers but which can still

form strong hydrogen bonds with the silanol groups of the silica gel. By exploiting such solvents, well dispersed organic–inorganic hybrids were formed with polymers including polystyrene (PS) and poly(vinyl chloride) (PVC). Alternatively, it has been shown that polymer/filler interactions, and hence dispersion of the filler in the final nanocomposite, can be improved through the introduction of groups into the polymer that can react with the silica, thereby preventing phase separation. One route to this involves the use of trialkoxysilane polymer end-groups although, by definition, this gives only a small degree of functionalization which, depending upon the nature of the intrinsic polymer/silica interactions and the chain length, may be insufficient to prevent phase separation. Consequently, incorporation of trialkoxysilane functionalities into the macromolecular backbone is a more effective strategy in leading to strong bonding between the polymer phase and the silica network through the formation of hydrolytically stable Si–C bonds. This approach involves the copolymerization of the monomer of interest with a co-monomer of appropriate functionality; the monomer most commonly used for this purpose is 3-(methacryloxypropyl)trimethoxysilane (MSMA). Examples of polymers that have been modified using this general strategy include polystyrene, PMMA, poly(butyl methacrylate) (PBMA) and acrylonitrile-butadiene-styrene (ABS) rubber. Where it is impractical to introduce the required functionality into the polymer, silane coupling agents can be reacted into the silica phase. In this way hybrid materials based on polyurethane (PU), PMMA and polyimides (PI) have been produced. A major interest in silica/polymer sol-gel systems concerns potential applications as optical materials and, consequently, many of the polymers cited above are of little technological importance from an insulation perspective. However, the approach has also been used successfully with epoxies, where the silica forms in parallel with the epoxy curing reaction. In this case, the use of amine hardeners has the advantage that they act both as epoxy crosslinking agents and as catalysts in the sol–gel process; as indicated previously, the inclusion of a coupling agent is generally beneficial in controlling phase separation. However, this duality in amine functionality does indicate that curing of the polymer and formation of the silica are not independent processes, a factor that must be remembered when considering the optimal stoichiometry of the system. Although most reported activity concerning the in-situ formation of a nanostructured inorganic phase within a polymeric matrix has concerned silica-based materials, analogous approaches have been used to generate nanocomposites containing titania, alumina and zirconia/silica. Elsewhere other in-situ approaches have been used to generate titania nanoparticles from titanium (III) chloride in aqueous solution, before dissolving PVA in the suspension to produce a PVA/titania nanocomposite. Gold nanoparticles have been produced in-situ in the presence of n-alkane-terminated PAA amphiphiles; although this was reported to give nanoparticles that exhibit lower crystallinity and less well controlled size distributions that those produced using alternative chemical strategies.

2.2. Characterization of Nanocomposites (Introductory Remarks)

In the account that follows, characterisation techniques are divided into three general categories: spectroscopy; microscopy; scattering. In each of the sections that follows, the same general approach is adopted; first, some background theory is given in order to provide an appreciation of how a particular technique works; what information can a particular technique provide? This theoretical understanding supports the various case studies described subsequently, which show how a particular technique has been used.

2.3. Spectroscopy

Although the term spectroscopy was initially used to refer to the dispersion of visible light, it has now grown to encompass any technique where some characteristic is measured as a function of wavelength or frequency. So, this general category of characterisation can include techniques as disparate as UV/visible spectroscopy which, in representing the “colour” of an object in terms of its absorption behaviour primarily at visible wavelengths is most

closely aligned with the original meaning of spectroscopy, through to mechanical relaxation spectroscopy, in which the frequency dependence of the stress in a sample is determined as a function of applied strain. In short, spectroscopy in the widest sense includes a vast range of techniques and, therefore, to provide a comprehensive description of the theory and uses of all techniques goes way beyond the scope of an article such as this.

2.3.1. UV/Visible Spectroscopy

Absorption of electromagnetic radiation of visible or ultra-violet wavelengths involves electronic transitions. As an example, consider the bright blue appearance of aqueous copper sulphate. In this case, coordination of the Cu^{2+} ion with water molecules induces non-degeneracy in the outer electronic d orbitals and an absorption of red light. In the case of an organic compound containing one C=C bond, this will absorb strongly in the far ultraviolet. As the extent of conjugation increases, so the absorption edge decreases in energy and, eventually, enters the visible spectrum. An example of this phenomenon is β-carotene ($C_{40}H_{56}$), which contains a long conjugated sequence of alternating double and single bonds such that the $\pi \rightarrow \pi^*$ transition occurs at a photon energy of ~2.5 eV. This transition has certain similarities with an electron being promoted from the valence band to the conduction band in a crystalline semiconductor. However, unlike in some other regions of the spectrum, these transitions do not occur simply but, rather, are "mixed" with other phenomena, notably vibrational modes, such that the wavelength of light that is absorbed is determined by the complete energetic conformations (electronic, vibrational, rotational) of the molecule before and after the transition. Nevertheless, UV/vis spectra can still contain a great deal of useful information, even if much of it is negative. For example, if an organic compound does not absorb in the range 200-800 nm, then it can be deduced that it contains no conjugated or benzenoid structure, no aldehyde or keto groups, etc.

2.3.2. UV/Visible Spectroscopy – Case Studies

Since UV-vis spectroscopy involves electronic transitions, its utilization with respect to nanocomposites is associated with systems that readily undergo electronic transitions and, predominantly, those containing metallic components; surface plasmon resonance effects are commonly studied using this technique. Colloidal systems composed of metallic nanoparticles have attracted interest in connection with many applications, including as novel sensor systems that exhibit macroscopic changes as a result of changes in aggregation state in response to some external stimulus. To this end, pH-dependent colour changes in colloidal dispersions of gold nanoclusters have demonstrated that significant red-shifts and peak broadening occur in the surface plasmon band of the gold nanoclusters as the pH of the system is reduced. Similar effects have also been associated with catalysis effects involving charge transfer and dipole-dipole interactions leading to aggregation. Li et al, 2009, synthesized cadmium sulphide (CdS) nanoparticles on nanofibres of bacterial cellulose; subsequent characterisation by UV/vis spectroscopy revealed a small absorption peak at 426 nm. That is, as a result of the finite size of the nanoparticles, the absorption was found to be blue shifted by 90 nm compared with bulk CdS. In contrast, in PANi systems containing both titania (TiO_2) nanoparticles and magnetic Fe_3O_4 micro-filler, the UV/vis spectrum was found to be independent of composition, implying that the presence of the filler affects neither the structure of the PANi nor the electronic transitions that occur within it; the $\pi - \pi^*$ transition was reported to occur at an invariant wavelength of 371 nm. An alternative interpretation of this is that if any interactions do occur between matrix and nanofiller, then the volume that is affected is too small to have a detectable effect on the spectrum. Similarly, silver loaded TiO_2 systems templated in a graft copolymer film have been synthesized and examined by UV/vis spectroscopy. The final system exhibited the characteristic plasmon peak of silver nanoparticles at 410 nm together with another feature at 294 nm, which the authors "assigned to the typical absorption edge of TiO_2" (Koh et al, 2009). An alternative use of UV/vis spectroscopy is as a means of simply evaluating optical clarity at

different wavelengths. The rationale behind this is that improved dispersion results in smaller aggregates and, therefore, increased clarity; evidently, while this philosophy has some validity for amorphous polymers, it cannot be applied simplistically to semicrystalline systems. The same approach has also been used to determining the degree of "yellowing" in clay/poly(ethylene terephthalate) (PET) system, an effect related to decomposition of the organic compatibilizers.

2.3.3. Raman / Infra Red Spectroscopy

Raman and infra red (IR) spectroscopies are associated with changes in the vibrational state of molecules. If the oscillations of a molecule produce an oscillating dipole moment, then the molecule can couple directly with an electromagnetic wave of appropriate frequency and absorb the radiation. In practice, this requires the exciting radiation to lie in the infra red region of the spectrum; homonuclear diatomic molecules, such as H_2, O_2, and N_2 on grounds of symmetry can never exhibit a dipole moment and, therefore fail to interact in the way described. In place of absorption, the incident radiation may be scattered. Simplistically, the electrons in the molecule can be considered to experience an intense oscillating electric field, which causes them to oscillate at the frequency of the exciting radiation. The result is the emission of electromagnetic radiation of the same frequency in all directions; Rayleigh scattering. However, if any vibrational mode involves changes in polarizability, then the emitted radiation will also contain components that are shifted in frequency from that of the exciting radiation; the Raman Effect. Although the elegant rules of group theory can be used to determine which vibrational modes of a given molecular structure will be IR or Raman active, in practice, both spectroscopies can be considered to provide similar, albeit complementary, information. The vibrational modes of molecular structures are dependent upon the symmetry of the molecules being irradiated and, as such, both Raman and IR techniques can be considered to reveal characteristic "fingerprints" of the specimen. However, in practice, the environment surrounding the molecules will also have an effect, such that more subtle effects are revealed and, in principle, the vibrational modes of the system may be affected in three ways. First, chemical interactions may serve to modify the response of the polymer as a result of interactions with the nanoparticles. Second, the limited extent of nanoparticles means that the translational symmetry of a macroscopic crystal will be broken at its surfaces, leading to the appearance of specific surface and interface vibrational contributions. Finally, the size of the nanoparticles may result in them existing in novel phases not seen in chemically equivalent macroscopic materials, which will exhibit their own unique spectral signature.

2.3.4. Raman Spectroscopy – Case Studies

In their excellent review, "Raman spectroscopy of nanomaterials: how spectra relate to disorder, particle size and mechanical properties", Gouadec and Colomban, 2007, describe two models by which particle sizes can be derived from Raman spectral data - the Phonon Confinement Model (PCM) and the Elastic Sphere Model (ESM). Such models contain parameters that have the dimensions of distance, but the precise interpretation of such parameters is far from straight forward. For example, the PCM model of Richter et al, 1981, is concerned with phonons confined within nanospheres of diameter L. Comparison of values of L derived from Raman scattering studies of ceria (CeO_2) with TEM data revealed an order of magnitude discrepancy. In this case, the key factor in determining L was not the size of the CeO_2 particles but, rather, the distance between defects in the oxygen lattice of the ceria. In germanium particles, it has been shown that the correct interpretation of L is itself size dependent; for larger grains, L does indeed correspond to the actual size for the grains. The Raman behaviour of disordered graphitic carbon has been studied extensively, both experimentally and theoretically and, for such systems, the ratio of the intensity of the so-called G and D bands has been suggested as a means of determining an average graphitic domain size. Although this approach has been widely used, theoretical

calculations indicate that size is not the only factor. Also, it has been suggested that resonance effects are important, such that the graphitic domains that are sampled in practice will simply be those that are of the correct size to be excited by the chosen laser. In short, although it is theoretically possible to use confinement effects to estimate phase size, in practice, this is not straightforward. In the case of nanocomposites containing multi-walled carbon nanotubes (MWCNTs), shifts in the position of the G and D bands have been associated with interactions been the polymer and the nanotubes. Proposed explanations include charge exchange between the polymer and the CNTs and chemical interactions between the matrix and the nanotube, which serves to affect the vibrational modes of the latter. Jeon et al, 2007, used Raman microprobe spectroscopy as part of a study of nanocomposites based upon high density polyethylene HDPE and single walled carbon nanotubes (SWCNT). A key feature of the Raman response of CNTs is the radial breathing mode, which is located in the Raman spectrum between 100 and 400 cm^{-1}, and is affected by such factors as nanotube dimensions, chirality, the surrounding matrix and the aggregation state of the nanotubes. In this work, a Raman feature around 266 cm^{-1} was ascribed to individual SWCNTs, while another close to 232 cm^{-1} was related to aggregated forms. In addition, these peaks were found to shift to higher frequencies in the presence of the polymer matrix; it is proposed that this is related to "some compressive effect on the nanotubes".

2.3.5. IR Spectroscopy – Case Studies

IR spectroscopy appears to be a very commonly used technique for the characterisation of nanocomposites; some 20 nanocomposite papers per month have been published during 2009 which use this technique and these range from routine characterisation to the provision of data that have been related to specific interactions. For example, the intensity of organoclay hydroxyl bands has been reported to decrease on introduction into polyamide-10, 6; shifts in IR peaks to lower wavenumbers in nanocomposites containing Fe_3O_4 nanoparticles have been associated with interactions between the nanoparticles and some surfactant coating. In hydroxyapatite/gelatin nanocomposites, a range of chemical changes within the hydroxyapatite galleries have been detected and associated with reactions with the polymer. A detailed study of the Si-O stretching region of the IR spectrum of MMT in melt mixed samples of PE and MMT containing a dimethyl-dialkyl-ammonium salt as comptabilizer, reported the emergence of additional spectral features in the region 960-1140 cm^{-1} as shown in Figure 2.3.1 (Tzavalas and Gregoriou, 2009). These changes were associated with an alteration in the environment of the MMT Si atoms, due to interactions between the MMT and either the polymer or the alkyl chains of the compatibilizer. In view of the uncertainty in the precise origin of the reported effects, the authors' claim that the emergence of these additional features constitutes "an efficient, fast and convenient way to monitor intercalation/exfoliation of polymer clay nanocomposites" seems somewhat optimistic. Nevertheless, whatever the precise origin of this specific effect, evidence does exist to suggest that changes in spectral line positions can occur as a result of chemical interactions at nanofiller surfaces. IR spectroscopy has been used to study the surface chemistry of nanosilica particles extracted from polyester polyol/nanosilica nanocomposites (a pre-cursor to the formation of PU-based systems). After extraction in acetone and repeated centrifugation and washing, the silica particles still exhibited a pronounced C==O peak at 1744 cm^{-1}, a result that was interpreted in terms of a polyester polyol residue that had been adsorbed onto the silica particles through hydrogen and/or chemical bonds and remained attached, despite the extended washing/recovery procedure employed. Evidently, mechanistic interpretations of subtle changes in the IR spectra obtained from nanocomposites are possible, but this is not necessarily straightforward. As such, most infra red studies of such systems have concentrated on the conventional wavenumber range. Nevertheless, near infra red (NIR) spectroscopy has not been completely ignored. Moghaddam et al, 2009, used this approach to study the effect of processing on PU/clay systems and,

by using spectral subtraction techniques, revealed some evidence of intensity changes as processing progressed. While it was possible to ascribe some of these features to specific processes (e.g. overlap of the overtone of the urethane N–H stretch and the third overtone of the carbonyl group), the origin of others remained unclear, as is often the case with NIR of even simple systems.

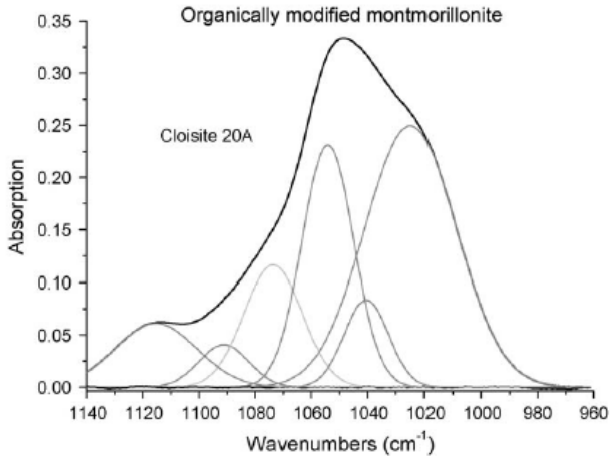

Figure 2.3.1 IR spectrum in the Si-O stretching region obtained from an MMT/PE system; the feature at around 1080–1090 cm^{-1} is not present prior to melt. Reprinted from *Vibrational Spectroscopy* 2009, 51(1), Tzavalas, S., and Gregoriou, V.G., 2009, Infrared spectroscopy as a tool to monitor the extent of intercalation and exfoliation in polymer clay nanocomposites, pp.39-43, with permission from Elsevier.

2.3.6. Nuclear Magnetic Resonance Spectroscopy (NMR)

Each electron in an atom can be through of as a charged spinning object with magnetic components $m_s = \pm½$. Similar processes occur in the nucleus such that nuclei with an even mass number, *A*, and even charge, *Z*, behave as if they were non-spinning bodies, whereas other nuclei where these conditions do not apply behave conversely. A spinning nucleus, like any spinning charge, generates a magnetic moment which will interact with any imposed external magnetic field, such that the nuclear magnetic energy levels are perturbed. Although the isotopes that can be studied include ^{19}F, ^{29}Si and ^{31}P, the two most practically important nuclei for NMR spectroscopy are ^{1}H and ^{13}C. These nuclei have a nuclear spin of magnitude ½, which give two possible states, corresponding to the nuclear spin aligned parallel or antiparallel to the field. At zero field the spin +½ and –½ states are degenerate but, as the applied field increases, their difference in energy progressively increases. Nevertheless, the energy difference between the two states always remains small so, practically, an NMR experiment involves exposing the sample of interest to a monochromatic beam of microwaves and sweeping the applied magnetic field. In practice, most NMR experiments interrogate the fine structure in the resonance of one nuclear species; this structure results from two distinct processes, which are termed the chemical shift and spin-spin coupling. Considering proton NMR as an example, every proton is surrounded by an electron cloud, which serves partially to shield it from the influence of the applied magnetic field. The result of this is a shift in the resonant frequency, which depends upon the chemical environment of the proton. Spin-spin coupling concerns the way in which the spin of one proton interacts with the spins of other neighbouring protons. Consider, for illustration, the three hydrogen atoms bonded to carbon in a methyl group. The result of spin-spin interactions will be to produce a quadruplet with approximate intensity ratio 1:3:3:1. These relative intensities derive from the fact that one combination of the three spins can give [+½, +½, +½], but there are three possible combinations which contain two +½ and one –½. In summary, NMR is a sensitive means of probing the chemical environment around the target nucleus.

2.3.7. NMR Spectroscopy – Case Studies

As described above, a key issue concerning the technological application of nanocomposites concerns the links that exist been processing, structure/dispersion and the macroscopic properties of interest. The paper by Gilman et al, 2003, "High throughput methods for polymer nanocomposites research: Extrusion, NMR characterization and flammability property screening" considers the utility of NMR as a potential on-line screening tool for characterizing dispersion in nanocomposites; the paper concentrates on PS/MMT systems processed by twin screw extrusion. The rationale behind the approach is that paramagnetic Fe^{3+} ions present in MMT as impurities will affect the proton longitudinal relaxation time in the polymer, a parameter termed T_1^H. In the case of protons located within about 1 nm of the MMT surface, T_1^H will be reduced directly, while so-called spin-diffusion results in this mechanism propagating into the bulk. Since the measured value of T_1^H will depend upon the concentration of Fe^{3+} ions in the system and their proximity to the polymer, the better the MMT dispersion, the greater the reduction in T_1^H compared with the value determined from the polymer alone. Comparison with more traditional techniques for assessing dispersion suggests that the methodology is valid. The same methodology has also been used to study clay structure in nylon-6/MMT systems via the ^{27}Al nucleus, demonstrating that the additional four-coordinated site seen in the nanocomposite is likely to be related to surface modification of the clay as a result of interactions with the polymer matrix. In nanocomposites based on MWCNTs in poly(3-hexylthiophene) (P3HT), numerous peak shifts have been reported as a result of local interactions between the polymer and graphitic structure of the CNTs; while a broadening of the aromatic hydrogens due to π-π stacking involving the P3HT thiophene ring and the graphitic benzene rings of MWCNTs is not unexpected, shifts in the methyl peak in the composites, is less intuitive, suggesting that CH-π interactions also occur. ^{13}C NMR has been used to study nanocomposites based upon styrene-butadiene rubber (SBR) and titania and has revealed significant shifts in peak positions, which have been taken to indicate interactions between nanoparticles and polymer chains. Somewhat surprisingly, spin lattice relaxation experiments suggest that the molecular mobility in is not affected by he introduction of the nanoparticles. As described previously, common way to compatibilize polymers and nanofillers is through surface functionalization of the latter. Pardal et al, 2009, used a combination of proton and ^{13}C NMR to study "co-telomerization" reactions on silica nanoparticles. Telomerization reactions are polymerization reactions that typically yield a degree of polymerization of the order of 3. In this case, the process was used to graft short chain oligomers onto the nanoparticle surface with controlled architectures and, in particular, with vinyl end groups that could be used as polymerization initiation or grafting sites. Elsewhere, ^{29}Si NMR has been used to probe study sol-gel processes in epoxy matrices, while nanocomposites of MMT and PCL have been studied in a comparable manner.

2.3.8. Electron Spin Resonance Spectroscopy (ESR)

ESR spectroscopy is the electronic equivalent of NMR and thus, in the presence of an external magnetic field, an unpaired electron's magnetic moment will align itself either parallel or antiparallel to the field, such that the initially degenerate states (spin up and spin down) split in energy – the so-called Zeeman effect. Thus, if a collection of paramagnetic centres is exposed to microwave radiation while the magnetic field is swept, at an appropriate splitting, the radiation will be absorbed as the unpaired electrons move between the two spin states. Evidently, in practical systems, electrons do not exist as solitary entities and, consequently, this process will be influenced by external factor. For example, interactions between the unpaired electron and its local environment will affect the shape of the ESR spectral line; alternatively, the magnetic moment of an atom with a non-zero nuclear spin will lead to hyperfine coupling, which splits the ESR signal into doublets, triplets etc as described above for NMR, so providing information on the host atom; anisotropy may be exhibited as a result of the

symmetry of the atomic or molecular orbital containing the unpaired electron. Consequently, ESR spectroscopy is used widely for the detailed study of paramagnetic centers, and particularly the free radicals.

2.3.9. ESR Spectroscopy – Case Studies

The nature of the interface between polymers and nanoparticles is at the centre of much of the interest in nanocomposites. ESR studies of pyrrole derivative/layered double hydroxide (LDH) systems has, for example, demonstrated the ability of this technique to reveal specific interactions; in this case, the ESR spectrum exhibited a hyperfine structure indicative of interactions between carboxylate radicals and nearby aluminium nuclei within the interlayer galleries. While such chemical interactions are important, in nanodielectrics, electrical factors are of particular relevance. Ai et al, 2008, studied the photochromic behaviour of nanocomposite films based upon nano-sized metal-oxygen cluster anions termed polyoxometalates (POM) in PVA. This study provided evidence of UV radiation-induced charge transfer between the PVA and the POM. MacCrone et al, 2007, attempted to probe the nature of the interface between nanosilica and crosslinked PE (XLPE) using ESR, in particular, in connection with oxygen radicals present in the system. This study acquired spectra while, simultaneously applying an electric field and concluded that "the oxygen radicals associated with the interfacial polymer have lower ligand field splittings compared to their counter-part oxygen radicals in the pure polymer", although the broad nature of the features reported and the complete absence of any clear fine scale features makes unambiguous interpretation problematical. In the above cases, the paramagnetic centre was believed to be a serendipitous consequence of processing; the alternative is to introduce such centres deliberately. However, ESR is capable of not only providing information concerning interfacial interactions, but also, the consequences of these for molecular dynamics. Miwa et al, 2006, studied nanocomposites of poly(methyl acrylate) (PMA) and synthetic fluoromica, in which the PMA had been modified to include a so-called spin label. That is, a stable free radical, commonly nitroxide, which is introduced into a material that does not have an intrinsic paramagnetic response. This work demonstrated the power of the approach and showed that, in exfoliated systems, the mobility of PMA chains is reduced due to interactions with the nanofiller. The thickness of the rigid interface region was estimated to be in the range 5-15 nm. In intercalated materials, similar results were obtained, in that a fraction of constrained chain segments were detected at the clay interface together another with a higher mobility fraction. The chain dynamics of PEO, in this case end-labelled with nitroxide radicals, have similarly been studied whilst intercalated within the galleries of a fluoromica clay through a combination of experiment and simulation. From this, it was concluded that while the PEO chains were strongly compressed in one specimen by the charged silicate platelets, so restricting chain mobility, while in others, both rapid and slow chain dynamics were seen as a result, respectively, of segments removed from and interacting with the gallery walls. The spontaneous polymerization of PMMA in the presence of hectorite has been studied and, in the case of hectorite containing VO^{2+} ions, changes in the ESR spectrum after exposure to the monomer were interpreted as being indicative of polymerization within the galleries. No equivalent changes were detected in the equivalent system containing Cu^{2+} ions.

2.3.10. Additional Spectroscopic Studies of Nanocomposites

Many other spectroscopic techniques have also been applied to study polymeric nanocomposites. For example, X-ray photoelectron spectroscopy (XPS) was used to study polymer/nanofiller interactions in PMMA/kaolinite (Li et al, 2008); an increase of 0.6 eV in the oxygen 1s energy was ascribed to hydrogen bonding between the carbonyl groups of the polymer and hydroxyl group in the kaolinite sheets, while changes in the silicon 2p peak were associated with exfoliation. XPS has also been used to demonstrate covalent bonding between carbon nanofibres and monomers, oligomers and polymers and to confirm the existence of an initiator

monolayer on the surface of nanosilica prior to further chemical treatment. In addition to the above techniques, which all involve photons of some wavelength, numerous other techniques are also sometimes categorised under the heading spectroscopy. Dielectric spectroscopy involves measuring the response of a specimen to an alternating electric field, while molecular relaxation spectroscopy involves measuring the relationships between oscillatory stresses and strains in solids terms of appropriate moduli and phase angles. In the liquid state rheometers can perform the same function. While such spectroscopies are generally considered to constitute measurements of material properties, rather than structural probes, there is one area where his approach has been used as an indicator of structure, or at least dispersion, in nanocomposites; that is, viscosity. This is particularly relevant, technologically, to systems based on liquid polymers such as epoxies.

Mohan et al, 2005, examined the rheological behaviour of epoxy-MMT nanocomposites containing organo-modified and unmodified MMT, and reported that the presence of the added MMT served to increase the viscosity, particularly when suitably compatibilized. Similar increases in viscosity on adding nanofillers have also been seen in a siloxane copolymer filled with an organically modified mica-type layered silicate and PP/clay systems. Wang et al, 2006, examined the rheological properties of epoxy resin/nanoclay systems processed without and with add solvent. In the former case dispersion of the organoclay was found to be relatively poor, with particles greater than 10 μm in size remaining after processing. Rheologically, the system processed with added solvent differed markedly from that processed directly. First, the absolute viscosity value was seen to be increased, second increased shear thinning was observed and, finally, comparison with Krieger-Dougherty theory suggested a dramatic difference is the shape of the included particles. However, viscosity is not simply related to the extent of dispersion, it is also affected by the *distribution* of particle sizes within the system. Examination of the flow characteristics of model polymer (ethylene oxide/propylene oxide triblock copolymers) latex sphere systems has shown that the relative viscosity decreases as the size distribution increases. Studies of the rheological response of an epoxy resin containing differently functioned organoclays has revealed yielding phenomena, which were was interpreted as being indicative of mechanical stresses breaking down physical networks within the resin.

2.4. Scattering

2.4.1. X-ray Diffraction

The most simplistic approach to the problem of X-ray diffraction concerns the situation of a plane wave that is incident upon a perfect, infinite array of scatters. In this case, if the waves scattered from two successive planes are in phase, then geometry leads to the Bragg equation:

$$n\lambda = 2d\sin\theta$$

where n is an integer, d is the interplanar spacing, θ is the Bragg angle and λ is the wavelength of the radiation. Alternatively, the in-coming plane wave can be represented by a wavevector $\underline{q_o}$, of magnitude $2\pi/\lambda$, while the diffracted wave is represented by $\underline{q'}$. From this, the scattering vector $\underline{q}$ can be defined:

$$\underline{q} = \underline{q_o} - \underline{q'}$$

The utility of this geometrical approach is best illustrated by considering an infinite perfect crystal, whereupon the lattice planes can be represented by an array of points – the reciprocal lattice. If the tip of the vector $\underline{q_o}$ is placed at the origin of the reciprocal lattice then, the Bragg condition equates to the condition that $\underline{q}$ extends from the origin to a reciprocal lattice point and diffraction from the corresponding crystalline planes will then be seen. For elastic scattering:

$$q_o = q$$

such that all possible scattered wavevectors correspond to the surface of a sphere of radius $2\pi/\lambda$. When this

surface intersects a reciprocal lattice point, Bragg's Law will be fulfilled and diffraction is observed – the so-called Ewald Sphere construction. For an infinite perfect crystal, the reciprocal lattice points will be infinitely small, such that the above criterion is severe; diffraction only occurs at a singular angular value and the diffraction peak becomes infinitely narrow. As the extent of the crystal decreases, so the size of the reciprocal lattice points in the appropriate direction increases, such that diffraction can occur over an increasing range of angles. The result is that the observed diffraction peak becomes broadened; diffraction peak widths are commonly used in X-ray diffraction to evaluate crystallite sizes using the Scherrer equation:

$$\beta = \frac{K\lambda}{L\cos\theta}$$

where β is the peak width, K is a constant close to unity and L represents the size of the scattering crystallites in the direction corresponding to the diffraction peak corresponding to β.

Finally, and of most general utility, if the incident plane wave is again represented by the wavevector $\underline{q_o}$, by which we define an arbitrary origin O, then the material can be considered to be composed of an assembly of scattering volume elements $d\tau$, each of which will act as a source of spherical elastically scattered waves. The magnitude of q can then be written:

$$q = \frac{4\pi}{\lambda}\sin\theta$$

and the amplitude A_o of the scattered wave arriving at a remote detector from O can be written:

$$A(0) = AP(0)d\tau$$

where $P(0)$ is related to the nature of the scattering and the density of the scattering matter at O. Similarly, the amplitude arriving from P can then be written:

$$A(\underline{r}) = AP(\underline{r})(\exp i\underline{K}.\underline{r})d\tau_r$$

Thus, the total amplitude scattered from the complete assembly with a wavevector $\underline{q}$ is given by:

$$A(\underline{q}) = A\int_{-\infty}^{+\infty} P(\underline{r})(\exp i\underline{q}.\underline{r})d\tau_r$$

such that the total scattered intensity can be written:

$$I(\underline{q}) = \left|A\int_{-\infty}^{+\infty} P(\underline{r})(\exp i\underline{q}.\underline{r})d\tau_r\right|^2$$

These final equations are the key general relationships between the quantity that is measured in practice (the scattered intensity as a function of angle, where the angle is synonymous with q) and the structural variation within the specimen (represented by $P(\underline{r})$).

In practice, the process by which material structure gives rise to a scattered intensity can be considered in terms of two elements. First there is the local crystal lattice and then there are other larger scale structural features which may relate to groups of atoms, groups of molecules or some other repeat units, each of which can be termed a motif. The effect of the motif on the underlying diffraction pattern can then be evaluated using the Convolution Theorem. That is, the "intensity" of reciprocal lattice points are modulated by the function that is the Fourier Transform (FT) of the motif. To illustrate this, consider limiting the extent of a perfect 1-dimensional crystal. The FT of a perfect infinite crystal gives an array of infinitely narrow reciprocal lattice points. The extent of the crystal is then limited by multiplying the initial infinite lattice by a chopping function, the value of which is 1 within the extent of new finite crystal and zero elsewhere. The FT of this motif then needs to be multiplied by the FT of the initial lattice to obtain the required result. If the structure, in fact, consists of a

regular array of these limited crystals, then this larger scale ordering can be represented by another motif, such that the above process is repeated.

To illustrate the above, consider the application of X-ray diffraction to a semi-crystalline polymer. Broadly, the approach can be subdivided into wide angle X-ray scattering (WAXS) and small angle X-ray scattering (SAXS). In the case of WAXS, the scattering angles, or the magnitude of the scattering vectors, are such that information concerning the crystalline lattice is obtained. For highly ordered materials such as monodisperse PE oligomers, diffraction peaks are sharp, and many diffraction orders are generally observed, such that the Bragg equation can be applied with confidence. For less ordered polymers, the extent of the disorder serves to perturb the diffraction pattern such that peaks become broadened as a result of the limited extent of the crystallites and only low orders are observed. Nevertheless, Bragg's Law can still be applied and, in concert with the Scherrer equation, much useful information can be obtained. Such materials contain lamellar crystals separated from one another by amorphous material and SAXS is widely used to study this arrangement. Although, in practice, such a structure possesses no periodicity, it can be handled in a similar manner to long range superlattice fluctuation (motif) superimposed upon the local order within the crystal although, strictly, this is merely a construction of convenience. Since the scattered intensity that is observed is the FT of the electron density distribution, the diffraction pattern observed from such a system is a convolution of the FT of the functions representing these two factors. Since the superlattice is highly disordered, information relating to it is only preserved in the zeroth order peak, at small scattering angles. Analysis of the intensity distribution in this region generally requires the application of some model of the structure, from which parameters such as the crystallite long period, the amorphous thickness, the aggregation state of lamellae etc can be obtained. However, as with all X-ray scattering, it is rarely possible to transform intensity data into a unique structure; in recording intensity information, related phase information is lost – the so-called Phase Problem.

To conclude, when considering X-ray data it is essential to consider that ordering will generally occur at a range of dimensional levels and, in principle, all of these will exert some influence over the diffraction pattern that is obtained. While Bragg's Law is a simple way to interpret diffraction data from well ordered systems it, in fact, merely represents a highly simplistic idealisation. For systems where the ordering is limited and occurs on a range of different dimensional levels it is essential that such factors are taken into account when considering the real structural implication of experimental data.

2.4.2. X-ray Diffraction Case Studies

In nanocomposite research, the area where X-ray scattering has been utilised most concerns studies of systems containing nanoclays. Here, the topics that have attracted particular attention concern issues such as the effect of intercalant chemistry on layer spacing and studies of the aggregation state of the clay within the polymer matrix. While it is perfectly reasonable to interpret changes in peak positions in terms of intercalation of polymer chains or the introduction or extraction of the compatibilizer, statements such as "there is the absence of diffraction peaks, indicating the silicate layer are completely exfoliated in the PU matrix" (Cai et al, 2007), which are common in the literature, should be treated with caution. A converse interpretation of the absence of a distinct Bragg peak is that it merely indicates that, whatever the aggregation state of the layered filler, it is merely too disordered for Bragg's Law to apply. Indeed, statements such as "the results suggest that the single sheets of LDH have been exfoliated in the polymer matrix" have been made even when clear peaks exist in the scattering pattern (Li et al, 2003). Of particular interest in this regard are studies that combine WAXS and transmission electron microscopy (TEM). For example, Tang et al, 2004, used these techniques in concert to study

PP/MMT/calcium carbonate nanocomposites; despite the existence of a weak Bragg peak in the WAXS pattern of their PP1 sample corresponding to a periodicity of 1.3 nm and high contrast structural features on the TEM, this paper still states that the "TEM image for sample PP1 .... shows individual silicate layers which can be seen to be well-dispersed

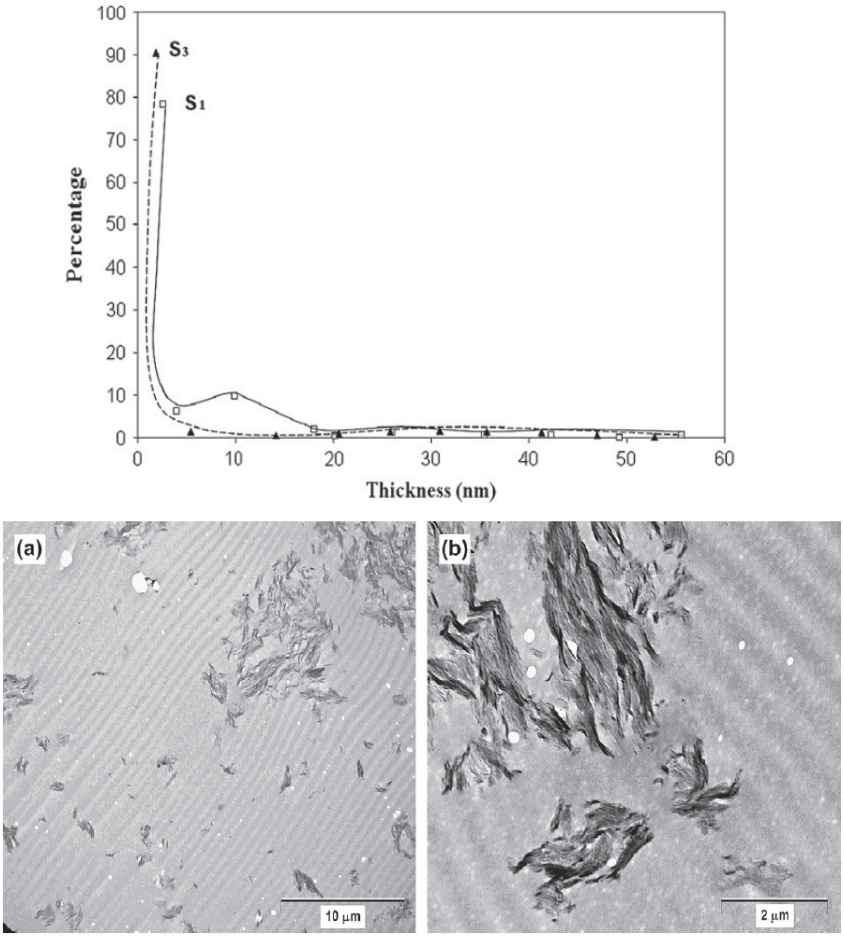

Figure 2.4.1 Comparison of the tactoid size distribution calculated from X-ray data with TEM images of the same sample (S_3). Reprinted from *Polymer* 2007, 48(14), Hernandez, M., Sixou, B., Duchet, J. and Sautereau, H., The effect of dispersion state on PMMA-epoxy-clay ternary blends: In situ study and final morphologies, pp.4075-4086, with permission from Elsevier.

(exfoliated) in the matrix". Gârea et al, 2009, used WAXS and TEM, together with many other techniques, in a comprehensive study of polybenzoxazine/MMT nanocomposites. Although the WAXS patterns only include broad, minor features, the TEM images clearly show a range of extensive tactoids. In a similar vein, the study of Hernandez et al, 2007, is unique to our knowledge in attempting to derive a numerical tactoid size distribution from X-ray data, as shown in Figure 2.4.1. The calculated size distribution shows that the number fraction of large aggregates in their material was exceedingly small. However, the TEM images well demonstrate that it was not zero. This highlights two important issues: while a number size distribution is easy to understand, perhaps a mass distribution is of more value; in certain applications, including those involving high electric fields, it may be the one large aggregate that is of more importance than the myriad of exfoliated layers. In short, much of the claims made about the dispersion state of layered systems in nanocomposites is based upon, at best, the inappropriate use of the idealised Bragg equation and, consequently, assertions based on this approach should be

treated with extreme caution.

In addition to studying the aggregation state of organoclays after dispersion into a polymeric material, WAXS has also been used to examine the introduction of monomers into inter-layer galleries prior to in-situ polymerisation. In the case of the polymerisation of sulfonate monomers within LDH systems, WAXS revealed evidence for the exchange of the chlorine anions by the monomer molecules. This resulted in a significant increase in the basal spacing of the host structure; the reported values are consistent with the inclusion of two monomer layers of monomer on each side of the gallery. In particulate systems, changes in order resulting from the inclusion of carbon black within PANi have also been reported using WAXS, although not quantified; elsewhere the Scherrer equation has been employed to evaluate the average metallic particle size in epoxy-based nanocomposites, containing metallic silver produced by the in-situ reduction of silver nitrate.

While it is possible to take a simplistic approach when dealing with WAXS data, even if this is invalid, the nature of SAXS data means that equivalent approaches cannot generally be used. Indeed, although SAXS can be highly informative, as explained by Paul and Robeson, 2008, "this technique has not been widely used except in a few laboratories probably because most laboratories do not have SAXS facilities or experience in interpreting the results." Nevertheless, Sedláková et al, 2009, used SAXS as part of a study of PBMA/MMT nanocomposite latexes; the resulting data were processed using Guinier analysis (plotting log $I(q)q2$ versus $q2$) and suggested that MMT existed in the form of sheet-like particles with a thickness of ~1.3 nm, a value that is in broad agreement with expectations. This form of data analysis was also used to give the radius of gyration of the plate thickness and the mass per unit area. Kim and Macosko, 2008, used SAXS, albeit with a different data processing methodology, to determine the structure of polyester/exfoliated graphite nanocomposites. In this case, TEM images suggested a high degree of exfoliation, an assertion supported by the absence of strong WAXS peaks; plotting log $I(q)$ against log q was interpreted in terms of the graphite layers existing in a fractal structure of dimensionality 2.0-2.3. The same data analysis methodology has been employed to study fractal structures elsewhere, including in titanium-oxo-cluster-based hybrid materials.

2.4.3. Additional Scattering Studies of Nanocomposites

While X-ray scattering is an electronic process, neutron scattering results from the same nucleon-nucleon forces that that hold atomic nuclei together. For any atom, the scattering factor is defined by the nuclear scattering length, which is dependent upon the constitution of the scattering nucleus, not upon the electronic configuration of the atom. As such, neutron scattering is isotope not element dependent. Therefore, a perfect crystal containing different isotopes of the same element can behave as a randomly disordered system, due to the different scattering lengths exhibited by the different isotopes.

In the case of systems containing polymers, this isotope dependence is of enormous value. Whereas X-ray diffraction is rather insensitive to the presence of hydrogen, the nuclei of both hydrogen and deuterium are strong neutron scatterers. Also, the neutron scattering lengths of these two isotopes are of opposite sign, such that a classic experimental approach involves introducing deuterated molecules into a hydrogenated matrix. This results in strong contrast, such that the conformation of the deuterated component can be studied within the chemically identical host. A second major advantage of neutron scattering is that, in practice, it is possible to obtain data over a very wide range of scattering vectors, characteristics that has proved particularly useful in the detailed study of disordered polymeric materials.

Galicia et al, 2009, observed a correlation peak at $q = 0.032$ Å^{-1} during a study of ferrogels based upon Fe_2O_3 nanoparticles incorporated into a polyacrylamide network. This was interpreted as indicting that the most

probable inter-particle distance was ~ 20 nm. However, at higher ferro-fluid volume fractions, the form of the structure factor at low scattering vectors indicated that the dispersion of the nanoparticles was highly heterogeneous. Jouault et al. 2009, used small angle neutron scattering (SANS) as part of as part of a study of PS/ silica nanocomposites to explore the network structure of the nanofiller. This paper provides a good illustration of both the kind of information that can be obtained in this way and the nature of the analysis required to extract potentially meaningful parameters. For example, a log log plot of scattering intensity against scattering vector, after appropriate correction of the raw data, was found to give a q^{-4}, dependence at intermediate q values, a finding that is characteristic of the scattering of a sharp well-defined interface between the nanosilica and the matrix. At low q, ($q < 10^{-2}$ Å^{-1}) the above plots tended to a plateau value, which is the signature of finite-size objects, termed primary aggregates, in the probed length scale. I larger agglomerates were to exist, then their signature could only have been detected by extending the experiments to lower scattering vectors. Further analysis suggests that the primary aggregates were fractal objects, which were on average composed of 15 nanoparticles and which have a fractal dimension of 2.5. Similar experiments on PEO/laponite hydrogels yielded a fractal dimensionality of between 2.6 and 2.8, depending upon the included sodium chloride concentration. Although, the precise origin of this fractal structuring was unclear, the disappearance of a plateau in the ultra-SANS region at high ionic strengths was taken to imply that adding NaCl results in an increase in size or density of the structural units. In laponite-based nanocomposites, including block copolymers, the lamellar texture of the block copolymer was observed in the small angle neutron scattering data; the associated dimension was found to increase on the introduction of the nanofiller. Nanocomposite hydrogels constitute ideal model systems in which to probe such issues, since substitution of H_2O with mixtures of H_2O and D_2O is a relatively easy means of inducing isotope contrast between the polymer and the solvent. In this way, for example, the deformation behaviour of clay based hydrogels has been examined in detail (Nishida et al, 2009). By recording two dimensional scattering patterns and then decomposing these into three partial structure factors, it was possible to explore the orientation of the clay and polymer components separately on deformation and to deduce that a polymer-enriched layer exists adsorbed onto the clay surfaces. Similar approaches have been employed elsewhere, but using other deuterated solvents.

Visible light has a wavelength of the order of 500 nm and therefore is, commonly used to study the solid state structure of crystalline polymers, primarily spherulitic dimensions, via the techniques of small angle light scattering. While optical clarity has been used as an indirect measure of the dispersion state of nanofillers in nanocomposites, the fact that the radius of gyration of polymer molecules in solution have long been determined through Rayleigh scattering theory and Zimm plots means that similar approaches can also be used in the study of polymer/nanoparticle systems. For example, dynamic light scattering (DLS) has been used in the study of microphase separation in poly(*N*-isopropyl acrylamide) (PNIPA)-clay nanocomposite hydrogels. In this work, the hydrodynamic radius of the clay, when dispersed alone in water, was found to be 16 nm, and independent of temperature, while the hydrodynamic radius of the polymer, in solution, was found to increase from 5 nm to 260 nm when the temperature was raised through the lower critical solution temperature. However, adding clay to the polymer solution was found to suppress this dramatic change. This result was interpreted in terms of suppression of aggregation of the PNIPA above the LCST as a result of strong interactions between the clay and the polymer. Tang and Dong, 2009, used DLS to study the size distributions generated as a result of using different emulsion-based synthesis routes for the preparation of ZnO nanocomposite latex based upon styrene. This work involved the initial treatment of the ZnO nanoparticles, in an attempt to render them more hydrophobic, and contains a detailed protocol for the surface treatment of nanoparticles with a silane coupling agent. Despite

this, contact angle measurements on treated ZnO sample were taken to indicated that only a limited increase in hydrophobicity is possible; this was found to be insufficient to prevent migration into the aqueous phase during emulsion polymerisation. Other examples of systems where DLS has been used to determine structural dimensions include aqueous solutions of fluorinated block copolymer and SWCNT, nanocomposites of poly(styrene-co-hexylacrylate) and cellulose whiskers, and C60/polymer colloid nanocomposites. Although DLS is essentially a technique for characterizing optical scatterers in a fluid, Foster et al, 2009, used it in connection with a study of processing conditions on the structure and properties of polypropylene/carbon nanofibre (CNF) nanocomposites. In this case, the CNFs were extracted from the each nanocomposite by dissolution and DLS was then used to determine the average fibre length.

2.5. Microscopy

Fundamental imaging theory indicates that the resolution limit of ideal optical system is related to the wavelength of the illuminating radiation. Consequently, since the prime objective of this article is to consider technique that are capable of providing useful information for the characterisation of nanocomposites, optical imaging is largely irrelevant. Here we will therefore focus on electron microscopy and scanning probe techniques. Electron microscopy can be subdivided into two broad categories, techniques where the electron beam is transmitted through a thin specimen (TEM) and those that involve emission of radiation from the surface of a bulk specimen (scanning electron microscopy - SEM). In addition, a number of related spectroscopic techniques should also be considered. A plethora of scanning probe microscopies (SPM) have been developed in recent times, since Rohrer and Binnig pioneering work in the 1980s that led to their receipt of the Nobel Prize for Physics in 1986.

2.5.1. Transmission Electron Microscopy

In the TEM, a thin film sample is irradiated with electrons and the transmitted radiation is imaged on a fluorescent screen or captured via an appropriate system. As such, a number of factors must be considered.

(i) An essential requirement is that the sample is sufficiently thin that useful transmitted radiation emerges. Thin specimens may be prepared in many ways but, for most practical specimens, ultramicrotomy is the most direct means of generating a thin specimen from a bulk artefact. However, the cutting process is generally far from straight forward and the forces involved are such that the resultant section may incur appreciable damage.

(ii) Energy is inevitably dissipated in a specimen when exposed to a beam of electrons and, indeed, such processes are critical to a number of analysis modes. However, polymers are, relatively speaking, much more radiation sensitive than many materials, such that covalent bonds are broken and permanent changes occur as a result of crosslink formation or chain scission.

(iii) If any imaging technique is to be of practical use, then the resulting contrast must be structurally meaningful. In TEM contrast can arise from variations in atomic number (Z-contrast), variations in specimen thickness (thickness contrast) or factors that are crystallographic in origin (Bragg or diffraction contrast).

2.5.2. TEM Case Studies - Electron Imaging

Even a cursory examination of the literature demonstrates that TEM is the most widely technique for the study of polymer-based nanocomposites, since the approach is extremely well suited to the examination of such systems. A key issue in the application of TEM to polymeric materials concerns the availability of suitable contrast mechanisms; most engineering plastics are not sufficiently ordered for diffraction-based imaging techniques to be

of great utility and the fact that such materials are generally composed of light elements, necessarily means that variations in electron density from place to place provide insufficient Z-contrast for this, in isolation, to give good images. In the case of nanocomposites, the differences in electron density between the matrix and the nanofiller means that this latter constraint is removed, such that the approach is an ideal means of studying dispersion and the aggregation state of the nanofiller.

Compatibility between nanofiller and matrix polymer is a major issue in the case of many nanocomposites, including those based upon the technologically dominant polymers, polyethylene and polypropylene. Consequently, the state of dispersion of nanofillers in such materials is of considerable interest. Copolymers of ethylene and vinyl acetate (EVA) are systems of considerable technological importance in many areas, including certain practical dielectric systems. Also, in many ways, they constitute idea model systems by which to study the influence of polarity on nanofiller dispersion and aggregation, since their degree of polarity can be varied by adjusting the relative proportions of ethylene and vinyl acetate in the polymer. Zhang et al, 2008, examined the structure of a range of EVA systems including 5-10% of a Zn/Al LHD and concluded that, while melt processing resulted in reasonable dispersion, this was somewhat inferior to that achieved through a prolonged (24 h) solution intercalation route; a more homogeneous dispersion of single LDH platelets was obtained via the latter route. Similar studies have been conducted on other layered systems, such as nanocomposites based upon graphite oxide. Elsewhere, the dispersion of ZnO nanoparticles within PMMA has been examined as part of a study of oxygen permeation in these systems; the resulting images revealed clear evidence of fractal-type structuring. Thus, while the dispersion was uniform on the scale of micrometres, significant local variations in particle densities were seen at smaller length scales.

Thermoplastic polyolefins (TPO) constitute a generic family of materials composed of blends of various propylene and ethylene copolymers, which have desirable mechanical properties for use in numerous areas. As such, the addition of nanoclays constitutes an attractive means of further enhancing properties and, consequently, the structure of such materials has been studied. Kim et al, 2008a, used TEM to study the structure of such systems, in particular, to understand the influence of maleic anhydride on composite morphology. This paper contains a selection of very high quality micrographs that well illustrate the advantages and limitation of bright field TEM for understanding such systems. First, the micrographs included clearly show the dispersion state of the clay, in this case MMT containing dimethyl, dihydrogenated tallow, within the polymer matrix; most of these appear to be oriented edge-on, whereupon the high electron density of the nanoclay layers means that they appear as thin dark lines within a light matrix. The use of TEM to study such systems is indeed generally associated with the examination of the edge-on view of sheets stacked to varying degrees, although it is possible to produce useful images of suitable small tactoids when the layers are oriented orthogonally. Indeed, it has been suggested that bright field TEM can be used directly to reveal changes in surface chemistry in MMT sheets oriented in this way. While this is an interesting concept, the image contrast is not easy to interpret. However, more detailed studies of surface modified TiO_2 nanoparticles using high resolution lattice imaging are much more convincing; prior to grafting, the crystal lattice of the TiO_2 can be seen throughout the nanoparticles while, after grafting, disordered surfaces layers 1-5 nm in thickness are clearly visible (Ngo et al, 2009). Equivalent specialist high resolution imaging techniques have also been utilized in the study of cerium based nanoparticles in PMMA where, quite remarkably, both lattice images and selected area diffracrtion patterns have been obtained from particles within the polymer matrix (Chai et al, 2009).

Composites based upon expanded graphite sheets have much in common with layered silicates. That is, graphite is also a layered structure and, by suitable processing, it can be expanded into nanosheets and dispersed within a matrix. Although most TEM studies of such systems have concentrated on the same bright field imaging techniques discussed above, selected area electron diffraction (SAED) has also used to examine systems based upon PS and graphite nanosheets, and a styrene-butyl acrylate copolymer and graphite oxide. Further extending the use of diffracted beams, Houdayer et al, 2007, applied dark field imaging to the study of PANi/antimony nanocomposites, although the paper does not seek to deduced any additional information from this approach.

Much of the interest in nanocomposites has related to their inclusion within thermoplastic systems, many of which are semicrystalline materials where macroscopic properties are strongly influenced by their lamellar and spherulitic morphology. However, while bright field imaging of the type described above is well suited to revealing the dispersion of the nanophase within the matrix, it cannot provide any information concerning the structure of the polymer. Traditionally, the lamellar texture of semicrystalline polymers requires the application of an appropriate staining or etching technique to provide useful image contrast. Surprisingly, we are not aware of any TEM studies that have sought to apply these well established approaches to semicrystalline nanocomposite systems; staining techniques would appear to be particularly appropriate as a means of studying nanoparticle/matrix interface structures, although careful optimization of the methodology would be required to ensure that the electron dense nanofiller could be unambiguously differentiated from the stained matrix. Studies of polymer blend systems illustrates a related problem inherent in bright field TEM techniques. Although TPOs, for example, are incompatible blend systems, both phases are of equal electron density and, therefore, appear equivalent when viewed in TEM bright field. This point is clearly made by comparing the TEM appearance of microtomed sections of multicomponent nanocomposites based upon MMT dispersed in a blend of polypropylene (PP), a polyamide-6 (PA6) and a Kraton block compolymer (Kusmono et al, 2008). Although the authors claim to be able to identify the Kraton in their thin sections, the dominant PP/PA6 phase structure is not readily visible. Despite this, the silicate layers are described as being homogeneously dispersed in the PA6.

2.5.3. Scanning Electron Microscopy

In the SEM, electrons are first accelerated to an energy in the range of 100 eV to 30 keV and, then, a de-magnified image of the source is focussed onto the sample surface and scanned across it in a raster pattern. Although such an imaging system cannot compete with TEM in terms of absolute resolution, ease of sample preparation and a depth of field extending to many micrometres are often more than adequate compensation. Nevertheless, the following fundamental issues need to be considered.

(i) In TEM, most of the incident electrons pass through the sample without undergoing any inelastic scattering processes whereas, in the SEM, the majority of the incident energy is dissipated in the sample. Consequently, particularly at high magnifications, it is important to optimize both the accelerating voltage and the probe current to minimize sample damage.

(ii) Electrons do not only result in radiation damage but, in the case of dielectric materials, also cause the sample to charge. The conventional means of avoiding this involves coating the sample with a suitable material and, although gold is most commonly used, carbon (reduced X-ray absorption) and chromium (reduced granulation but reduced long term environmental stability) both have their utility.

(iii) When a primary electron beam, energy ~10 keV and ~10 nm in diameter is incident upon a bulk sample, multiple scattering results in an interaction volume that extends for ~1 μm into the sample and which, at

its maximum extent, is of a comparable diameter. Throughout this volume, many processes occur, including the production of electrons, ranging in energy from some tens of electron volts to the energy of the primary beam, and X-rays. Secondary electrons (SE) are low energy electrons (~30 eV) and therefore are only able to emerge from the specimen when produced near the surface (~10 nm), where the diameter of the interaction volume is comparable to that of the primary beam. The number of electrons that escape is then dependent upon the local surface topography. Backscattered electrons (BSE) are also produced throughout the interaction volume and because, of their high energy, are able to escape from well within the specimen. The resolution obtainable in BSE imaging mode is therefore limited by the dimensions of the interaction volume, not the primary beam, although the resultant images do contain some atomic number information.

2.5.4. SEM Case Studies

SEM is a technique that is primarily associated with the examination of surfaces and therefore it can be applied in a number of ways to characterize nanocomposite systems; the simplest approach involves the direct examination of an external surface. For examples, Jia et al, 2008, used SEM in this way as part of a study of the tribological performance of an epoxy resin modified with PU and MMT. In this case, where the objective was to examine the wear pattern, the approach is entirely justified. Other subject areas where no sample preparation is required prior to SEM examination include the study of nanoparticles themselves, mechanically failed specimens, chars produced during studies of the effect of nanoadditives on flame retardency, laser ablation characteristics and surface erosion by electrical discharge erosion. However, in general, external surfaces will not be typical of a bulk material and, therefore, it is generally preferable to combine SEM with some prior sample preparation technique, the sophistication of which can vary greatly.

A commonly used and straightforward technique for exposing internal surfaces is cryo-fracture. In this case, the significance of the term “cryo” is that it implies that the process is conducted well below the glass transition temperature (T_g) of the specimen, such that it undergoes brittle fracture. However, even for polymers with a relatively high T_g it appears common practice to cool the specimen prior to fracture. Examples of systems where this technique has been used with success include an EVA copolymers containing nano-titania and a PU/titania nanohybrid membrane. Filippi et al, 2008, used cryo-fracture to examine the effects of the preparation procedure on the morphology of HDPE grafted maleic anhydride/organoclay nanocomposites. These workers specifically chose to examine samples that were not coated prior to insertion into the SEM but, rather, to employ an ESEM operating under a moderate vacuum. This approach, they claim, results in increased contrast between the phases; the images included in the paper certainly do contain high contrast, although it is difficult to determine exactly why this occurs. Lin et al, 2008, examined the structure and electrical properties of nanocomposites based upon copper nanowires in a PS matrix; in this case, the Z-contrast inherent in BSE imaging was used to reveal the location of the copper within the carbon-based matrix. Although these workers employed an accelerating voltage of 20 kV, whereupon the BSE excitation volume would be large, they nevertheless still claim to be able to distinguish single nanowires and aggregates of just two or three. An alternative means of opening up an internal surfaces is, simple, to cut the sample open; again, this is best performed below T_g to minimize sample deformation and the generation of cutting artefacts. In appropriate circumstances, where cutting damage is inconsequential and some inherent contrast mechanism exists, then the sample can be examined directly. Such an approach has been used in the study of electrical discharge characteristics of an epoxy resin filled with a combination of micro-silica and a layered silicate to provide nano-reinforcement of the resin phase. But exposing an internal surface orthogonal to the external surface that had experience electrical activity it proved possible both to quantify

the depth of erosion and image the internal structure of the resin, at least at the level of the micro-silica.

In the SEM, a key element of secondary electron imaging is surface topography and therefore the next step in increasing sample preparation sophistication involves post-processing the exposed internal surface in order to induce surface topographies that provide additional information concerning the morphological characteristics of interest, such as the distribution of the nano-additive or the effect of the nanofiller on the matrix microstructure. In the case of many polymeric systems, a wide range of different etching techniques have been developed to perform just his function but, somewhat surprisingly, few attempts appear to have been made to adapt these established and extremely powerful techniques to the study of nanocomposites. Wang et al, 2008, used cryo-fracture in concert with solvent etching (exposure to boiling toluene) to examine rather complex rubber toughened poly(trimethylene terephthalate)/organoclay ternary nanocomposites; in this case the objective of this approach was specifically to extract the rubber phase to re-examine both the phase structure of the matrix and the partitioning of the organoclay between the two polymers. Elsewhere, permanganic etching has been used with success to study PE-based systems.

2.5.5. Spectroscopy in the Electron Microscope

Inelastic scattering processes occur in both SEM and TEM. In the former instrument, these most significantly result in the production of X-rays, which contain information concerning the elemental composition within the sample – X-ray spectroscopy, which is most commonly analyzed via energy dispersive instrumentation (EDS/EDX). If the electron probe is fixed at one point on the specimen then the X-ray spectrum that is acquired will represent the complete range of elements present within the excited volume. As such, spatial resolution is not related to the size of the exciting electron beam but, rather, is limited to the micrometre scale. Conversely, if a fine electron probe is generated in the TEM, as in scanning transmission electron microscopy (STEM) for example, then the limited thickness of the specimen means that the exited volume, and consequently the spatial resolution, is of a comparable scale to the diameter of the exciting electron beam. In both SEM and TEM, the exciting probe can be rastered across the sample, such that a compositional image is built up sequentially, pixel by pixel, albeit with very different spatial resolutions in the two instruments. However, it is not only resolution that is affected by the extent of the excitation volume in the SEM since, after production, they may interact with the sample *en route* to the detector, such that the signal is perturbed through fluorescence and absorption effects. Where the sample is thin, (e.g. TEM) these effects are negligible and, therefore, EDS is much more of a quantitative tool in the TEM/STEM than in the SEM. In the TEM, the inelastic scattering processes that result in the X-ray spectra described above are also reflected in the energy spectrum of the transmitted electron beam. That is, the transmitted beam contains a spectrum of energies that can be used to characterise the elemental composition of the specimen via electron energy loss spectroscopy (EELS). Using this approach, elemental maps may be built up sequentially, pixel by pixel, using the same STEM techniques mentioned above in connection with EDS or, simultaneously, through the use of suitable electron energy filtering techniques by which an image is formed from electrons with an energy loss that coincides with the absorption edge of an element of interest.

2.5.6. Spectroscopy in the Electron Microscope – Case Studies

As described above, the attainable resolution using EDS in the SEM is insufficient to facilitate the detection of individual nanoparticles. Nevertheless, the approach has been used as a means of determining the chemical composition of nanoparticles and as a means of imaging gross spatial variations in composition. A study of PS-based nanocomposites (Umek et al, 2009) used this approach to demonstrate the superior dispersion of titania nanoribbons, compared with titania nanotubes, a result that was ascribed to the tendency of the latter to form

clusters; no reason for this was proposed. An SEM/EDS study of PMMA/silica hybrid sol–gel materials demonstrated that this synthetic route did not result in any large silica aggregates (Yeh et al, 2006). However, examination of the images presented does appear to indicate variations in X-ray intensity on the micrometre scale at low silica levels and, at higher levels, an apparent assembly of the silica into striking elongated features; no comment is made concerning this. Whilst elemental maps that plot detected X-ray intensity within an energy window corresponding to the element of interest are most commonly used to reveal dispersion, a less commonly used alternative is to show representative spectra. This does have the advantage of enabling peak ratios to be compared. Casciola et al, 2005, used EDS in their study of PVDF/zirconium phosphate nanocomposites; in this case, the fluorine line could be used to represents the local signal obtained from the polymer, while the Zr and P peaks were used as markers for the nanoparticles. Although the Zr/P ratio was found to be spatially invariant, the ratio of Zr/F changed significantly from place to place. In addition to using this approach n this SEM, these workers also exploited the high resolution available in TEM/EDS to confirm the nanometric nature of their ZrP particles and to reveal the precise distribution present in a number of different systems. The composition of nanocomposites containing palladium and titania and systems containing nano-silver within a PANi matrix have also been studied in this way, but most investigations that have exploited this approach would seem to have employed it as a means of characterizing nanoparticles. It can therefore be concluded that the use of TEM/EDS for the study of polymeric nanocomposites has been limited, while the ultilization of EELS, in its various guises, for the direct examination of polymer-based nanocomposites appears even more restricted. The approach has been used in the study of and nano-palladium in the conjugated polymer poly(5-amono-*ortho*-cresol), although the

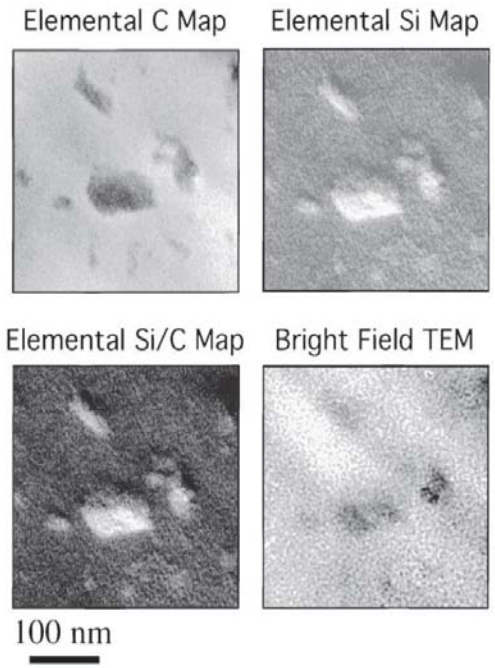

Figure 2.5.1 Comparison of a conventional TEM of a polymer containing POSS nanoparticles with image obtained at different energy loss values. Reprinted from *Polymer* 2002, 43(15), Li, G.Z., Wang, L., Toghiani, H., Daultonc, T.L., and Pittman Jr, C.U., Viscoelastic and mechanical properties of vinyl ester (VE)/ multifunctional polyhedral oligomeric silsesquioxane (POSS) nanocomposites and multifunctional POSS-styrene copolymers, pp.4167-4176, with permission from Elsevier.

potential of the approach is better demonstrated by Li et al's 2002 study of nanocomposites based upon a commmercial vinyl ester resin containing polyhedral oligomeric silsesquioxane (POSS) nanoparticles, as shown in Figure 2.5.1. Despite the differences in electron density between the nanofiller and the matrix, bright field TEM was unable to reveal the POSS, whereas energy filtering produced clear images.

2.5.7. Scanning Probe Microscopies

A broad range of scanning probe microscopies have evolved from the initial concept of scanning tunnelling microscopy (STM). In STM, an atomically sharp probe is scanned across a sample surface and the tunnelling current between the tip of the probe and the surface of the specimen is monitored; as such, two basic modes of operation are possible. First, the separation between the tip and the sample can be maintained at a constant value. Because the tunnelling current depends upon the wavefunction overlap between probe and surface, this can provide a topographical image of the sample surface with atomic resolution. Alternatively, the tip can be scanned across the surface at constant height, whereupon, the resultant variations in current can be related to local variations in charge density. Both of the modes described above provide image contrast that is a convolution of the electronic structures of the sample and probe tip. When the latter contribution is minimal, information is obtained that pertains to just the sample; both topographic data and spectroscopic data are then attainable. Tunnelling spectroscopy can be performed in the STM by locating a feature of interest and then monitoring the current as a function of applied voltage at a fixed separation, whereupon the resulting data are then related to the local density of states in the sample.

In other SPM systems, the tunnelling current is replaced by an alternative physical process; the underlying principles of imaging and spectroscopy nevertheless, still apply. Possibly the most widely used SPM variant today is atomic force microscopy (AFM). As in STM, this also relies upon an atomically sharp tip being scanned across the specimen but, now, it is mechanical interactions rather than electrical ones that provide the image contrast. The mechanical interactions serve to deflect the cantilever upon which the probe in mounted, and these deflections can be monitored. The resultant modes can be illustrated by a number of examples. First, the tip can be scanned across and in contact with the sample to provide topographical information. Similar information can be obtained without contact by adjusting the separation of the sample and probe such that the defection remains constant; a non-contacting constant force topographic image. Alternatively, in tapping modes, an oscillation can be applied to the cantilever whereupon images can be generated not just from the deflection but also from phase information. Finally, force spectroscopy can be performed by measuring the deflection as a function of sample / probe separation. Experiments include nano-indentation, in which the probe is pushed into the sample surface, or single molecule “stress / strain” measurements.

Other techniques included scanning near-field optical microscopy (SNOM), in which a tapered fibre is used to probe the optical properties of the sample with a resolution ~100 nm, scanning thermal microscopy, in which a thermocouple/heater assembly replaces the AFM tip in order to probe the thermal properties of the surface, and a gamut of electrical techniques such as electrostatic probe microscopy, in which a bias potential is applied to the probe and the defection results from interactions with surface charges. In short, any physical process can be used as the basis for an SPM, provided the probe / surface interactions can be localised and the probe can be scanned across the surface to provide an image.

2.5.8. AFM Case Studies

Although STM was the first SPM technique to be developed and has great advantages when it comes to the examination of particular systems, the requirement to be able to sustain a tunnelling current between the probe tip and the sample necessarily limits its utility where dielectric materials are of interest. For such systems, the most commonly used technique is AFM due to its relative ease of use, range of available imaging modes and cost. Consequently, AFM has been widely used to study many different nanocomposite systems.

Song et al, 2008, used AFM in tapping mode to produce topographical images of the distribution of gold

nanoparticles within polyacrylamide networks. Because the gold nanoparticles stood proud of the polymer network, this simple approach was able to provide excellent image contrast, clearly revealing the size of the nanoparticles and their distribution within the system. Similar images have also been generated using non-contacting mode and, through quantitative profilometry, it has been concluded that the nanoparticles typically stood about 5 nm proud of the background. Elsewhere, such a direct approach has been less successful and a number of reasons can be proposed for this. One study of the structure and optical properties of titania-based nanocomposites (Rao and Chen, 2008) reported a surface roughness value of just 0.45 nm, a result the authors associated with excellent dispersion of the titania within the polymeric matrix. However, external polymer surfaces are well known to be unrepresentative of the bulk so the generality of this conclusion is open to some debate - the accompanying TEM micrographs appear to show detectable granularity. Huang et al, 2008, used AFM in tapping mode/phase imaging to study the effect of aluminium nano- and microparticles on morphological evolution in low density polyethylene; that is, to examine the effect of the filler on the matrix. Although this is one of relatively few investigations to use microscopy to focus on the matrix polymer rather than just the distribution of nanoparticles, the work could be criticized in that these workers only examined potentially unrepresentative external surfaces of bulk compounded samples.

To overcome such issues, Kim et al, 2008, cryogenically microtomed their samples prior to examination. Where such a procedure is used in conjunction with SEM, as described above, it is then necessary to introduce some structurally meaningful topography prior to examination. In this study of nanocomposites based upon TPO, the difference in the mechanical properties of the various components of the TPO were sufficient to reveal the phase structure of the blend; with the exception of microtome damage, surfaces exposed in this way should be flat. However, this approach did not reveal the physical state of the nanoclay and, for this, TEM was used. Neither TEM nor AFM were able simultaneously able to image both the nanoclay distribution and the structure of the matrix polymer. Although this study does not explicitly state that it is differences in mechanical properties that are exploited to generate image contrast, other work has clearly shown that high modulus tactoids of functionalised organoclay in a polymer matrix can be revealed though AFM tapping mode/phase imaging. Ganß et al, 2008, used microtomy to expose internal surfaces of PP/MWNT composites and used AFM phase imaging to reveal a relatively homogeneous distribution of loosely packed assemblies of MWNTs with dimensions ~1 μm. AFM has been used study of the effect of nanoalumina on the electrical surface erosion behaviour of an epoxy resin. In this case, topographical images of eroded surfaces clearly showed increasing roughness as degradation progressed, an observation that was interpreted as the formation of a surface layer rich in nanoparticles.

Other systems where AFM topographical images have been used to reveal the distribution of nanoparticles within a polymer include gold nanoparticles within polyacrylamide networks (tapping mode), zinc sulphide nanocrystal quantum dots in poly(vinylpyrrolidone), PU/nanosilica and PET/MMT.

2.5.9. Additional SPM Studies of Nanocomposites

Apart from AFM, the most commonly used scanning probe techniques for the study of nanocomposites are based upon electrical measurements. The original scanning probe microscopy was STM, which relies upon a tunnelling current flowing from the probe tip to the sample. As such, this initially seems well suited to studying local variations in electrical behaviour and was applied to the study of conducting polymer/SWCNT nanocomposites (Tamburri et al, 2005). However, since the tunneling current will be dependent upon both the electrical; properties of the sample and its topography, it is not clear how the images presented in this paper should really be interpreted. Elsewhere, variations in the electrical characteristics along the length of individual carbon

nanotubes have been interpreted as corresponding to single functional groups (Cahill et al, 2004). The partitioning of conducting inclusions between phases in a block copolymer leads to variations in the local electrical properties, rendering this problem amenable to study by electrostatic force microscopy (EFM), a technique that probes local variations in electric field gradient above the specimen surface. In this way, variations in the local composition of systems containing functionalized graphene and silver nanoparticles have been imaged. While this approach is readily used to provide image contrast, quantitative interpretation of the data is more problematical. Nevertheless, Gramse et al, 2009, have proposed a means by which quantitative measurements of the local dielectric constant can be made using EFM. Ramasundaram et al, 2009, imaged the local ferroelectric response of thin nanocomposites films of an organically modified silicate in poly(vinylidene fluoride) using dynamic contact-EFM. In this, a DC voltage was first applied to a Ti/Pt coated conductive tip to pole the sample locally, pixel by pixel. To probe the resulting ferroelectric response, a high frequency AC signal was applied to the tip together with a DC offset of opposite polarity to that used in the write phase, and the probe was scanned across the specimen to form the required image. Other similar studies include measurements of the work function of PANi films, before and after gold-cluster nucleation, using scanning Kelvin probe microscopy and a study of nanocomposites of titania and PPV using a combination of SNOM and EFM (Liu, 2009). This paper is particularly useful not only in illustrating the nature of the images that such techniques can provide, but also in describing the theoretical principles that underpin the extraction of meaningful data from the electrostatic interactions that occur between a sample surface and an electrically biased conducting probe tip.

References

Ai, L.-M., Feng, W., Chen, J., Liu, Y., and Cai, W.M., 2008, Evaluation of microstructure and photochromic behavior of polyvinyl alcohol nanocomposite films containing polyoxometalates, *Materials Chemistry and Physics*, 109(1), pp.131-136.

Cahill, L. S., Yao, Z., Adronov, A., Penner, J., Moonoosawmy, K. R., Kruse, P., and

Goward, G. R., 2004, Polymer-functionalized carbon nanotubes investigated by solid-state nuclear magnetic resonance and scanning tunneling microscopy, *J. Phys. Chem. B*, 108(31), pp.11412-11418.

Cai, Y., Hu, Y., Song, L., Liu, L., Wang, Z., Chen, Z. and Fan, W., 2007, Synthesis and characterization of thermoplastic polyurethane/ montmorillonite nanocomposites produced by reactive extrusion, *J. Mater. Sci.*, 42(14), pp.5785-5790.

Casciola, M., Donnadio, A., Pica, M., Valentini, V., and Piaggio, P., 2005, Characterization of Zr phosphate/PVDF nanocomposites by vibrational spectroscopy, *Macromol. Symp.*, 230, pp.95-104.

Chai R., Lian H., Li C., Cheng Z., Hou Z., Huang S., and Lin J., 2009, In Situ Preparation and Luminescent Properties of CeF3 and CeF3:Tb3+ Nanoparticles and Transparent CeF3:Tb3+/PMMA Nanocomposites in the Visible Spectral Range, *J. Phys. Chem. C*, 113(19), pp.8070-8076.

Ciardelli, F., Coiai, S., Passaglia, E., Pucci1, A., and Ruggeri, G., 2008, Nanocomposites based on polyolefins and functional thermoplastic materials, *Polym. Int.*, 57(6), pp.805-836.

Filippi, S., Marazzato, C., Magagnini, P., Famular, A., Arosio, P., and Meille, S.V., 2008, Structure and morphology of HDPE-g-MA/organoclay nanocomposites: Effects of the preparation procedures, *Eur. Polym. J.*, 44(4), pp.987-1002.

Foster, R.J., Hine, P.J., and Ward, I.M., 2009, Characterisation and modelling of polypropylene/carbon nanofibre nanocomposites, *Polymer*, 50(16), pp.4018–4027.

Galicia, J.A., Cousin, F., Dubois, E., Sandre, O., Cabuil, V. and Perzynski, R., 2009, Static and dynamic structural probing of swollen polyacrylamide ferrogels, *Soft Matter*, 5(13), pp.2614–2624.

Ganß, M., Satapathy, B.K., Thunga, M., Weidisch, R., Pötschke, P., and Jehnichen, D., 2008, Structural interpretations of deformation and fracture behavior of polypropylene / multi-walled carbon nanotube composites, *Acta Materialia*, 56(10), pp.2247-2261.

Gârea, S.A., Iovu, H., Nicolescu, A. and Deleanu, C., 2009, A new strategy for polybenzoxazine–montmorillonite nanocomposites synthesis, *Polymer Testing*, 28(3), pp.338-347.

Gilman, J.W., Bourbigot, S., Shields, J.R., Nyden, M., Kashiwagi, T., Davis, R.D., Vanderhart, D.L., Demory, W., Wilkie, C.A., Morgan, A.B., Harris, J., and Lyon, R.E., 2003, High throughput methods for polymer nanocomposites research: extrusion, NMR characterization and flammability property screening, *J. Mater. Sci.*, 38(22), pp. 4451–4460.

Gouadec, G., and Colomban, P., 2007, Raman Spectroscopy of nanomaterials: how spectra relate to disorder, particle size and mechanical properties, *Progress in Crystal Growth and Characterization of Materials*, 53(1), pp.1-56.

Gramse, G., Casuso, I., Toset, J., Fumagalli, L., and Gomila, G., 2009, Quantitative dielectric constant measurement of thin films by DC electrostatic force microscopy, *Nanotechnology*, 20(39), 395702.

Hernandez, M., Sixou, B., Duchet, J. and Sautereau, H., 2007, The effect of dispersion state on PMMA-epoxy-clay ternary blends: In situ study and final morphologies, *Polymer*, 48(14), pp.4075-4086.

Houdayer, A., Schneider R., Billaud D., Lambert J., and Ghanbaja J., 2007, Preparation of new antimony(0)/polyaniline nanocomposites by a one-pot solution phase method, *Materials Letters*, 61(1), pp.171-176.

Huang, X., Jiang, P., Kim, C., Duan, J., and Wang, G., 2008, Atomic force microscopy analysis of morphology of low density polyethylene influenced by Al nano- and microparticles, *J. Appl. Polym. Sci.*, 107(4), pp.2494-2499.

Jang, B.Z., and Zhamu, A., 2008, Processing of nanographene platelets (NGPs) and NGP nanocomposites: a review, *J. Mater. Sci.*, 43(15), pp.5092-5101.

Jeon, K., Lumata, L., Tokumoto, T., Steven, E., Brooks, J., and Alamo, R.G., 2007, Low electrical conductivity threshold and crystalline morphology of single-walled carbon nanotubes-high density polyethylene nanocomposites characterized by SEM, Raman spectroscopy and AFM, *Polymer*, 48(16), pp.4751-4764.

Jia, Q., Shan, S., Wang, Y., Gu L., and Li, J., 2008, Tribological performance and thermal behavior of epoxy resin nanocomposites containing polyurethane

and organoclay, *Polym. Adv. Technol.*, 19(7), pp.859-864.
Jouault, N., Vallat, P., Dalmas, F., Said, S., Jestin, J., and Boué, F., 2009, Well-dispersed fractal aggregates as filler in polymer-silica nanocomposites: long-range effects in rheology, *Macromolecules*, 42(6), pp.2031-2040.
Kickelbick, G., 2008, The search of a homogeneously dispersed material—the art of handling the organic polymer/metal oxide interface, *J. Sol-Gel Sci. Technol.*, 46(3), pp.281-290.
Kim D.H., Fasulo P.D., Rodgers W.R., and Paul D.R., 2008, Effect of the ratio of maleated polypropylene to organoclay on the structure and properties of TPO-based nanocomposites. Part II:Thermal expansion behavior, *Polymer*, 49(10), pp.2492-2506.
Kim, H. and Macosko, C.W., 2008, Morphology and properties of polyester/exfoliated graphite nanocomposites, *Macromolecules*, 41(9), pp.3317-3327.
Koh, J.K., Seo, J.A., Hwan Koh, J., and Kim, J.H., 2009, Templated synthesis of Ag loaded TiO2 nanostructures using amphiphilic polyelectrolyte, *Materials Letters*, 63(15), pp.1360–1362.
Kusmono, Mohd Ishak, Z.A., Chow, W.S., Takeichi T., and Rochmadi, 2008, Influence of SEBS-g-MA on morphology, mechanical, and thermal properties of PA6/PP/organoclay nanocomposites, *Eur. Polym. J.*, 44(4), pp.1023-1039.
Li, B., Hu, Y., Liu, J., Chen, Z. and Fan, W., 2003, Preparation of poly (methyl methacrylate)/LDH nanocomposite by exfoliation-adsorption process, *Colloid. Polym. Sci.*, 281(10), pp.998-1001.
Li, G.Z., Wang, L., Toghiani, H., Daultonc, T.L., and Pittman Jr, C.U., 2002, Viscoelastic and mechanical properties of vinyl ester (VE)/multifunctional polyhedral oligomeric silsesquioxane (POSS) nanocomposites and multifunctional POSS-styrene copolymers, *Polymer*, 43(15), pp.4167-4176.
Li, X., Chen, S., Hu, W., Shi, S., Shen, W., Zhang, X., and Wang, H., 2009, In situ synthesis of CdS nanoparticles on bacterial cellulose nanofibers, *Carbohydrate Polymers*, 76(4), pp.509-512.
Li, Y., Zhang, B., and Pan, X., 2008, Preparation and characterization of PMMA–kaolinite intercalation composites, *Composites Science and Technology*, 68(9), pp.1954-1961.
Lin, B., Gelves G.A., Haber, J.A., Pötschke P., and Sundararaj, U., 2008, Electrical, morphological and rheological study of melt-mixed polystyrene/copper nanowire nanocomposites", *Macromol. Mater. Eng.*, 293(7), pp.631-640.
Liu, P., 2007, Polymer modified clay minerals: a review, *Applied Clay Science*, 38(1-2), pp.64-76.
Liu, R., 2009, Imaging of photoinduced interfacial charge separation in conjugated polymer/semiconductor nanocomposites, *J. Phys. Chem.*, C 2009, 113(21), pp.9368-9374.
MacCrone, R.K., Nelson, J.K., Schadler, L.S., Smith, R., and Keefe, R.J., 2007, The use of electron paramagnetic resonance (EPR) in the probing of the nanodielectric interface" *proc.* ***IEEE International Conference on Solid Dielectrics*****, July 8-13 2007, Winchester UK. Pp.428-431.**
Miwa, Y., Drews, A.R., and Schlick, S., 2006, Detection of the direct effect of clay on polymer dynamics: the case of spin-labeled poly(methyl acrylate)/clay nanocomposites studied by ESR, XRD, and DSC, *Macromolecules*, 39(9), pp.3304-3311.
Moghaddam, L., Martin, D.J., Halley, P.J., and Fredericks, P.M., (2009), Vibrational spectroscopic studies of laboratory scale polymer melt processing: application to a thermoplastic polyurethane nanocomposite, *Vibrational Spectroscopy*, 51(1) pp.86–92.
Mohan, T.P., Kumar, M.R., and Velmurugan, R., 2005, Rheology and Curing Characteristics of Epoxy-Clay Nanocomposites. *Polymer International*, 54(12), pp1653-1659.
Ngo V.G., Bressy C., Leroux C., and Margaillan A., 2009, Synthesis of hybrid TiO_2 nanoparticles with well-defined poly(methyl methacrylate) and poly(tert-butyldimethylsilyl methacrylate) via the RAFT process, *Polymer*, 50(14), pp.3095-3102.
Nishida, T., Endo, H., Osaka, N., Li, H.J., Haraguchi, K., and Shibayama1, M., 2009, Deformation mechanism of nanocomposite gels studied by contrast variation small-angle neutron scattering, *Phys. Rev. E*, 80(3), 030801 (R).
Pardal, F., Lapinte, V., and Robin, J.-J., 2009, Modification of silica nanoparticles by grafting of copolymers containing organosilane and fluorine moities, *J. Polym.Sci.: Part A: Polym. Chem.*, 47(18), pp.4617–4628.
Paul, D.R. and Robeson, L.M., 2008, Polymer nanotechnology: nanocomposites, *Polymer*, 49(15), pp.3187-3204.
Rao, Y., and Chen, S., 2008, Molecular composites comprising TiO_2 and their optical properties", *Macromolecules*, 41(13), pp.4838-4844.
Ramasundaram, S., Yoon, S., Kim, K.J., Lee, J.S., and Park, C., 2009, Crystalline structure and ferroelectric response of poly(vinylidene fluoride) / organically modified silicate thin films trepared by heat controlled spin coating, *Macromol. Chem. Phys.*, 210(11), pp.951-960.
Raquez, J.-M., Narayan, R., and Dubois, P., 2008, Recent advances in reactive extrusion processing of biodegradable polymer-based compositions, *Macromol. Mater. Eng.*, 293(6), pp.447–470.
Richter, H., Wang, Z.P., and Ley, L., 1981, The one phonon Raman-spectrum in microcrystalline silicon, *Solid State Comm.*, 39(5), pp.625-629.
Sedláková, Z., Plešti, J., Baldrian, J., Šlouf, M. and Holub, P., 2009, Polymer-clay nanocomposites prepared via in situ emulsion polymerization, *Polym. Bull.*, 63(3), pp.365-384.
Song, Y., Li, Z., Wang, L., Yao, Y., Chen, C., and Cui, K., 2008, One-step preparation of hybrid materials of polyacrylamide networks and gold nanoparticles", *Microscopy Research and Technique*, 71(6), pp.409-412.
Sudeep, P.K., and Emrick, T., 2007, Polymer-nanoparticle composites: preparative methods and electronically active materials, *Polymer Reviews*, 47(2), pp.155-163.
Tamburri, E., Orlanducci, S., Terranova, M.L., Valentini, F., Palleschi, G., Curulli, A., Brunetti, F., Passeri, D., Alippi, A., and Rossi, M., 2005, Modulation of electrical properties in single-walled carbon nanotube/conducting polymer composites, *Carbon*, 43(6), pp.1213-1221.
Tang, E. and Dong, S., 2009, Preparation of styrene polymer/ZnO nanocomposite latex via miniemulsion polymerization and its antibacterial property, *Colloid Polym. Sci.*, 287(9), pp.1025-1032.
Tang, Y., Hu, Y., Zhang, R., Wang, Z., Gui, Z., Chen, Z. and Fan, W., 2004, Investigation Into poly(propylene)/montmorillonite/ calcium carbonate nanocomposites, *Macromol. Mater. Eng.*, 289(2), pp.191-197.
Thomas, V., Namdeo, M., Murali Mohan, Y., Bajpai, S.K. and Bajpai, M., 2008, Review on polymer, hydrogel and microgel metal nanocomposites: a facile nanotechnological approach", *J. Macromol. Sci., Part A: Pure Appl. Chem.*, 45(1), pp.107-119.
Tzavalas, S., and Gregoriou, V.G., 2009, Infrared spectroscopy as a tool to monitor the extent of intercalation and exfoliation in polymer clay nanocomposites, *Vibrational Spectroscopy*, 51(1), pp.39-43.
Umek, P., Huskić, M., Škapin, A.S., Florjančič, U., Zupančič, B., Emri, I., and Arčon, D., 2009, Structural and mechanical properties of polystyrene nanocomposites with 1-D titanate nanostructures prepared by an extrusion process, *Polymer Composites*, 30(9), pp.1318-1325.
Wang, H., Hoa, S.V., and Wood-Adams, P. M., 2006, New method for the synthesis of clay/epoxy nanocomposites. *J. Appl. Polym. Sci.*, 100(6), pp4286-4296.
Wang, K., Chen, Y., and Zhang, Y., 2008, Effects of organoclay platelets on morphology and mechanical properties in PTT/EPDM-g-MA/organoclay ternary nanocomposites, *Polymer*, 49(15), pp.3301-3309.
Yeh, J.-M., Weng, C.-J., Huang, K.-Y., and Lin, C.-C., 2006, Effect of baking treatment and materials composition on the properties of bulky PMMA-silica hybrid sol-gel materials with low volume shrinkage, *J. Appl. Polym. Sci.*, 101(2), pp.1151-1159.
Zhang M., Ding P., Du L., and Qu B., 2008, Structural characterization and related properties of EVA/ZnAl-LDH nanocomposites prepared by melt and solution intercalation, *Materials Chemistry and Physics*, 109(2-3), pp.206-211.

Chapter 3 Macroscopic Properties – Measurement and Assesment

3.1. An Introductory Comment

When comes the time to give an appraisal of the performance gain from developing nanodielectrics, the preparation techniques and nature/state of the materials studied must be considered. New challenges have appeared associated with dispersing nanoparticles into polymeric matrices or polymer microcomposites. Quality of dispersion affects the improvement of the material properties. The “nanometric” context has also brought upon new sensitivities of the developed materials in regards of the initial electric charge trapping, the ingression of water molecules and interplay at interfaces (Zhou *et al* 2008), the stability of the material in regards of different annealing processes, etc.

At the present time, mostly non-optimized nanodielectrics have been studied. This reflects into the observed properties and their variability. Overall, the properties gleaned here refer mostly to hybrid polymer composites. They are nanocomposites containing some non-negligible structures of micrometric size, formed of nanostructures and/or particles. Properties are found to be affected by the preparation and the storage conditions (Sami *et al.* 2008). Annealing parameters (Yeh *et al* 1976) and ageing will also be important in determining the properties. All the above remarks apply to the properties reported in the following sections.

The best improvement in properties is found when the inorganic nanoparticles are pre-treated. For instance, silane treatment functionalizes the surfaces, increases interactions with the polymer matrix, and helps in the dispersion process. It also affects the interaction zone which is believed to play a determinant role in polymer nanocomposites (Tanaka *et al* 2005). Indeed, in its present state-of-the-art, nanodielectrics properties are dominantly controlled by the interfaces (particle/matrix). However, the nanodielectric concept (Fréchette *et al* 2001) is more general and, in some circumstances, will permit building blocks and interfaces to both play determinant roles (Fréchette 2009).

To give a flavour of the effect of nanostructuration on the dielectric properties improvement of polymer nanocomposites, let us mention the substantial increase of the nanodielectric surface resistance to discharge erosion and an observed reduced of space charge accumulation. Then, let us discover the detailed properties presented in the following sections.

References

Fréchette MF, Trudeau M, Alamdari HD et al S (2001) Introductory Remarks on Nano-Dielectrics”, Ann. Rept. CEIDP, Kitchener CAN, Oct. 14-17

Fréchette MF (2009) Innovation in Dielectric Materials : from Macro to nanoscales, Invited Keynote, Electrical Insulation Conference (EIC), Montréal, Québec, Canada, 1-3 June

Sami A, Fréchette MF, David E et al (2008) Water as a digression relative to the dielectric response in the frequency domain for polymer composites Ann Rept CEIDP Québec city, Qc, Canada, Oct. 26-29th

Tanaka T, Kozako M, Fuse N et al (2005) Proposal of a multi-core model for polymer nanocomposite dielectrics. Trans IEEE DEI-12-4:669-681

Yeh GSY, Hosemann R, Loboda-Cackovic el al (1976) Annealing effects of polymers and their underlying molecular mechanisms Polymer Vol.17 April pp 309-318

Zou C, Fothergill JC, Rowe SW (2008) The effect of water absorption on the dielectric propertiesof epoxy nanocomposites. Trans IEEE DEI-15-1:106-117

3.2. Dielectric Spectroscopy

3.2.1. Introduction

In this chapter the study of the behaviour of nano-composites in the frequency domain is discussed. Dielectric spectroscopy (DS) is a commonly used technique to record the behaviour of the complex permittivity as a function of frequency for different temperatures. The technique is based on the application of a voltage of varying frequency to a test specimen and measurement of the resulting current and phase shift between current and applied voltage. From these data, the complex permittivity is derived:

The real and imaginary component of ε, plotted against frequency show the dielectric relaxation phenomena in this frequency range. Any change of the molecular structure of a dielectric, due to ageing processes or due to the addition of fillers, will show up in such a plot if the related relaxation phenomena occur in the measured frequency range. The frequency range of commonly used DS analyzers is quite broad, ranging from µHz to GHz. Especially in the lower frequency ranges information is contained about the inter-action of fillers and host material. For a thorough treatment of DS the reader is referred to Kremer (2003), for more information on dielectric polarisation Jonscher (1983) would be an excellent choice.
Conventional (micro-sized) fillers are commonly used to improve thermal/mechanical properties and to reduce cost, often at the expense of a reduction of dielectric properties. The bonding of the host polymer to the filler will give rise to a local immobilization of the polymer chains, thus affecting the properties of the composite system (Nelson et al. 2002). Usually, large filler weight percentages are used, up to 70%. Characteristic for micro-composites is the occurrence of Maxwell-Sillars-Wagner (MSW) polarization at the interfaces between filler and host.

Although a large amount of literature is available on DS applied on nano-composites, we will focus on the literature on nano-composite dielectrics for electric insulation. The emphasis will be on the most common base polymers, i.e. epoxy resin and polyethylene and their response to the addition of nanoparticles. Further, this chapter will be restricted to some remarkable observations using DS on nanocomposites.

3.2.2. Effects of nanoparticles in the low frequency region of the DS spectrum

Perhaps the first paper in this field was the one of Nelson et al. (2002). In this paper, the results are presented of DS on standard Bisphenol-A epoxy resin composites with Titanium Dioxide (TiO_2) particles of nano and micro-size. In the paper it is not reported whether the particles were surface treated before mixing them with the resin. For 10% filler loading a marked difference was found in the low frequency region between nanocomposites and microcomposites. For the former, a flat tan delta response was found in contrast to the latter. This was possibly attributed to a percolation conduction process in the nanocomposites. For particle loadings of 1%, the low frequency response of the nanocomposites resembled the response of microcomposites and base resin. The conclusion was drawn that “changes engineered by the nanomaterials require loadings greater than a few percent”.

In more recent years, more attention was paid to the dispersion of nano particles in the host matrix. Also it became evident that the dispersion needs to be checked by means of for instance TEM.

Ambid et al. (2004) studied nanocomposites obtained from polypropylene and orhanophilic layered silicate (clay). The addition of nanoparticles to two different types of polypropolene resulted in a clear relaxation peak which was absent in the base polymer. The relaxation peak shifted to higher frequencies when the temperature was increased. It was put forward that this relaxation was linked either to the interfaces between nanoparticles and

the polymer matrix or to the filler itself.

In 2007 Roy et al. (2007) showed the effect of surface modification on the dielectric spectrum of polyethylene-SiO_2 composites. The nanosilica was either untreated, or surface modified using triethoxyvinylsilane (TES), *n*-(2-aminoethyl) 3-aminopropyl-trimethoxysilane (AEAPS), or hexamethyldisilazane (HMDS). The latter two are of a polar nature, thus creating an incompatible interface with the XLPE. Treatment with TES results in a real part of the permittivity being lower than for the base XLPE, while AEAPS and HMDS lead to significantly larger values for the permittivity. The tan delta at low frequencies however is lower for AEAPS and HMDS than for TES or for the base XLPE. The broad loss peak that appears for the micron size composites is absent in the nanocomposites. This was attributed to a confinement of the polymer reducing chain movement. Untreated nanoparticles show a strong increase in losses at low frequencies which was assumed to be caused by percolation conduction or quasi-dc conduction.

Hallouet et al. (2009) investigated epoxy resin based composites with dispersed magnetite nano-particles (Fe_3O_4) with diameters between 20 and 30 nm and micro-particles with diameters between 0.5 and 5 µm. Temperature dependent DS between 50 Hz and 1 GHz showed that neither the micro-particles nor the nano-particles affected the molecular dynamics. An important result was that the intrinsic relaxation strength of the matrix polymer in the nano-composites increased, proportional to the volume fraction of particles. In the micro-composites there was no such effect. A tentative explanation was given based on the total area of interfaces in the composite.

3.2.3. Reduction of the real part of the permittivity

Imai et al. (2002) were probably the first to notice a decrease of the real part of the permittivity in nanocomposites, although the layered silicate filler had a higher permittivity than the base epoxy resin.

Most authors agree that the reduction of the real part of the permittivity is due to the interaction between nanoparticles and host polymer, resulting in a reduced mobility of polymer chains. This is true for smaller filler fractions while for larger filler fractions (roughly > 5%), the effect of the high bulk permittivity of the nanofiller becomes more important in determining the permittivity of the composite

In 2004 Fothergill et al. (2004) presented the results of a study in which three different types of nanoparticles, TiO_3, Al_2O_3 and ZnO, were compared. Again, a Bisphenol A epoxy resin was used. A remarkable finding was the fact that the nanocomposites exhibited a real value of the permittivity that was smaller than that of the base resin. The microcomposite showed a higher value of the real value of the permittivity than the nanocomposite and the base resin which was attributed to interfacial polarization. No rules of mixtures could explain this finding. Again, for the low frequencies, a flat tan delta response was found for the nanocomposites, which was explained by assuming percolation conduction. A similar behavior was again reported by Nelson et al (2005) in a paper that presents a.o. DS results at very low frequencies for TiO_2 – epoxy nanocomposites and microcomposites with 10% filler. The nanocomposites showed a noticable dispersion in the mid-frequency range, in contrast to the microcomposites.

Singha et al. (2008) also studied TiO_3, Al_2O_3 and ZnO epoxy nanocomposites and confirmed the reduction of the real part of the permittivity for low filler fractions below 5%. Kochetov et al (2009) studied boron nitride (BN) and aluminum nitride (AlN) epoxy nanocomposites and found a decrease of the real part of the permittivity for filler fractions below 5% for BN and below 2% for AlN.

3.2.4. The effect of humidity on the dielectric spectrum

The presence of water or water shells in nanocomposites significantly affects the low frequency DS results. Zou et al (2008) showed that in “wet” epoxy resin nanocomposites with SiO_2 nanoparticles, the slopes of the real and imaginary part of the complex capacitance were parallel, indicating percolation conductivity or quasi-dc behavior. In the dry composites, the real part of the capacitance kept constant and there was no such relation. A “water shell” model was proposed to explain this behavior.

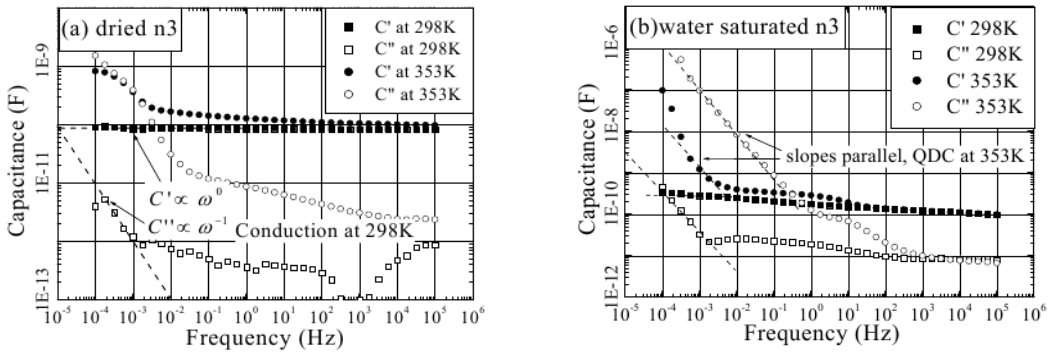

Figure 3.2.1 Complex capacitance of dried (left) and wet (right) silica nanocomposites, Zou et al (2008)

Zhang et al (2008) studied the dielectric response of polar (epoxy) and non-polar (polyethylene) nanocomposites. They compared DS of alumina-epoxy alumina-polyethylene nanocomposites before and after an extensive drying process. No difference was found between neat epoxy and the nanocomposite at dry condition. The responses are very different however when they had absorbed about 0.4% water. The polyethylene nanocomposites showed negligible differences before and after drying, which is attributed to the very low water absorption. The addition of nano-alumina leads to a dielectric loss peak in the low frequency region which moves to higher frequency with increasing nano-alumina content. It is suggested that the sites for absorbed water in the nanocomposites are very different to those in the pure polymer due to the large amount of interfaces in the former. This was confirmed by DS on the dry and wet nano-alumina powder.

Fréchette et al. (2009) also studied the effect water on the dielectric response of nanostructured epoxy microcomposites (60% weight percent micro quartz + 0.45% nanoclay) and reference microcomposites. Pre-treatment by heating the epoxy samples at a temperature of 160^{o}C under vacuum for 48 hours resulted in a significant decrease of the real and imaginary part of the permittivity of the nanostructured composites.

DS can be successfully used to determine the quality of nanocomposites. Huang et al. (2007) studied the electrical properties of polyethylene/aluminum nanocomposites. They recorded an increase of real and imaginary permittivity with filler content, up to a filler loading of 24%. Above 24%, both the real and imaginary permittivity decreased with filler loading. This was attributed to voiding from imperfect filler packing and solvent evaporation. The number of voids and pores was found to be considerably larger in samples with filler loadings above 24%.

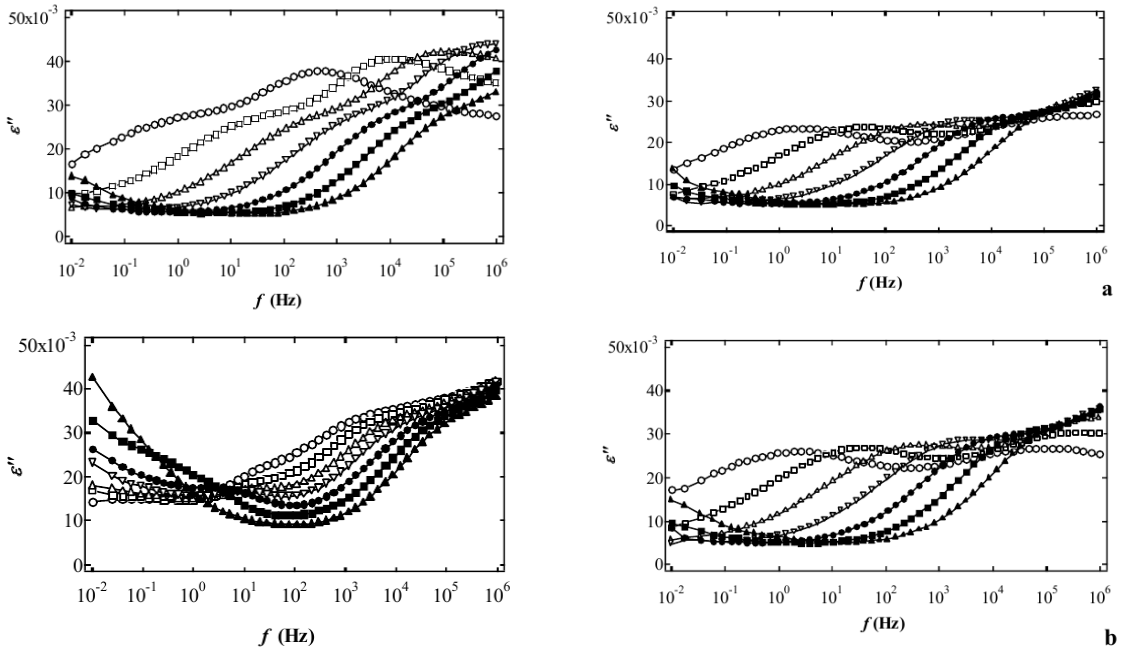

Figure 3.2.2 Frequency dependence of dielectric loss at -50, -30, -10, 10, 30, 50 and 70 ^{o}C. a) left: base epoxy, before drying; right: base epoxy, after drying. b) left: nanocomposite, before drying; right: nanocomposite, after drying. Zhang et al. (2008)

References

Ambid M, Mary D, Teyssedre G, Laurent C, Montanari GC, Kaempfer D, Mülhaupt R (2004) Effect of filler concentration on dielectric behaviour and on charge trapping in PP / clay nanocomposites. Annual Rept. IEEE-CEIDP: 389-392

Fothergill JC, Nelson JK, Fu M (2004) Dielectric properties of epoxy nanocomposites containing TiO_2, Al_2O_3 and ZnO fillers. Annual Rept. IEEE-CEIDP: 406-409

Fréchette MF, David E, Martinez HD, Savoie S (2009) Post-heat treatment effect on the dielectric response of epoxy samples. Annual Rept. IEEE-CEIDP: 705-708

Hallouet B, Desclaux P, Wetzel B, Schlarb AK, Pelster R (2009) Analysing dielectric interphases in composites containing nano- and micro-particles. J. Phys. D: Appl. Phys. 42: 1-10

Huang XY, Jiang PK, Kim CU (2007) Electrical properties of polyethylene / aluminum nanocomposites. Journal of Applied Physics 102: 124103

Imai T, Hirano Y, Hirai H, Kojima S, Shimizu T (2002) Preparation and properties of epoxy-organically modified layered silicate nanocomposites. Conference record IEEE ISEI: 379-383

Jonscher AK (1983) *Dielectric relaxation in solids*. London: Chelsea Dielectric Press

Kremer F (2003) *Broadband Dielectric Spectroscopy*. Berlin: Springer

Kochetov R, Andritsch T, Lafont U, Morshuis PHF, Picken SJ, Smit JJ (2009) Preparation and dielectric properties of epoxy – BN and epoxy –AlN nanocomposites. Proc. IEEE EIC: 397-400

Nelson JK et al (2002) Towards an understanding of nanometric dielectrics. Annual Rept. IEEE-CEIDP: 295-298

Nelson JK, Hu Y (2005) Nanocomposites dielectrics – properties and implications. J. Phys. D:Appl. Phys., 38: 213-222

Roy M, Nelson JK, MacCrone RK, Schadler LS (2007) Candidate mechanisms controlling the electrical characteristics of silica/XLPE nanodielectrics. Journal of Materials Science, 42-11: 3789-3799

Singha S, Thomas MJ (2008) Dielectric properties of epoxy nanocomposites. IEEE Trans. DEI 15-1:12-23

Zhang C, Stevens GC (2008) The dielectric response of polar and non-polar nanodielectrics. IEEE Trans. DEI 15-2: 606-617

Zou C, Fothergill JC, Rowe SW (2008) The effect of water absorption on the dielectric properties of epoxy nanocomposites. IEEE Trans. DEI 15-1:106-117

3.3. DC Conductivity at Low and High Field

It is well known that the relationship between current density, *J*, and electric field, *E*, is not linear for polymeric insulating materials in a wide range of electric field. At low field, where the injected charge is small, an ohmic behavior, $J=\sigma E$, is often observed, and the electrical conductivity, σ, is independent of *E*. At higher field, on the contrary, a strong dependence of σ on *E* is observed. Indeed, if the electric field applied to an insulation system is above the threshold for space charge accumulation, electronic charge injection from the electrodes becomes larger and larger and the electric field distribution may depart from the Laplacian field. It has been demonstrated that this threshold coincides with the onset of the space charge limited current (SCLC), (Dissado et al. 2005), which can be determined as the change of slope in the *J-E* characteristic (Fig. 3.3.1). Often the Schottky law is used to describe the injection mechanism at medium-high field (Dissado et al. 1992):

$$J = AT^2 \exp\left(-\frac{\Delta W - \beta_s \sqrt{E}}{kT}\right) \quad \beta_s = \sqrt{\frac{e^3}{4\pi\varepsilon}} \tag{3.3.1}$$

where *A* is a constant of the material, *k* is Boltzmann's constant, ΔW is the activation energy (injection barrier), and *e* is the electron charge.

The traditional framework of charge transport involves hopping between traps with charge mobility and conductivity limited by trap density and trap depth distribution: the deeper the traps the lower the mobility and, thus, the conductivity.

In addition to electronic charge injection, also ionic charges may play an important role in conduction mechanism. However it is quite hard to distinguish between electronic and ionic conduction mechanisms. In general, we can say that the latter may be prevalent at low field, where injection is small, and in materials including additives.

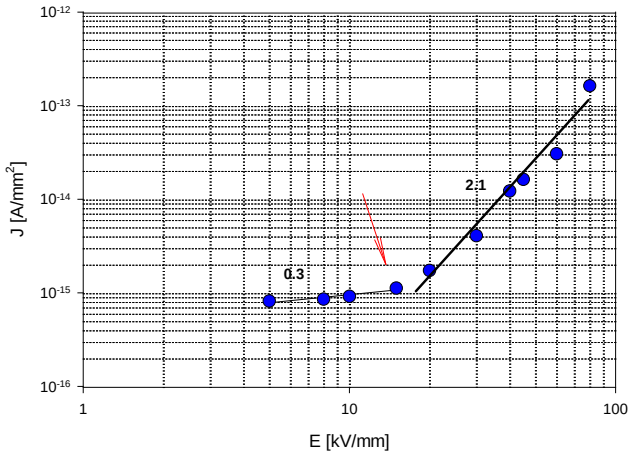

Figure 3.3.1 Current density vs. field for a polyethylene specimen. The onset field of SCLC is indicated by the arrow. The slopes of the interpolation lines are also reported.

DC conductivity can be evaluated by means of polarization current measurements, according to the following procedure. A given field is applied to the specimen and polarization current is monitored through an electrometer. The conduction current is measured after polarization is completed, i.e. when the current reaches the steady state. Current density can be calculated known the specimen geometry and the J-E characteristic can be plotted (Fig. 3.3.1) by performing tests at different fields.

Conduction current depends largely on chemical/physical properties of the material, e.g. morphology,

microstructure, crystallinity. In particular, conduction current of nanostructured materials can be larger/smaller than that of the base material, depending on the kind and concentration of the nanoadditive dispersed in the matrix, the cleanness, the compatibilization treatments, and the presence of water. Table 3.3.1 summarizes the main results shown in literature and obtained with different combinations of host/nanoadditive materials.

Table 3.3.1: Summary of the main conductivity results on nanocomposite insulating materials from literature.

Host material	Nanofiller	Results
Polyamide	SiO_2	conductivity decreases with nanofiller density increase at high temperature and low field. At lower temperature large nanofiller density lead to an increase of conductivity, particularly at high field (Cao et al. 2004)
PP and EVA	layered silicates	conductivity increases at high field (> 30 kV/mm) at room field, particularly for EVA (effect of moisture absorbed by the nanofiller) (Montanari, Fabiani et al. 2004)
Epoxy	TiO_2, Al_2O_3, ZnO	conductivity increase for small filler density (<2%) due to increased ionic conduction in the epoxy matrix (Singha et al. 2008)
Epoxy	layered silicate	conductivity decrease at low field (< 10 kV/mm), and high temperature (>60°C) with nanofiller density increase (Frechette et a.l 2008)
LDPE	MgO	increasing MgO density conductivity decreases largely (Chakradhar et al. 2008)
LDPE	MgO	conductivity decreases as nanofiller density increases up to 4% (Murakami et al. 2008)

The results reported in Table 3.3.1 show that the addition of nanofillers is able to modify significantly conduction current of the host material, affecting both charge injection and transport mechanisms. On one hand, indeed, the presence of the nanoadditive at the electrode/insulation interface can increase/decrease the injection barrier ΔW, affecting injection current, see equation (3.3.1). On the other hand, the nanofiller can alter trap distribution (in number and depth), affecting the transport current. The overall effect of the nanofiller on conduction current is, obviously, obtained as a balance of injection and transport mechanism, depending not only on the nanofiller concentration, but also on the electric field and temperature. For instance, the addition of nanofillers introducing deep traps or increasing the injection barrier lead to a nanocomposite material showing lower conductivity than the base material.

DC conductivity can be affected significantly by several factors during material manufacturing. For instance, contaminants left by the filler compatibilization process can increase noticeably electrical conductivity of a nanostructured material with respect to the base material, due to the introduction of extra ionic species in the matrix.

Intense washing treatments can reduce the presence of contaminants for those materials that need a compatibilization process (Montanari, Cavallini et al. 2004), but this makes more complex and expensive material manufacturing.

Another kind of material contamination which can increase remarkably conduction current is relevant to the water absorbed by hydrophilic nanofillers (e.g. silica and nanoclays) that can form a thin shell around the particle if the fillers are not properly dried before manufacturing the final nanocomposite (Chen et al. 2008), (Fabiani et al. 2009). Moreover, different nanofiller shapes give rise to different modifications of the conductivity process of the nanocomposite, and relatively small amounts of adsorbed water can affect in radically different ways the final

nanocomposite performances, particularly in relation with the filler aspect ratio. This is shown in Fig. 3.3.2 (Fabiani et al. 2009), where the conduction currents for two different nanoclays, namely boehmite and fluorohectorite, before (wet) and after (dry) an intense drying treatment to remove water molecules attracted by the nanoparticles, are reported. The aspect ratio of boehmite and fluorohectorite is 1 and >100, respectively. An increase of conduction current can be observed for the 'wet' specimens with respect to the 'dry' ones, particularly for the fluorohectorite specimens (almost 2 orders of magnitude). This can be explained considering that in the case of boehmite, which has particles with low aspect ratio, the formation of a thin shell of water around the filler particles does not modify significantly the conduction properties of the composite, because the thickness of the shell is much smaller than the average distance among the particles and the formation of percolation paths on a large scale is very unlikely. On the contrary, for fillers with high aspect ratio, such as the layered silicates (e.g., fluorohectorite), when a critical amount of water is adsorbed and accumulated around the particles, percolation paths are formed, leading to an increase of the conductivity of the specimens and of the loss factor. In this case, a drastic reduction of dielectric strength is also observed (Fabiani et al. 2009).

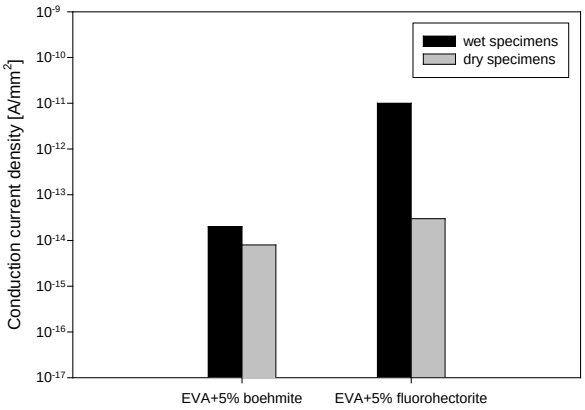

Figure 3.3.2 Steady state conduction current for wet and dry nanocomposite specimens. Electric field = 10 kV/mm (Fabiani et al. 2009).

Concluding, nanocomposite materials having tailored dielectric properties, e.g. a given electrical conductivity, can be realized provided that manufacturing process does not introduce contaminants that can lead to unexpected values of the material properties.

References

Cao Y, Irwin PC and Younsi K (2004) The future of nanodielectrics in the electrical power industry. Trans. IEEE DEI-11:797-807.

Chakradhar C and Ramu TS (2008) Polymer nanocomposites as insulation for HV DC cables - Investigations on the thermal breakdown. Trans. IEEE DEI-15:221-227.

Chen Z, Fothergill JC and Rowe SW (2008) The effect of water absorption on the dielectric properties of epoxy nanocomposites. Trans. IEEE DEI-15:106-117.

Dissado LA and Fothergill JC (1992) Electrical degradation and breakdown in polymers. Peter Peregrinus, London, U.K.

Dissado LA, Laurent C, Montanari GC et al (2005) Demonstrating a threshold for trapped space charge accumulation in solid dielectrics under DC field. Trans. IEEE DEI-12:612-620.

Fabiani D, Montanari GC and Testa L (2009) Effect of Aspect Ratio and Water Contamination on the Electric Properties of Nanostructured Insulating Materials", accepted for publication on Trans. IEEE DEI.

Frechette MF, Larocque RY, Trudeau M et al (2008) Nanostructured polymer microcomposites: A distinct class of insulating materials. Trans. IEEE DEI-15:90-105.

Montanari GC, Cavallini A, Guastavino F et al (2004) Microscopic and nanoscopic EVA composite investigation: Electrical properties and effect of purification treatment. Proc. IEEE-CEIDP:318-321.

Montanari GC, Fabiani D, Palmieri F et al (2004) Modification of electrical properties and performance of EVA and PP insulation through nanostructuration by organophilic silicates. Trans. IEEE DEI-11:754-762.

Murakami Y, Nemoto M, Okuzumi S et al (2008) DC conduction and electrical breakdown of MgO/LDPE nanocomposite. Trans. IEEE DEI-15:33-39.

Singha S and Thomas MJ (2008) Dielectric properties of epoxy nanocomposites. Trans. IEEE DEI-15:12-23.

3.4. Space Charge Measurement

3.4.1. PEA & PWP Measurements

3.4.1.1. What can we find using space charge measurement techniques

Space charge accumulates in insulating material when an electric high field is applied to the material. Since the accumulation of the space charge distorts the electric field distribution in the material, a breakdown sometimes occurs at a lower applied average electric field than its intrinsic dielectric strength. Figure 3.4.1 shows a typical example of the breakdown in low-density polyethylene (LDPE) as a result of distortion electric field by space charge accumulation (Matsui *et al.* 2005). The thickness of LDPE is *ca* 150 μm and the applied average electric field is about 330 kV/mm. The result is obtained using the pulsed electro-acoustic (PEA) method. It is found that a so-called packet-like charge, which was firstly observed by Hozumi *et al.* (1994), is injected from anode and it moves towards cathode side with increasing its amount of charge. Consequently, the electric field near cathode gradually increases and finally the breakdown is observed. When the breakdown occurred, the largest electric field in the sample was more than 500 kV/mm. Matsui *et al.* (2008) also gave a numerical analysis for this phenomenon.

Furthermore, the space charge sometimes shows the predictive information about degradation of insulating material. Figure 3.4.2 shows a typical example that the space charge accumulation may show the degradation of the material (Kishi *et al.* 2009). In this figure, the average dc electric field of 150 kV/mm is applied to a commercially available polyimide film of 125 μm thick at 80 ˚C. It is found that so-called hetero space charges are observed near electrodes before breakdown. When the breakdown occurs in this sample, the hetero space charges are always observed. Therefore, the hetero space charge may be used as the predictive information for breakdown.

As mentioned above, since the space charge measurement provide us some useful information about performance of insulating materials under high electric field, many researchers have still improved the measurement systems.

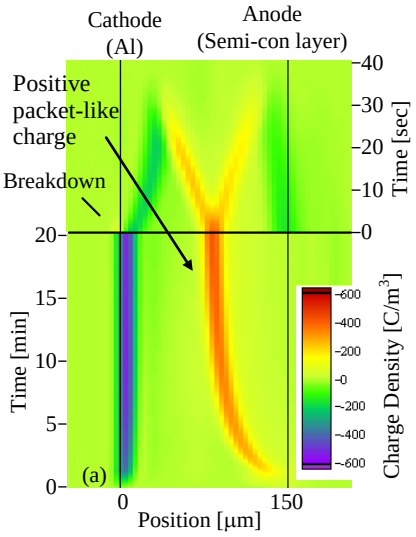

Figure 3.4.1 Typical example of time dependent space charge distribution in LDPE under applied dc electric field of 330 kV/mm including breakdown (Matsui *et al.* 2005).

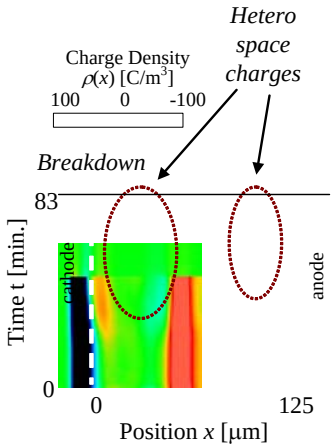

Figure 3.4.2 Typical example of time dependent space charge distribution in polyimide film under applied dc electric field of 150 kV/mm at 80 ˚C including breakdown (Kishi *et al.* 2009).

3.4.1.2. Typical measurement technique using acoustic wave propagation.

Many complicated measurement results about conduction and breakdown in dielectric materials under high dc electric field were expected due to existence of space charge accumulation (Bradwell *et al*.1971). However, when there was no effective observation technique for space charge distribution, it was difficult to show obvious result for the relationship between the space charge accumulation and these phenomena. About 20 years ago, some effective observation techniques for space charge distribution had been developed. Some of them are measurements using thermal wave propagation and others are those using acoustic wave propagation. Later techniques are classifiable as two major types. One is so called PWP (Pressure wave propagation) and another is PEA (Pulsed electro-acoustic) methods. Here, the brief principles of the two methods are introduced.

PWP method

PWP method is based on the displacement current measurement through the external circuit connected to a sample including the space charge in the bulk when the acoustic wave is traveling through the sample. Figure 3.4.3 (a) and (b) show schematic diagrams of the principle of PWP method. In these methods, a pulsive acoustic wave generated by acoustic source propagates through the sample. Since the pulsive acoustic wave is a compressed or an expanded layer of the material, the distance between space charge layer and electrode is slightly changed when it is propagates in the sample. The change of the distance between electrodes and the charged layer induces the displacement current in the external circuit connected to the electrodes. The amplitude and the timing of the measurement current depend on the amount of accumulated charge and position of the pulsive acoustic wave, respectively. Therefore, we can measure the space charge distribution by measuring the time sequential external current (Takada *et al* 1998).

The PWP methods are classified by the method how to generate the pulsive acoustic wave. The LIPP (Laser induced pressure wave propagation) is one of major PWP method (Laurenceau *et al.* 1977, Sessler *et al.*1982). In this method, the pulsive acoustic wave is generated by irradiation of strong laser pulse to a target put on the sample as shown in Figure 3.4.3(a). The target is heated rapidly by the laser irradiation, and a slight part of the target vapors. The reaction of the evaporation generates an acoustic wave. When the duration of the laser pulse is very short, we can have a very short acoustic pulse. Since the positional resolution of the PWP measurement depends on the pulse width of the propagating acoustic wave, the LIPP method is expected to obtain a high positional resolution.

On the other hand, there is a method using the pulsive acoustic wave generated from a piezoelectric-device. When a pulse voltage is applied to a piezoelectric-device, a pulsive acoustic wave generates as shown in Figure 3.4.3(b) (Eisenmenger and Haardt 1982). The intensity and duration of the pulsive acoustic wave from the piezoelectric-device are not so large either short compared with the laser induced one. However, it is easy to generate the acoustic pulses repeatedly and stably. Therefore, in this method, the averaging technique is available. By using the averaging technique, relatively sensitive measurement is carried out.

In the case of the PWP method, however, the sample is consisted in the measurement circuit as shown in Figure 3.4.3 (a) and (b). Therefore, the change of environments like temperature or electric field in the sample ~~is~~ strongly affects to the measurement results. For example, when the breakdown occurs in the sample under high stress, the amplifier must be broken. Therefore, it is necessary to be careful to observe such environment in this method.

PEA method

Figure 3.4.3 (c) shows a schematic diagram for Principle of PEA method (Takada *et al.* 1998). This method is a symmetrical technique to PWP method as shown in Figure 3.4.3. In this method, the acoustic wave is used as a signal, while it is used as exiting source for displacement current signal in PWP. When a relatively high voltage pulse is applied to the sample including accumulated space charge, the charge layer is forced by the pulse electric field in the bulk. The force generates an acoustic wave, and then it propagates in the sample. When the acoustic wave reach at the piezoelectric device put behind the electrode, it is converted into voltage signal. The amplitude of the acoustic wave is proportional to the charge density, and the delay of traveling time through the sample is proportional to the position of the charge. Therefore, we can measure the charge density distribution in the sample by measuring the time sequence of acoustic wave amplitude.

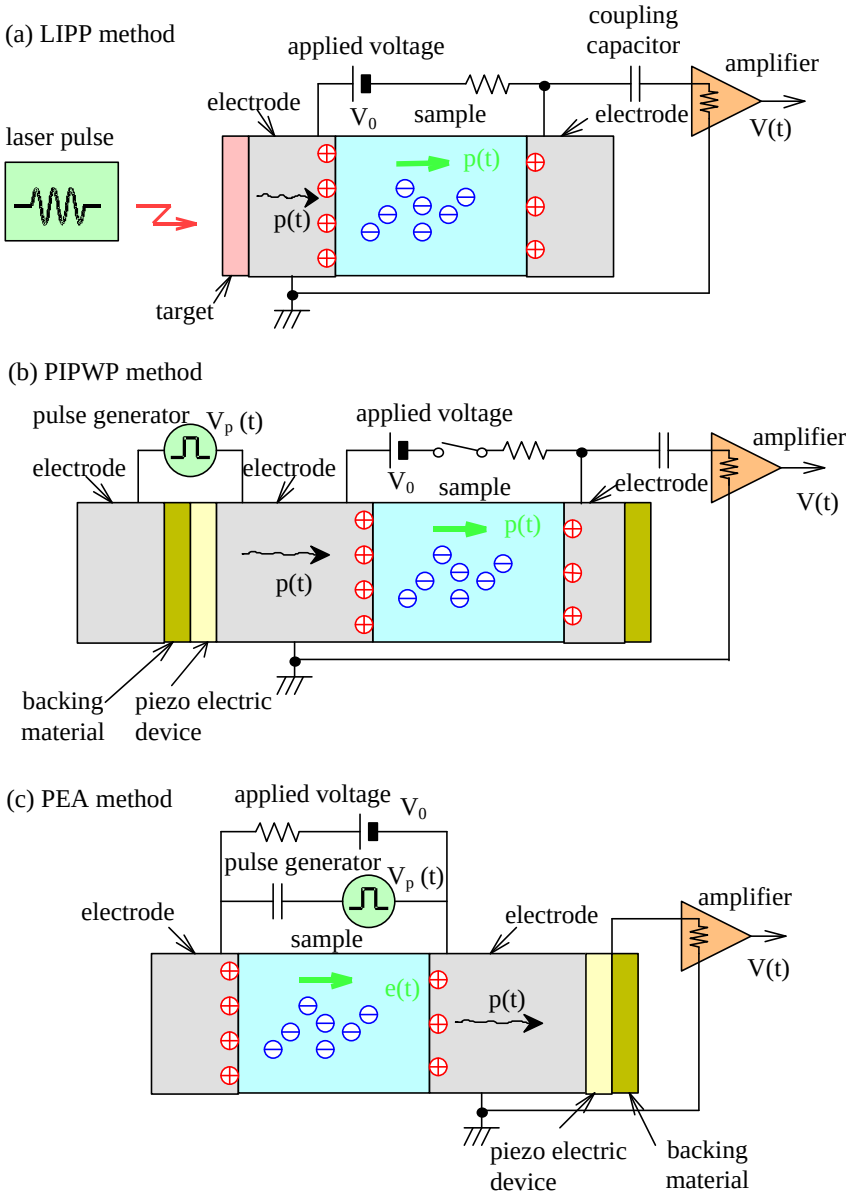

Figure 3.4.3 Schematic diagrams of measurement principles for (a) LIPP, (b) PIPWP and (c) PEA methods.

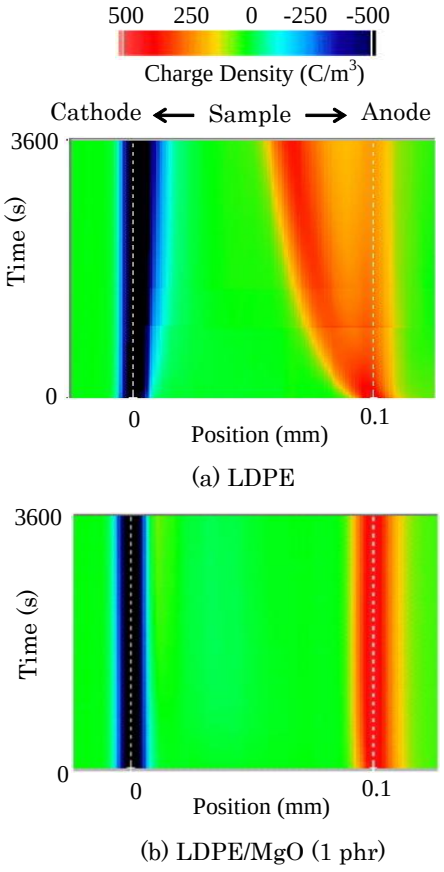

Figure 3.4.4 Time dependent space charge behavior in (a) LDPE and (c) LDPE/MgO (Hayase *et al.* 2006)

In the PEA system, since the piezoelectric sensor is put in the grounded shield box, the measurement is not affected by the environment of the sample. Therefore, the system is available even under high electric field near breakdown of the sample or at high temperature. Actually, many measurement results obtained under very sever conditions have been reported. In other words, the PEA system is an effective tool to understand the dielectric properties under accelerated test condition.

Measurement example of PEA method applied to nano-composite materials

Some measurement results obtained using PEA method on nano-composite materials have reported. In the case of nano-composite samples based on low density polyethylene (LDPE), they have reported the enhancement of charge injection by adding nano-filler to the base materials under relatively low dc electric field (Smith *et al* 2008, Chen *et al* 2007, Yin *et al* 2006). However, Hayase *et al.* (2006) and Murakami *et al* (2008) have reported that a nano-composite material shows a good resistance to accumulate space charge under relatively high electric field. Figure 3.4.4 shows a typical measurement result. The sample is a nano-composite material (LDPE/MgO) consisted of low density polyethylene (LDPE) with nano-size filler of Magnesium oxide (MgO). The LDPE/MgO has been reported that it shows high breakdown strength under high dc stress (Murata *et al.* 2005). As shown in Fig. 3.4.4(a), the packet-like charge is observed in LDPE under high dc stress and it sometimes leads to breakdown as shown in Fig. 3.4.1. However, as shown in Fig. 3.4.4(b), the sample including the MgO nano-filler shows no such packet like charge even under high dc stress. It is thought that the disappearance of packet-like charge by adding MgO nano-filler to LDPE is one of reasons why the LDPE/MgO shows the good performance under high dc stress. As to the reason why the packet-like charge is not generated in LDPE/MgO, it is expected that the MgO filler plays a role of trap site for the injected charges (Hayase *et al.* 2009). As mentioned above, PWP and PEA methods are useful tools to evaluate the performance of nano-composite materials as insulating materials.

3.4.2. Thermal Step Method

This section deals with space charge measurements dedicated to the characterization of epoxy nanocomposites (nanostructured microcomposite epoxies). Space charge measurements have been performed by using the Thermal Step Method (TSM) on samples with and without nanoparticles. By this way, a comparison of the behavior of each material has been highlighted regarding their ability to accumulate or to flow the space charges. Experiments have been performed by varying several poling parameters like temperature, electric field and time (ageing).

• Measurements were carried out after having maintained the samples during 30 minutes in short-circuit condition after each electrical poling;

• The cathode (ground electrode) is at the left on all the space charge distributions.

3.4.2.1. Space charge vs. poling temperature

The following results are showing the influence of the poling temperature on space charge accumulation on samples with and without nanoclays: respectively called EPON7A or EPON7B for samples with nanoclays and EPO8 or EPO9 for samples without nanoclays. The experimental results presented hereafter were obtained according to the following process:

• Space charge measurements after dc poling (5 kV, 60°C and 120°C, 1 hour) for EPON7A and EPO9 samples;

• Space charge measurements after dc poling (10 kV, 60°C and 120°C, 1 hour) for EPON7B and EPO8 samples;

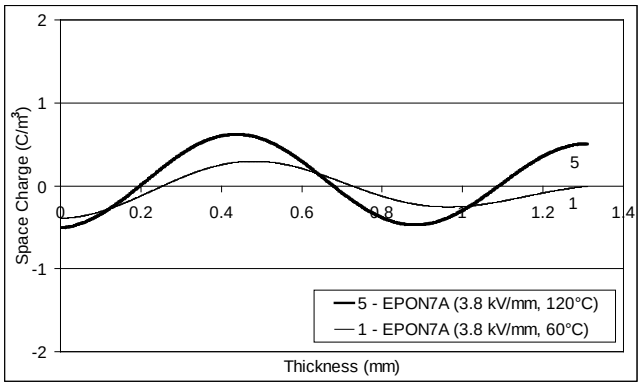

Figure 3.4.5 Space charge profiles on sample with nanoclays EPON7A

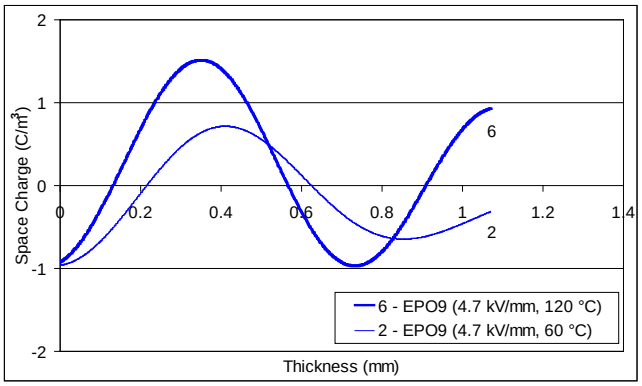

Figure 3.4.6 Space charge profiles on sample without nanoclays EPO9

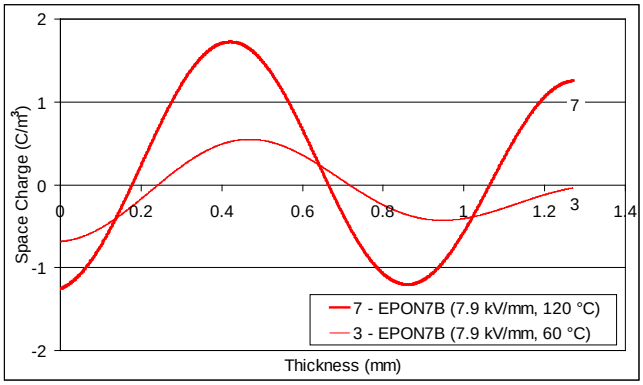

Figure 3.4.7 Space charge profiles on sample with nanoclays EPON7B

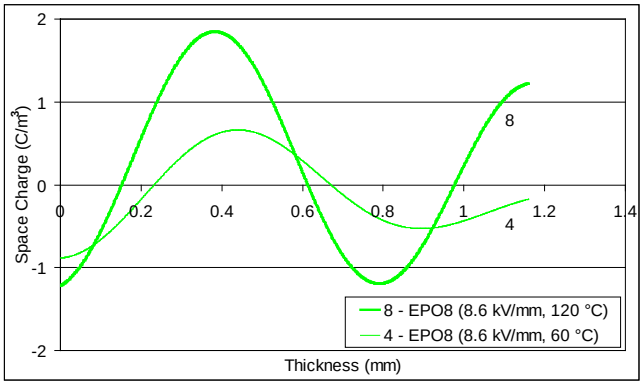

Figure 3.4.8 Space charge profiles on sample without nanoclays EPO8

All the space charge profiles reveal the presence of homocharges close to the cathode whatever conditioning conditions. In addition, we observe the presence of heterocharges close to the anode for the temperature of poling of 60°C and the presence of homocharges at the anode also with 120°C whatever the applied voltage of poling. All the samples accumulate more space charges for 120°C than for 60°C. We can note that for the "weaker" poling electric fields (Figures 3.4.5 and 3.4.6), sample EPON7A with nano clays stores less space charge than sample EPO9 without nano clays. On the other hand, for the "stronger" poling electric fields (Figures 3.4.7 and 3.4.8) the levels and the profiles of space charges obtained on samples EPON7B and EPO8 with and without nano clays appear similar. The effect of the poling electric field seems to be much more significant on the samples with nano clays than on those without nano clays. The following paragraph deals with space charge measurements performed after increasing the poling electric field up to 32.7 kV/mm and demonstrate an increasing in the differences between the samples for higher applied electric field (Frechette et al. 2009).

3.4.2.2. Space charge vs. applied electric field

Space charge measurements were performed on samples with and without nanofiller in order to compare their ability to accumulate and / or to flow space charges when they are submitted to applied voltages between 10 kV and 35 kV at 60 °C during 17 hours. These applied voltages correspond to applied electric fields from 7.6 kV / mm to 32.7 kV / mm.

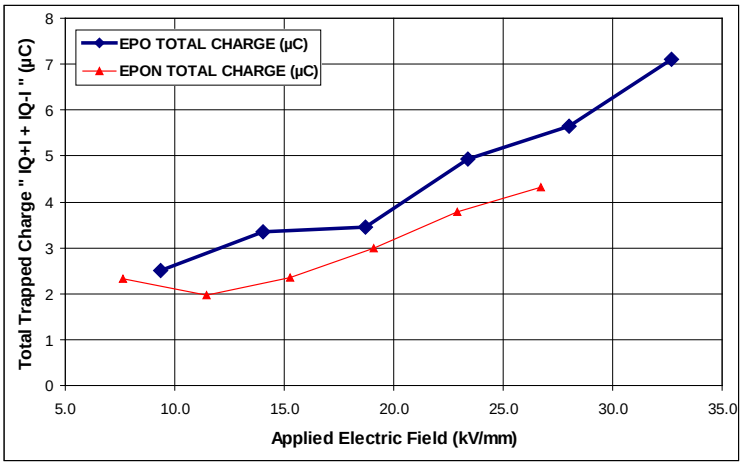

Figure 3.4.9 Evolution of the total trapped charge Abs(Q+) + Abs(Q-) versus Applied Electric Field

Figure 3.4.9 shows the evolution of the total quantity of trapped charge in each sample (sum of absolute values of the total positive and negative charge) versus applied electric field. For "weak" applied electric fields, it appears little differences in space charge levels between the sample with and without nano fillers. However, the nano-filled sample presents lower space charge levels.

The differing levels of space charges, between the two types of samples, are more pronounced with a "strong" applied electric field than a "low" applied field. Whatever, the value of applied electric field, space charge distributions exhibit homocharges close to the electrodes representative of a charge injection phenomenon.

The results show an increase in the level of total trapped charge with an increase in the applied electric field for both samples (Castellon et al. 2008). Note that this trapped charge is representative of a health of the material. However, the increase in the level of space charges seems to be limited in the case of nanofilled sample. Two explanations are possible: either this sample stores less space charge (less defects), or the space charge flow is more pronounced. Indeed, it is known, in the case of nanocomposite materials, electric fields nearby nanoparticles, because of the nano filler shape, can be strong and start volume conduction phenomena that facilitate the flow of space charges.

3.4.2.3. Space charge vs. ageing time

The space charge measurements were performed on samples with and without nano fillers in order to measure the evolution of charges trapped in the insulation during ageing.

The applied experimental protocol corresponds to an electrical ageing up to 1611 hours under 15 kV/mm at 60°C then under 20 kV/mm between 1611 hours and 1927 hours;

The first remark is concerned with the levels of the trapped charge: in both cases (positive and negative charge), the sample with nano clays exhibits the lowest level of trapped charge. This means that the nano fillers have a beneficial effect in regard with space charge accumulation vs. ageing (Castellon et al. 2009).

Then, we can observe stronger oscillations on the trapped charge of the sample without nano clays. This could be explained by considering that the sample must reach a significant level of local electric field before starting the flow of charge. As against in presence of nano fillers the flow of charges starts for lowest electric field levels. For

information, after 954 hours, the local electric field of the EPO sample can reach 26 kV/mm. These strong oscillations can result in the long term by a premature ageing of the material. We can observe also a higher level of negative trapped charges; this is due to a dominant injection of electrons during the ageing.

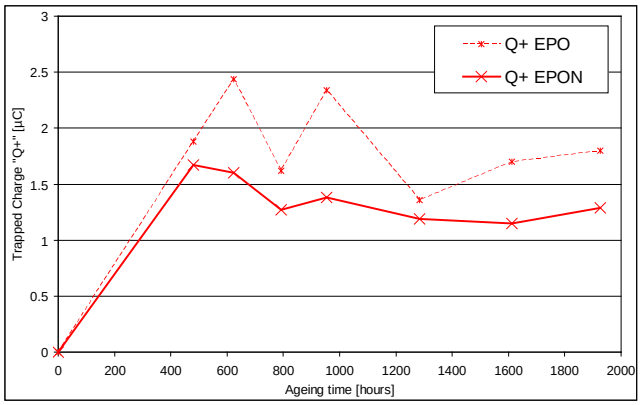

Figure 3.4.10 Evolution of the positive trapped charge versus ageing duration

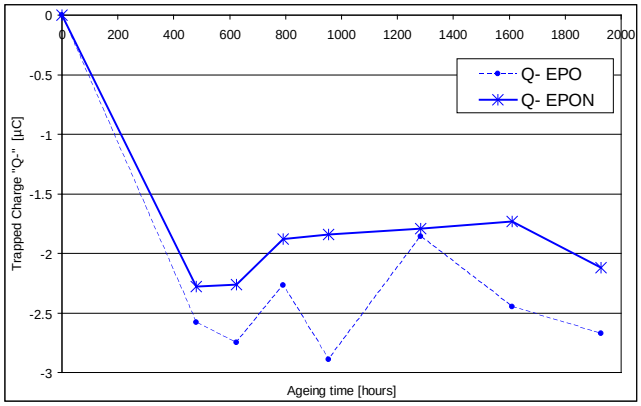

Figure 3.4.11 Evolution of the negative trapped charge versus ageing duration

Figures 3.4.10 and 3.4.11 exhibit a linear extrapolation between 0 and 480 hours of ageing, so it is not probably the real evolution of the trapped charges. This means that the sample has initial defects probably due to the manufacturing process but these defects (assimilated to traps) are empty of space charge. By applying an electric field during a short time, we tend to fill these defects relatively quickly.

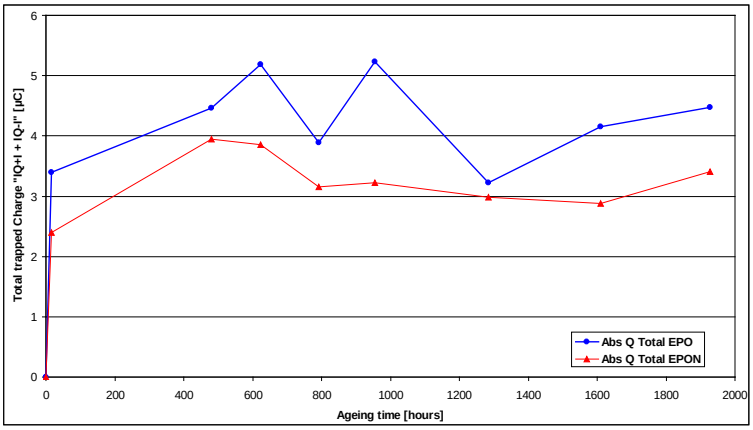

Figure 3.4.12 Evolution of the total trapped charge Abs(Q+) + Abs(Q-) versus Ageing duration

Figure 3.4.12 shows the evolution of the total quantity of trapped charge (Abs(Q+) + Abs(Q-)) observed in Figure 3.4.2.6 and 3.4.2.7 versus ageing time including the value of total trapped charge obtain in Fig. 5 for 15 kV/mm at 60°C during 17 hours. Finally, between 1611 and 1927 hours, we observe an increase of the trapped charge due to the increasing of the applied electric field (from 15kV/mm up to 20 kV/mm).

The evolution of the total trapped charge tends to decrease in ageing time; this means that we did not create new defects during ageing. Consequently, we cannot talk about ageing, considering ageing as an irreversible change of the material properties.

References

Bradwell A, Cooper R and Varlow B (1971) Conduction in polyethylene with strong electric field and the effect of prestressing on the electric strength. Proc. IEE., Vol. 28, pp. 247-254

Castellon J, Agnel S, A. Toureille A et al (2008) Space Charge Characterization of multi-stressed microcomposite nano-filled epoxy for Electrotechnical Applications, Proc. IEEE-CEIDP.

Castellon J, Nguyen HN, Agnel S et al (2009) Electrical and thermal ageing of microcomposite nano-filled epoxy: influence on space charge accumulation, Proc. IEEE-CEIDP.

Chen G, Zhang C and Stevens G (2007) Space Charge in LLDPE Loaded with Nanoparticles. Annual Rep. 2007 CEIDP, pp.275-278

Eisenmenger W and Haardt M (1982) Observation of Charge Compensated Polarization Zones in PVDF Film by Piezoelectric Acoustic Step Wave Response. Solid. State. Commun., Vol.41, pp917-920

Fréchette M, Larocque RY, Trudeau M et al (2008) Nanostructured polymer microcomposites : a distinctive class of insulating materials, Trans. IEEE-DEI-15-1:90-105.

Hayase Y, Tanaka Y, Takada T, Murata Y, Sekiguchi Y and Reddy CC (2009) Space Charge Suppression Effect of Nano-size Filler Added in Polymeric Materials. 2009 Dielectric meeting, Reading University, UK, (Journal of Physics: Conference Series (to be published.))

Hayase Y, Aoyama H, Matsui K, Tanaka Y, Takada T and Murata Y (2006) Space Charge Formation in LDPE/MgO Nano-composite Film under Ultra-high DC Electric Stress. IEEJ Trans. FM, Vol. 126, No. 11, pp. 1084 – 1089

Hozumi N, Suzuki H, Okamoto T, Watanabe K, Watanabe A (1994) Direct observation of time-dependent space charge profiles in XLPE cable under high electric fields. IEEE Trans. DEI, Vol. 1, No. 6, pp. 1068-1076

Kishi Y, Hashimoto T, Miyake H, Tanaka Y and Takada T (2009) Breakdown and Space Charge Formation in Polyimide Film under DC High Stress at Various Temperatures. 2009 Dielectric meeting, Reading University, UK, (Journal of Physics: Conference Series, Vol. 183, 012005, 2009)

Laurenceau P, Dreyfus G and Lewiner J (1977) New Principle for the Determination of Potential Distribution in Dielectrics. Phys. Rev. Lett. Vol. 38, No. 1, pp. 46-49

Murakami Y, Nemoto N, Okuzumi S, Masuda S, Nagao M, Hozumi N, Sekiguchi Y and Murata Y (2008) DC Conduction and Electrical Breakdown of MgO/LDPE Nanocomposite. IEEE Trans. DEI, Vol. 15, No. 1, pp.33 – 39

Murata Y, Sekiguchi Y, Inoue Y and Kanaoka M (2005) Investigation of Electrical phenomena of Inorganic-filler/LDPE Nanocomposite Material. Proc. 2005 International Symposium on Electrical Insulating Materials, pp.650-653

Matsui K, Tanaka Y, Takada T, Fukao T, Fukunaga K, Maeno T and Alison JM (2005) Space Charge Behavior in Low-density Polyethylene at Pre-breakdown. IEEE Trans. DEI, Vol. 12, No. 3, pp. 406-415

Matsui K, Tanaka Y, Takada T and Maeno T (2008) Numerical Analysis of Packet-like Charge Behavior in Low-density Polyethylene under DC Electric Field. IEEE Trans. DEI, Vol. 15, No. 3, pp. 841 – 850

Takada T, Tanaka Y, Adachi N and Qin X (1998) Comparison Between the PEA Method and the PWP Method for Space Charge Measurement in Solid Dielectrics. IEEE Trans. DEI, Vol.5, No. 6, pp.944-951

Sessler GM, West JE, Gerhard G (1982) High Resolution Laser Pulse Method for Measuring Charge Distributions in Dielectrics. Phys. Rev. Lett., Vol.48, No.8, pp.563-566

Smith RC, Liang C, Landry M, Nelson JK and Schadler LS (2008) The Mechanisms Leading to the Useful Electrical Properties of Polymer Nanodielectrics. IEEE Trans. DEI, Vol. 15, No. 1, pp. 187-196

Yin Y, Dong X and Li Z (2006) Space Charge Distribution Behavior of Nano-SiOx and Low-density Polyethylene Composite. Proc. 8th ICPADM, Vol.1, pp. 77- 80

3.5. Dielectric Breakdown

The dielectric breakdown property gives an indication of the maximum voltage that an insulation material can sustain, i.e. its electrical performance or electrical endurance (O'Dwyer 1973, Coelho 1979, Tanaka et al. 1983, Dissado et a.l 1992). Generally, polymeric insulation exhibit an intrinsic breakdown strength up to 8 MV/cm at room temperature, but in practice this performance drops significantly of several MV/cm due to defects or impurities. In the long term, these latter will also contribute to partial discharge and treeing, reducing the electrical endurance of polymeric insulation. The expectation of nanoparticles as fillers is precisely to counterbalance or at least reduce the impact of these defects or impurities on their extrinsic short and long term electrical performance.

On the other hand, the dielectric breakdown voltage or strength measurement depends on the sample geometry and homogeneity, the shape of electrodes, the type of voltage [alternative (AC), direct current (DC), impulse], the laboratory, etc… Furthermore, the dielectric breakdown is mostly a statistical event, i.e. is not reproducible and has a range of values due to its extrinsic nature (presence of defects, voids, crystalline and amorphous regions, molecular length, impurities, etc…). Several studies have indeed demonstrated the benefits of nano.fillers on the dielectric breakdown of polymers. The type of nano.filler and/or if is treated or not may have a great influence on this electrical property. Because of the numerous polymer nanocomposites proposed on this subject, we will concentrate only on the most popular ones polyethylene and epoxy nanocomposites.

3.5.1 Polyethylene nanocomposites

AC breakdown

The use of nanofillers can improve the short and long terms electrical performance of low density polyethylene (LDPE). Guastavino et al. (2009) have demonstrated that the AC breakdown (ACBD) strength of LDPE increases roughly 25% by adding nano silicate clays such as montmorillonite (MMT) alone, and some 8% in combination with sepiolite (SEP), as shown in Fig. 3.5.1. In long term aging, the combination of the two nanofillers gives the best results compared when they are considered separately and this particularly to LDPE itself, as evidenced in Fig. 3.5.2. This improvement brought by the combination of two nanofillers, an increase of time to failure near four orders of magnitude, is explained in terms of different aspect ratio inside the same material: the MMT enhancing short term breakdown and the SEP acting positively on the homogeneity of the nanocomposite. Similar results were obtained by Roy et al (2005) with crosslinked polyethylene (XLPE) and nano silica and particularly the vinylsilane-treated one, which show an increase of more than two orders of magnitude. This significant improvement is attributed by the authors to the strong covalent bonding between the matrix and the nanofiller, reducing the formation of interfacial defects such as microvoids.

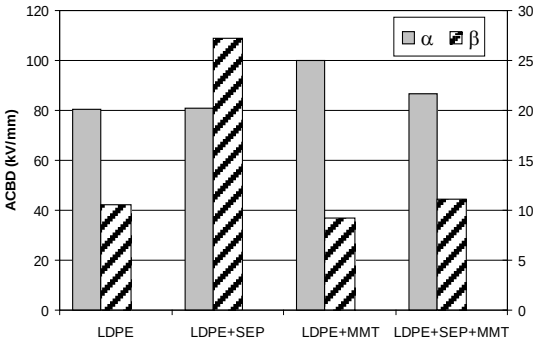

Figure 3.5.1 AC breakdown Weibull parameters ♋ and ♌ (right scale) for LDPE and nanocomposites

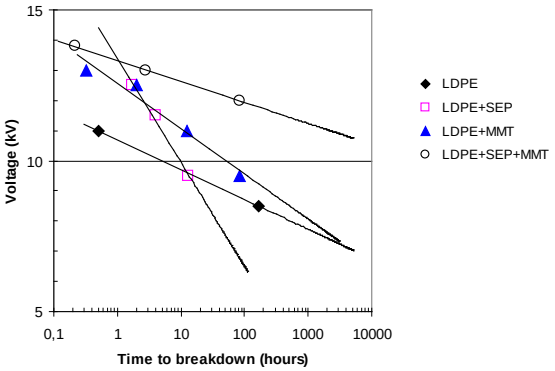

Figure 3.5.2 Voltage lifetime for LDPE and nanocomposites

DC and Impulse breakdown

Other nano fillers have been employed to improve the DC and impulse breakdown of LDPE. Okuzumi et al. (2008) using nano magnesium oxide (MgO) obtained increases of +32% and +19% respectively for DC and impulse BD strength, as indicated in Fig. 3.5.3. On the other hand, Ma et al. (2004) found a decrease of DCBD strength of nearly -38% with titania nano filler (TiO_2), but just -7% by drying the TiO_2 nanoparticles, and -18% modifying the surface of the TiO_2 nanoparticles with a silane coupling agent (AEAPS). The improvement obtained by drying the TiO_2/LDPE nanocomposite does not result just from the water removal, but this process has induced morphology and interface changes. The use of coated TiO_2 nanoparticles introduces at the interface polar groups that act as charge scattering centres or traps in the electrical process (Ma et al, 2005). The DCBD strength increase of MgO/LDPE nanocomposite, compared to bare LDPE, is also observed not only at room temperature (Murakami et al. 2008), but also at 60 and 90°C respectively reaching +13% and +22%, as shown in Fig. 3.5.4. The suppression effect of the conduction current determined by the space charge explains, by the authors, the greater DCBD strength at each temperature, the local field at the anode being reduced by the MgO nano filler under high electrical field.

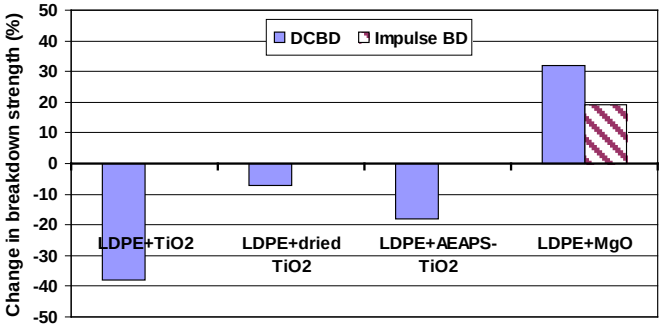

Figure 3.5.3 Change in DC and impulse breakdown for two nanocomposites LDPE compared to LDPE

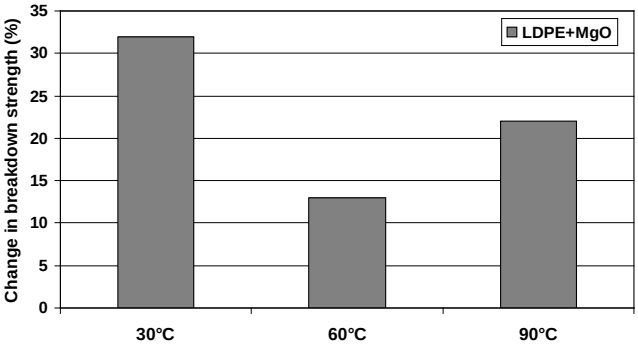

Figure 3.5.4 Change in DCBD strength MgO/LDPE nanocomposite compared to LDPE

3.5.2. Epoxy nanocomposites

Contrary to polyethylene, the electrical performance of epoxy can be enhanced with TiO_2 nano filler. Hu et al. (2006) have shown, Fig. 3.5.5, that the DC, AC and impulse breakdown strength of epoxy increase by 18, 9 and 2% respectively using nano TiO_2, but decrease in the same order by 10, 16 and 2% with micro TiO_2. The greater surface area of the nano filler and the improved dispersion method used (dual asymmetric centrifuge) have contributed indeed to these increases in breakdown characteristics. Although, Singha et al. (2006) observed rather a decrease for the ACBD strength of epoxy/TiO_2 micro and nano composites, they confirm the influence of the mixing or the importance of the nano filler dispersion in the epoxy matrix, as evidenced in Fig. 3.5.6 using ultrasonic and/or mechanical mixing. This difference in ACBD strength may come from the difference in sizes between the nano and micro TiO_2, they both use: on average respectively 40 nm and 0.5 µm for Singha et al. (2006), and roughly 23 nm and 1.5 µm for Hu et al. (2006). More recently, Singha et al. (2008 and 2009) obtained similar results with epoxy/Al_2O_3 and epoxy/ZnO nanocomposites, which have nano sizes around 45 and 65 nm respectively. Hence a much greater nano filler surface area together with proper mixing and dispersion in the polymer matrix appears to hinder the treeing and breakdown mechanisms improving thus electrical performance (Danikas et al. 2009).

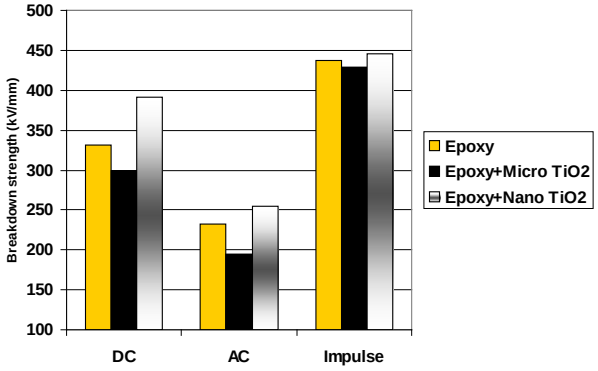

Figure 3.5.5 BD strength (Weibull scale parameter) of epoxy-TiO_2 formulations

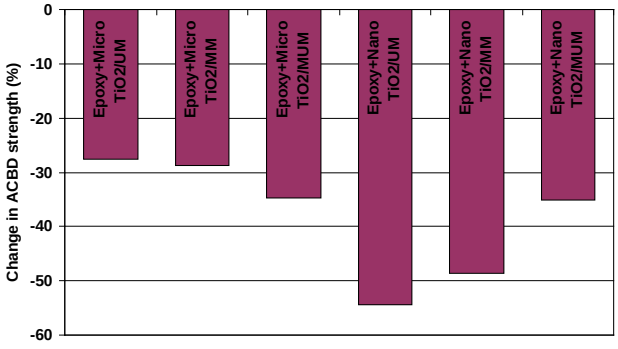

Figure 3.5.6 Change in ACBD strength of epoxy/ TiO_2 micro and nano composites compared to epoxy

The electrical performance of epoxy can be further improved with silicate (SiO_2) nano filler, particularly the long term performance. Fig. 3.5.7 gives the results obtained by Imai et al. (2005) showing an increase of the epoxy short term ACBD strength of 10, 14 and 22% by adding respectively nano layered SiO_2, micro SiO_2 or a mixture of them, and this relatively to base epoxy. The interpretation of these improvements is that the fillers, nano and/or micro, contribute to increase the branches of the electrical treeing delaying the breakdown failure, whereas with the base epoxy the tree propagation is relatively straight. This appears even clearer with the long term ACBD, shown on Fig. 5.3.8, with the same epoxy-SiO_2 formulations and also at three temperatures (Imai et al. 2006): a time to breakdown more than 800 and 80 times greater respectively at 20 and 145°C. Similar results were obtained by Iizuka et al. (2007) using Aerosil® nano silica leading to a time to breakdown almost 15 times greater compared to the base epoxy.

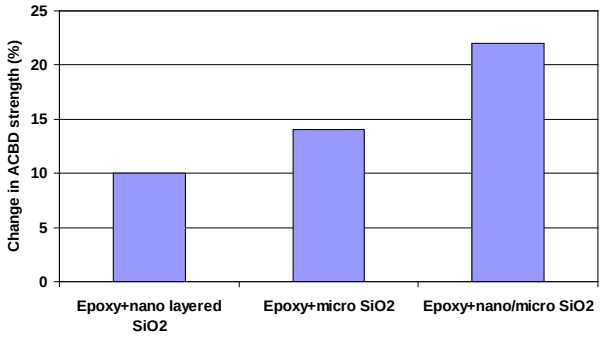

Figure 3.5.7 Change in ACBD strength of epoxy-SiO_2 formulations compared to epoxy

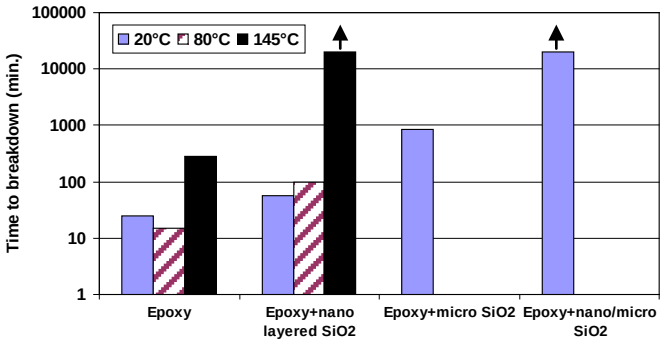

Figure 3.5.8 Time to breakdown (10 kV – 1 kHz) of epoxy-SiO_2 formulations at three temperatures; the arrows indicate no breakdown were obtained.

There is no doubt that nano fillers have a positive impact on the short and long term electrical performance of polymers. The type and size of nano fillers, their treatments or surface modification, the type of mixing and their dispersion in the matrix resin, etc… have however a major impact on this dielectric property. As it was well summarized by Danikas et a.l (2009) nanoparticles behave like barriers obstructing electrical failure path and delaying dielectric breakdown.

References

Coelho R (1979), *Physics of Dielectrics for the Engineer*, Elsevier Scientific Publishing Co..

Danikas M.G., Tanaka T. (2009) Nanocomposites – A review of electrical treeing and breakdown, IEEE Elect. Insul. Mag., Vol. 25, No. 4, 19-25.

Dissado LA, Fothergill JC (1992), *Electrical Degradation and Breakdown in Polymers*, Peter Peregrinus Ltd, Institution of Electrical Engineers.

Guastavino F, Dardano A, Squarcia S, Tiemblo P, Guzman J, Benito E, Garcia N (2009) Breakdown and electrical aging tests on different nanocomposite materials, Proc. Conf. IEEE-ISEI, 529-533.

Hu Y, Smith RC, Nelson JK, Schadler LS (2006) Some mechanistic understanding of the impulse strength of nanocomposites, Proc. IEEE-CEIDP: 31-34.

Iizuka T, Uchida K, Tanaka T (2007) Different voltage endurance characteristics of epoxy/silica nanocomposites prepared by two kinds of dispersion methods, Proc. IEEE-CEIDP: 236-239.

Imai T, Sawa F, Nakano T, Ozaki T, Shimizu T, Kuge S, Kozako M, Tanaka T (2005) Insulation Properties of nano- and micro-filler mixture composite, Proc. IEEE-CEIDP: 171-174.

Imai T, Sawa F, Ozaki T, Shimizu T, Kido R, Kozako M, Tanaka T (2006) Influence of temperature on mechanical and insulation properties of epoxy-layered silicate nanocomposite, IEEE Trans. DEI 13-1, 445-452.

O'Dwyer JJ (1973), *The Theory of Dielectric Breakdown in Solids*, Clarendon Press.

Okuzumi S, Murakami Y, Nagao M, Sekiguchi Y, Reddy CC, Murata Y (2008) DC breakdown strength and conduction current of MgO/LDPE composite influenced by filler size, Proc. IEEE-CEIDP: 722-725.

Ma D, Siegel RW, Hong JI, Schadler S, Mårtensson E, Önneby C (2004) Influence of nanoparticle surface on the electrical breakdown strength of nanoparticle-filled low-density polyethylene, J. Mater. Res., Vol. 19, No. 3, 857-863.

Ma D, Hugener TA, Siegel RW, Christerson A, Mårtenson E, Önneby C, Schadler LS (2005) Influence of nanoparticle surface modification on the electrical behaviour of polyethylene nanocomposites, Nanotechnology, 16, 724-731.

Murakami Y, Okazaki T, Okuzumi S, Nagao M, Sekiguchi Y, Reddy CC, Murata Y (2008) Temperature dependent space charge formation up to the breakdown under DC ramp voltage in MgO/LDPE nanocomposite, Proc. IEEE-CEIDP: 686-689.

Roy M, Nelson JK, MacCrone RK, Schadler LS, Reed CW, Keefe R, Zenger W (2005) Polymer nanocomposite dielectrics – The role of the interface, IEEE Trans. DEI 12- 4, 629-643.

Singha S, Thomas MJ (2006) Polymer composite/nanocomposite processing and its effect on the electrical properties, Proc. IEEE-CEIDP: 557-560.

Singha S, Thomas MJ (2008) Dielectric properties of epoxy nanocomposites, IEEE Trans. DEI 15- 1, 12-23.

Singha S, Thomas MJ (2009) Influence of filler loading on dielectric properties of epoxy-ZnO nanocomposites, IEEE Trans. DEI 16- 2, 531-542.

Tanaka T, Greenwood A (1983), *Advanced Power Cable Technology, Volume I: Basic Concepts and Testing*, CRC Press.

3. 6. Treeing Resistance of Polymer Nanocomposites

3. 6.1. Treeing lifetime

Figure 3.6.1 shows a classical representative data to demonstrate that treeing lifetime can be dramatically extended (Nelson et al. 2004), when polymers such as epoxy are nanostructured by the addition of small amount of nano fillers such as titania especially under relatively low electric stress. Similar data were obtained for PE/MgO, epoxy/silica, and epoxy/boehmite alumina nanocomposites. Silane couplings will work to increase treeing lifetime.

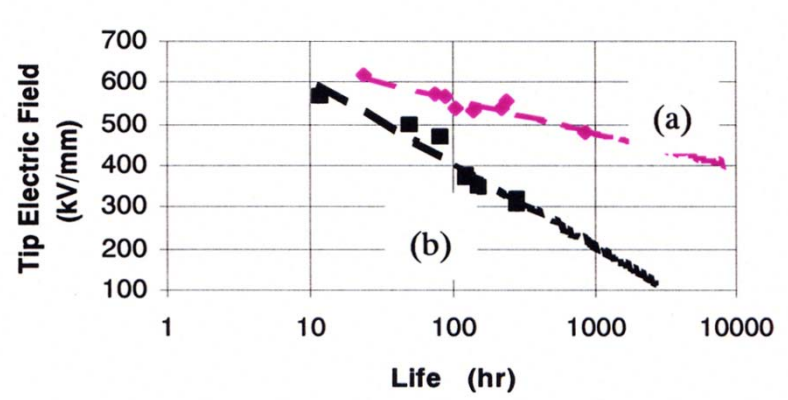

Figure 3.6.1 Treeing lifetime vs. applied voltage for (a) epoxy/titania nancomposite and (b) conventional filled epoxy (Nelson 2004)

Tree growth characteristics are represented by Fig. 3.6.2 (Vogelsang 2004). There are three stages or periods, i.e. an incubation period, a growth period, and a tree channel widening period. In general, no breakdown takes place, even if a thin tree channel reaches the opposite electrode. There is some time needed for breakdown. This phenomenon can be observed in many insulating materials such as pure epoxy, polyethylene, and nanocomposites.

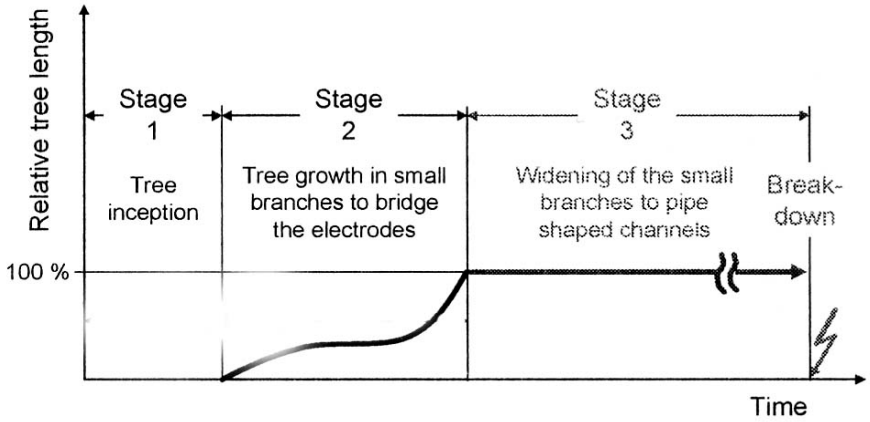

Figure 3.6.2 Tree growth characteristic (Vogelsang 2004)

A crossover phenomenon is observed under a certain condition as shown in Fig 3.6.3 (Tanaka et al. 2006). Tree growth speed is different between base epoxy and its nanocomposite under different voltage condition. At low

voltage like 10 kV, the tree growth speed for nanocomposite is slower than that for base epoxy. On the contrary, at high voltage like 25 kV, the former is faster than the latter. It is concluded that erosion type of degradation takes place under low voltage condition, while progressive type of degradation occurs under high voltage condition.

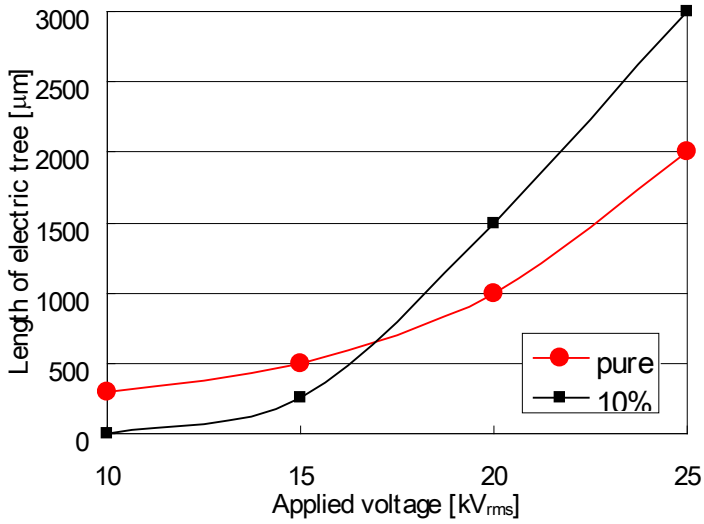

Fig. 3.6.3 Crossover phenomenon in tree length vs. voltage for epoxy/boehmite alumina nanocomposite (Tanaka et al. 2006)

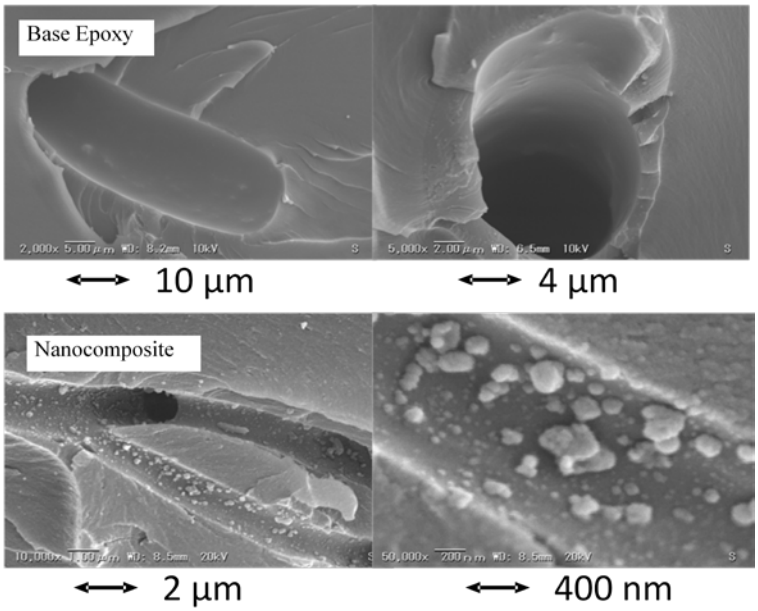

Fig. 3.6.4 Internal surfaces of trees formed in epoxy and epoxy/boehmite alumina nanocomposite (Tanaka et al. 2006)

Microscopic images of internal surfaces of trees formed in epoxy and epoxy/boehmite alumina nanocomposite are shown in Fig. 3.6.4 (Tanaka et al. 2006). Internal surface of a tree channel is smooth for base epoxy, while it is rough for nanocomposite. The latter has agglomerated filler particles on its inner surface. These particles are considered to be formed during the period in which an incipient thin channel is widened from inside by PD attack.

A narrow tree channel grows rather rapidly up to the opposite electrode, but does not cause directly material breakdown or failure. After that, partial discharges will erode the inside of the tree. This corresponds to the stage 3,

as indicated in Fig. 3.6.2. Narrow channels are formed due to solid dielectric breakdown, while wide channels are generated by PD attack afterwards. Dramatic treeing lifetime extension is considered to be related to PD degradation process inside a tree under moderate applied voltage condition. Similar results were obtained in PE/MgO nanocomposite (Kurnianto et al. 2007), where three kinds of characteristic time, i.e. time to reach the opposite electrode, time to breakdown and time lag to breakdown are separately obtained.

3.6.2. Possible effects of nano fllers on treeing

A progressive type of tree growth process is illustrated in Fig. 3.6.5 in the case of rather high voltage application. Tree channels are formed by successive solid breakdown at a tip of trees. It should be noted that this process is totally different from an erosion process caused by gaseous partial discharges inside tree channels. Trees are formed in either of the two following processes.

(1) Electrons are accelerated by the electric field, but decelerated by the nano particles.
(2) Electrons are accelerated by the electric field, and furthermore accelerated by the nano particles.

Deceleration and acceleration take place due to attractive and repulsive forces generated around the nano particles, respectively. Electric field is induced around the Debye shielding distance due to the formation of the electric double layers.

A strange phenomenon is observed that solid state breakdown (thin channel formation) occurs more easily in nanocomposite than in base epoxy. To understand this phenomenon, it is considered that repulsive force generated in epoxy nanocomposite will work against accelerated electrons. Such high energy electrons transport only in epoxy space between neighboring nano particles, being influenced by the repulsive force. In the case of LDPE/MgO nanocomposite, a thin tree formation (solid state breakdown) is retarded by the addition of nano fillers. This may correspond to the deceleration case. Such two different processes can be understood by the difference of the tendency of the triboelectricity to cause the far-distance interactive force. It is closely related to the electric double layers.

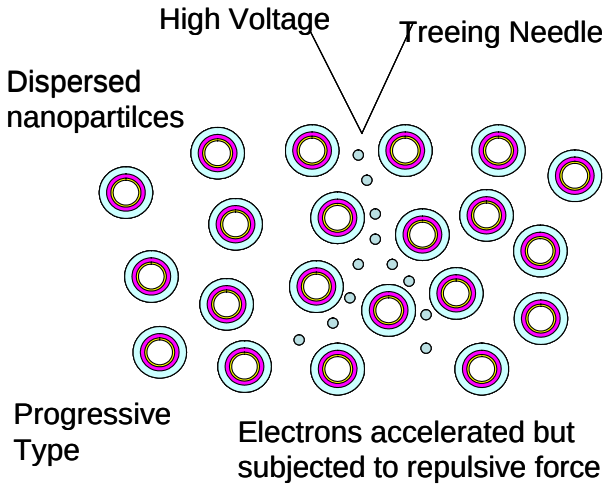

Figure 3.6.5 Possible mechanism for high voltage tree formation

3.6.3. Tree initiation

No pure tree initiation data are available as for nanocompoistes. Tree initiation is governed by an electron injection and extraction process. How the potential barrier at the electrodes is influenced by the inclusion of nano fillers. It is demonstrated in the literature (Tanaka et a.l 2005) that negative charge is formed near the electrodes in the case of the negative triboelectricity. This suppresses electron injection and thereby tree initiation. This model will also apply to the threshold for space charge formation and electroluminescence.

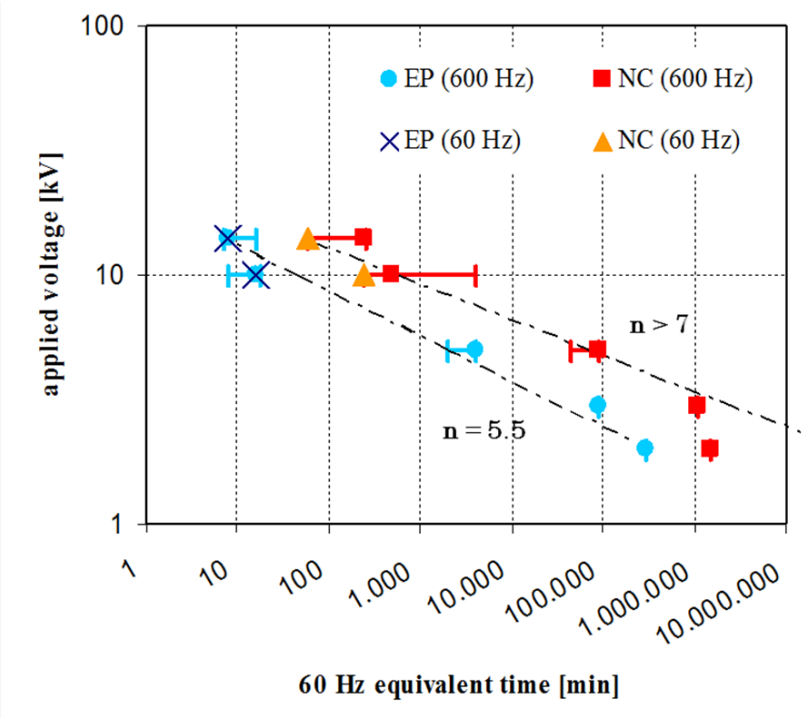

Figure 3.6.6 Treeing lifetime vs. applied voltage for neat epoxy and epoxy/layered silicate nanocomposite (Raetzke et al. 2008)

Note: Data taken under 600 Hz voltage instead of 60Hz for acceleration

V-t characteristics for quasi-initiation for treeing in epoxy/layered silicate nanocomposite specimens is shown in Fig. 3.6.6 (Raetzke et al. 2008), which are similar to treeing breakdown V-t characteristics as previously shown in Fig. 3.6.1. Advantage of nanocomposites is clearly confirmed, but tree length when we recognize tree initiation is about 100 μm. It means we have not observed pure tree initiation but it includes some early growth process in which inner surfaces must be subjected to internal partial discharges.

References

Kurnianto R, Murakami Y, Nagao M et al (2007) Treeing breakdown in inorganic-filler/LDPE nano-composite material. IEEJ Trans. FM 127-1:29-34

Nelson JH, Hu Y (2004) The impact of nanocomposite formulations on electrical voltage endurance. Proc. IEEE-ICSD, No. 7P-10: 832-835

Tanaka T, Kozako M, Fuse N et al (2005) Proposal of a multi-core model for polymer nanocomposite dielectrics. IEEE Trans. DEI 12-4:.669-681

Tanaka T, Matsunawa A, Ohki Y et al (2006) Treeing phenomena in epoxy/alumina nanocomposite and interpretation by a multi-core model. IEEJ Trans. FM., 126-11:1128-113

Rätzke S, Ohki Y, Imai, T et al (2008) Enhanced performance of tree initiation V-t characteristics of epoxy/clay nanocomposite in comparison with neat epoxy resin. Annual Rept. IEEE-CEIDP 6-2:528-531

Vogelsang R (2004) Time to breakdown of high voltage winding Insulations with respect to microscopic properties and manufacturing qualities. PhD. Diss. ETH No. 15656

3.7. Partial Discharge Resistance of Polymer Nanocomposites

3.7.1. Polyamide/layered silicate nanocomposites

It was first found in polyamide that partial discharge resistance or PD resistance is enhanced by transformation from base polyamide (PA) to polyamide layered silicate nanocomposite (Tanaka 2005). Further investigation was carried out to throw light on its mechanism. Surface of polyamide sheets are exposed to partial discharges using the IEC (b) electrode, and evaluated by the surface roughness measured by an AFM (atomic force microscope). One of the typical data is shown in Fig. 3.7.1 (Kozako et al. 2004) for the average surface roughness for base PA, PA naocomposite specimens with nano-filler content 2, 4, and 5 wt% as a function of time under ac 6 kV voltage application. This clearly demonstrates that PD resistance is enormously enhanced by nanostructuration.

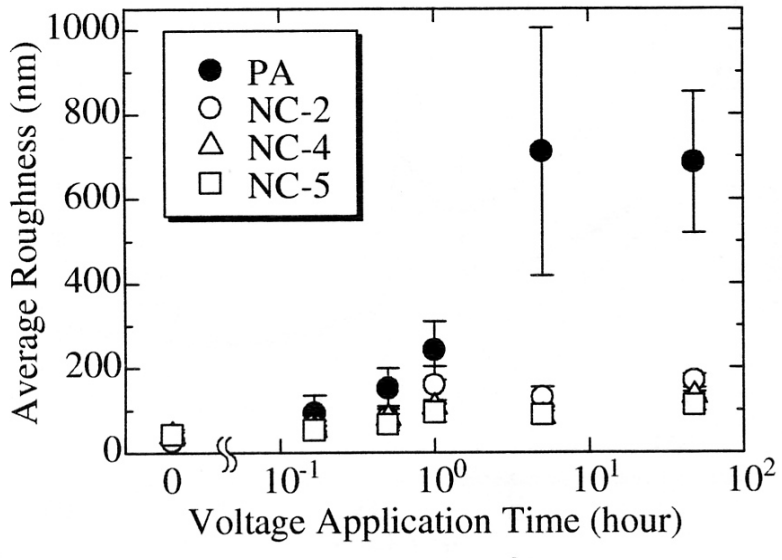

Fig. 3.7.1 Surface roughness change with time for base polyamide and nano-filled polyamide subjected to partial discharges (Kozako et al. 2004) Remark: NC-2, NC-4 and NC-5: layered silicate content 2, 4 and 5 wt%, respectively.

PD resistance improves in polyimide by nanostructuration with layered silicate. Such a positive effect is confirmed for silicone elastomer nanocomposites with 2 % silica and 5 % layered silicate, either, by the infrared spectroscopy. Radicals such as CH in CH_3, CH_3-Si-CH_3 group, and Si-O-Si group are watched for evaluation. It is recognized that they are greatly reduced by nanostructuration. For explanation of how PA layered silicate nanocomposite is against PD's, the following four points are considered as influencing factors.

(i) bonding strength between fillers and matrices

(ii) inter-filler space or matrix volume surrounded by neighboring fillers

(iii) morphology in the inter-filler space

(iv) mesoscopic interaction

In the light of the multi-core model, the first layer can be ascribed to the above item (i). Ionic bonding is suggested in this case, where the surface organically modified layered silicate is combined to the surrounding PA matrix. Items (ii) and (iii) should be modified into the second and third layers of the multi-core model. The second layer or some ordered structure such as spherulites and crystallites are created around the first layer, which is

evident from the WAXA, either. The third layer is amorphous more or less, and get in contact to the third layer of the nearest neighbor fillers. A diffuse layer must overlap the three layers. And therefore, these structures might be formed electrochemically by the mesoscopic interaction. The second layer of the multi-core model is considered to be almost adjacent to that of its nearest neighbor filler, and then will occupy almost whole volume of PA layered silicate nanocomposite. If spherulites formed around the filler as the second layer are strong against PD's compared to the original PA matrix, PA layered silicate nanocomposite becomes PD resistive. PD degradation must start in the amorphous region between the neighboring third layers or the less PD resistant third layer and proceed into the more PD resistant second layer. A same process will go in its next filler environment, as PD's enter the next the amorphous region, the third layer, and the second layer. An erosion process is illustrated in Fig. 3.7.2 (Tanaka, Kozako et al. 2005). Similar discussion can be made for silicone silica and layered silicate nanocomposites, and for polyimide layered silicate nanocomposite, too, on the basis of the multi-core model.

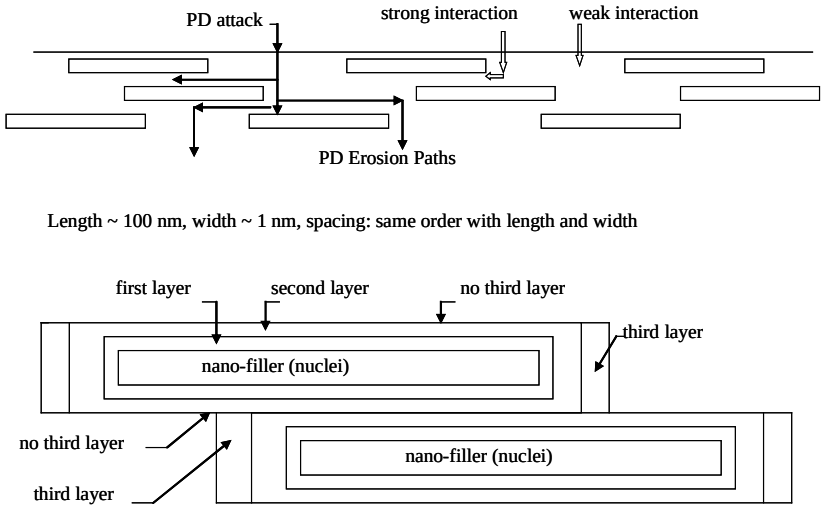

Fig. 3.7.2 PD erosion process for polyamide/ layered silicate nanocomposite (Tanaka, Kozako et al. 2005)

3.7.2. Epoxy nanocomposites

PD resistance characteristics of epoxy / titania nanocomposites are shown in Fig. 3.7.3 (Tanaka, Ohki, Shimizu et al. 2006). A rod-to-plane electrode system was used instead of IEC (b) electrode system. It was confirmed for different materials and electrodes that there is a similar positive effect of nano fillers on PD resistance. PD resistance is strengthened about 3 times at ageing time 90 hrs. Figure 3.7.4 shows the dependence of PD erosion depth on filler size and the effects of silane coupling on erosion depth (Tanaka T, Kuge S et al. 2006). It is clarified that PD resistance tends to increase with the decrease of filler size between 1.2 nm and 1.6 μm. Therefore the following conclusions can be obtained.

(1) There is a positive effect of nano fillers on PD resistance. Both particle-like fillers such as silica and titania and belt-like fillers such as layered silicate have a similar effect.
(2) Tight interfaces and well ordered morphology will increase PD resistance. Silane couplings and grown spherulites are some of the examples for that.
(3) Two and three dimensional segmentation of organic polymers by inorganic fillers seems to work well against the material attack by partial discharges

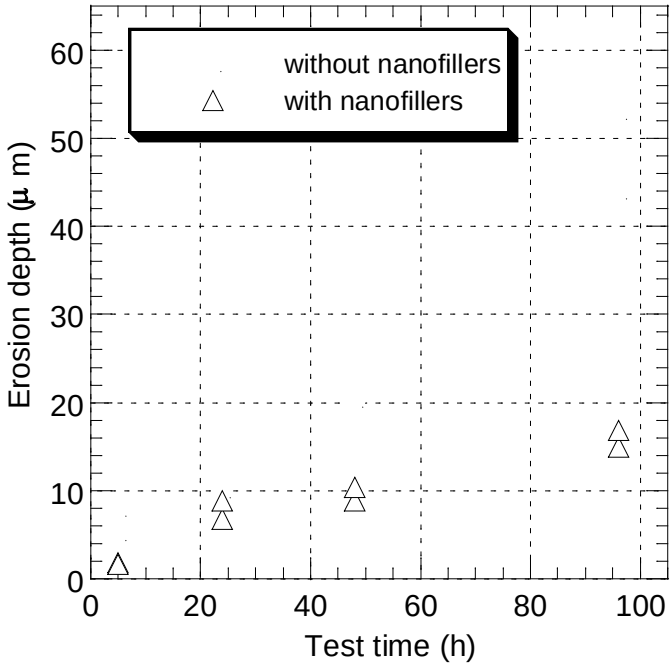

Fig. 3.7.3 Erosion depth vs PD time for epoxy /titania nanocomposites: 60 Hz, 6 kV (Tanaka, Ohki, Shimizu et al. 2006)

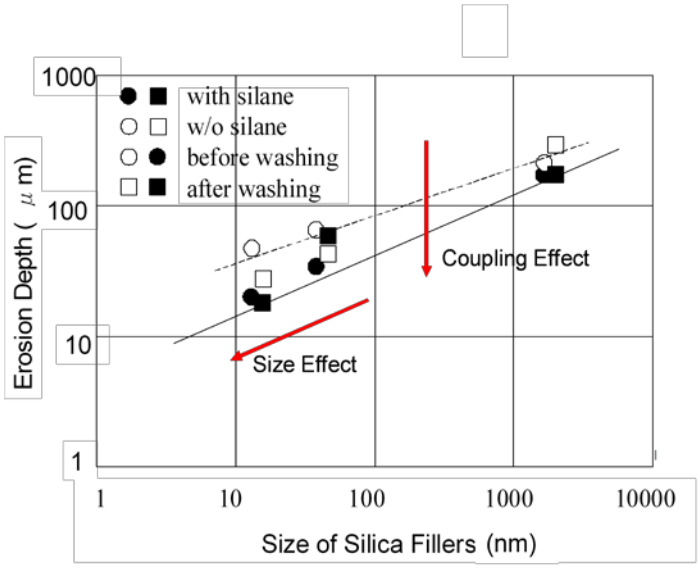

Fig. 3.7.4 Dependence of PD Erosion Depth on the Size of Silica Fillers at Aging Time 1440 h (Tanaka T, Kuge S et al. 2006)

Similar results were obtained for example in epoxy/alumia nanocomposites (Kozako et al. 2006), epoxy/alumina and titania nanocomposites (Maity, Basu et al. 2008), (Maity, Kasisomayajula et al. 2008), and epoxy/silica and alumina (Preetha et al. 2008). It was found (Maity, Kasisomayajula et al. 2008) that heating of nano fillers in vacuum before mixing and silane coupling treatment are essential to obtain nanocomposites with excellent properties. Heating must free up the hydroxyl groups on the surface of nano particles to make them available for hydrogen bonding with polymer matrices. It is further believed that functionalization by silane will help form covalent bonding such as Si-O-Al bonds. An epoxy/nano SiC system is also investigated (Tanaka, Matsuo et al. 2006), which shows almost the same results with epoxy/silica nanocomposites.

3.7.3. Polyethylene and polypropylene

Depth of erosion caused by PD depends on the content of nano-fillers as shown in Fig. 3.7.5 (Tanaka, Nose et al. 2006). It decreases with the increase of nano-fillers. In addition, it is worthwhile to mention that big improvement is observed, when only 1 phr of nano-fillers is added. Investigation is made on polypropylene nanocomposite in use for capacitors (Takala et al. 2008).

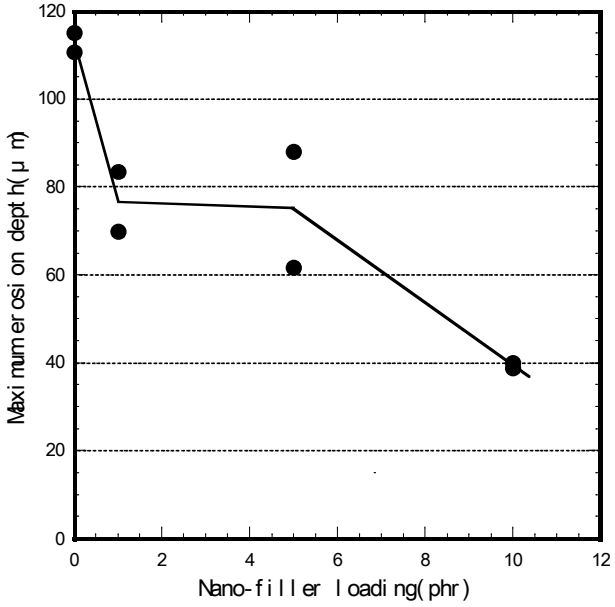

Fig. 3.7.5 PD resistance of LDPE/MgO nanocomposite (Tanaka, Nose et al. 2006)

3.7.4. Possible mechanism for PD erosion

A possible mechanism for erosion of nanocomposites subjected to partial discharges is illustrated in Fig. 3.7.6. A nanocomposite substance is eroded mainly in its polymer regions. Inorganic filler materials are far more PD resistive than organic polymers. Therefore, PDs will attack organic polymer regions preferentially. Segmentation of organic substances into many small area and/or volume is considered to be effective against PD attack. Inorganic filler materials are higher in permittivity than organic polymers, and then are subjected more to PDs than the latter. This phenomenon will help increase PD resistance, too. As a whole, it can be said that nanometer scale segmentation is more favorable than micrometer scale segmentation as for PD resistance. How does the multi-core model perform against PD attack? Nano segmentation or mesoscopic segmentation is a major factor to PD ageing. The first layer corresponds to the silane coupling region for both of polyamide and epoxy. The second layer is related to the spherulites in polyamide and the stoichiometrically crosslinked region in epoxy. The first and second layers will help increase PD resistance. Both of them will resist against extraction of nano fillers from the nanocomposite, as indicated in Fig. 3.7.6 Polyethylene is probably protected against PD's by the nano segmentation only.

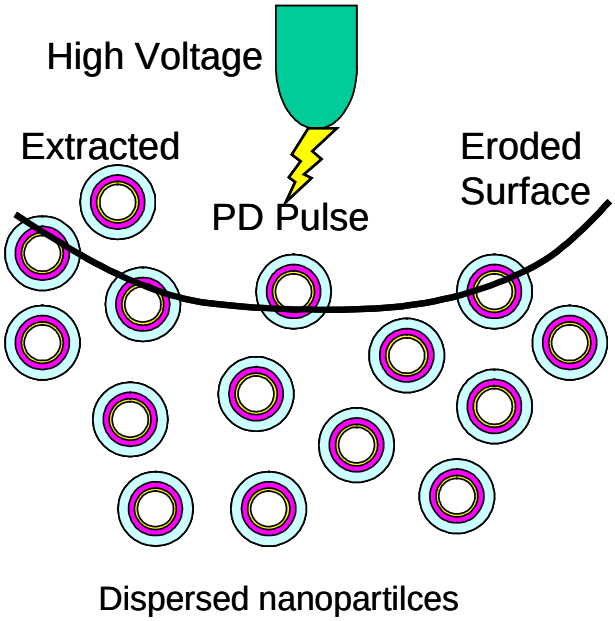

Fig. 3.7.6 Possible mechanism for PD erosion

References

Kozako M, Fuse N, Ohki Y et al. (2004) Surface Degradation of Polyamide Nanocomposites Caused by Partial Discharges Using IEC (b) Electrodes IEEE Trans. DEI 11-5: 833-839.

Kozako M, Ohki Y, Kohtoh M et al. (2006) Preparation and Various Characteristics of Epoxy/Alumina Nanocomposites IEEJ Trans. FM 126-11: 1121-1127.

Maity P, Basu S, Parameswaran V et al. (2008) Degradation of Polymer Dielectric with Nanomteric Metal-oxide Fillers due to Surface Discharges IEEE Trans. DEI 15-1: 52-62.

Maity P, Kasisomayajula SV, Parameswaran V et al. (2008) Improvement in Surface Degradation Properties of Polymer Composites due to Pre-processes Nanometric Alumina Fillers IEEE Trans. DEI 15-1: 63-72.

Preetha P, Alapati PS, Singha S et al.(2008) Electrical Discharge Resistant Characteristics of Epoxy Nanocomposites 2008 Annual Rept. CEIDP No.8-4: 718-721.

Takala T, Sallinen T, Nevalainen P et al. (2008) Surface Degradation of Nanostructured Polypropylene Compounds Caused by Partial Discharges Proc. IEEE ISEI No. S3: 205-209

Tanaka T (2005) Dielectrics Nanocomposites with Insulating Properties IEEE Trans.DEI 12-5: 914 – 928

Tanaka T, Kozako M, Fuse N et al. (2005) Proposal of a Multi-core Model for Polymer Nanocomposite Dielectrics IEEE Trans. DEI 12-4: 669-681.

Tanaka T, Ohki Y, Shimizu T et al. (2006) Superiority in Partial Discarge Resistance of Several Polymer Nanocomposites CIGRE 2006 Paper D1-303: pp8.

Tanaka T, Kuge S, Kozako M et al. (2006) Nano Effects on PD Endurance of Epoxy Nanocomposites Proc. ICEE No.ME1-01: pp. 4.

Tanaka T, Matsuo Y and Uchida K (2006) Partial Discharge Endurance of Epoxy / SiC Nanocomposite 2008 Annual Rept. CEIDP No.1-1: 13-16.

Tanaka T , Nose A , Ohki Y et al. (2006) PD Resistance Evaluation of LDPE/MgO Nanocomposite by a Rod-to-Plane Electrode System Proc. ICPADM 2006: 319-322.

3.8. Resistance to Tracking and Erosion

Though during recent years numerous original publications and review papers have been devoted to nanodielectrics, information concerning their resistance to erosion caused by different types of electric surface discharges is still scarce. Among the types of the surface discharges evaluated, one may list corona, partial discharges, gliding discharges and arcing. Since all these discharge types have detrimental impact on material performance, it has been of vital importance to investigate how much the use of nano-fillers may affect performance and reliability of insulation systems operating under conditions where the risk for surface discharge appearance exists. Investigations had revealed that nano-composites have satisfying resistant performance under the action of the surface electrical discharges.

When tracing a few years back, Lei and Xishan (2002) reported first on the resistance to tracking and erosion (according to IEC 60587) of room temperature vulcanized silicone rubber (RTV) coatings filled with nano-silica and nano-layered silicate. The authors concluded that the flame suppression mechanisms of the nano-filled composites were absolutely different from that of traditionally ATH filled RTV, and the sphere and layered shaped nano-filler particles could take over the role of flame retardant. Later on, Lei *et al.* (2004) extended the work to investigations of the materials to corona discharges and proved that nano-filled RTV performed much better than the virgin RTV material. It also was shown that nano-layered silicate filler could be dispersed in the SIR matrix uniformly and with only 5 wt% concentration contributed to improvements in tracking resistance and mechanical properties (Dengke *et al*.2004).

More or less at the same time El-Hag *et al.* (2004) showed, by means of ASTM 2303 inclined plane tracking and erosion test (IPT), that performance of silicone rubber (SIR) filled with 10 wt% of fumed nano-silica was similar to that of 50 wt% micro-filled one. The third harmonic component of the leakage current showed good correlation to the eroded mass measured. The authors also applied laser ablation technique to evaluate the erosion performance of the samples (El-Hag *et al.* 2006). An infrared laser was used as the source of heat to erode the SIR samples in addition to IPT. A hypothesis was formulated that formation of silica like layer helped to resist the degradation of SIR in nano-filled samples, which resulted from the strong bonding between nano-filler particles with the rubber matrix. Despite of the differences in erosion resistance, the investigations revealed that both nano- and micro-silica filled SIR retained similar thermal conductivity. The nano-silica filled RTV was also suggested to be better employed for contaminated environments than micro-silica filled RTV since test results had shown that nano-silica filled RTV had higher erosion resistance than micro-silica filled one (Meyer *et al.* 2006).

In parallel, Rätzke and Kindersberger (2005) evaluated the effects of silica and alumina nano-fillers on the resistance to arcing of silicone elastomers. The authors demonstrated a longer test time duration with increased filler concentration and pointed to the importance of good filler dispersion. The necessary good dispersion could only be achieved in case of nano-silica, while alumina nano-filler agglomerated and rather acted as ordinary micro-filler. However, the enhanced resistance to arcing became only evident with relatively high concentration (~40 wt%) of the silica nano-filler. Further investigations were done using a silicone rubber with a precipitated (silica 1) and a fumed (silica 2) silica nano-filler (Rätzke and Kindersberger 2009), (Rätzke and Kindersberger 2010). Both filler types were untreated and hydrophilic. The results showed a highly improved resistance to high voltage arcing and resistance to tracking and erosion (Figure 3.8.1) already at low filler contents (< 5 wt%) of the precipitated silica compared to the silicone rubber without fillers.

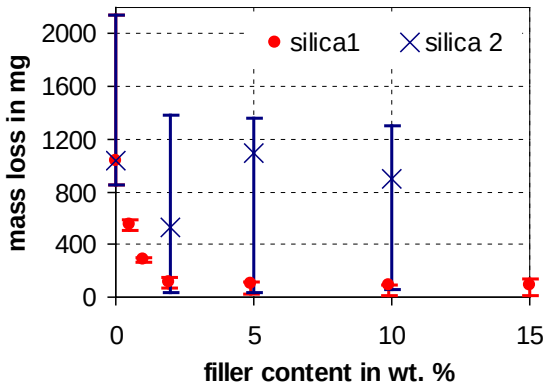

Figure 3.8.1 Median, maximum and minimum values of the mass loss occurring during the tracking and erosion test (according to IEC 60587) of a silicone matrix material with two different silica filler materials for three samples each.

For the materials with fumed silica no significant improvement was observed. The different behavior was explained by the estimated interphase content, which seems to be high for strong interactions between filler and matrix material and small for weaker interactions. This assumption was supported by TGA measurements (Figure 3.8.2) which showed a much higher thermal resistance for materials with the precipitated silica than for materials with the fumed silica (Rätzke and Kindersberger 2010).

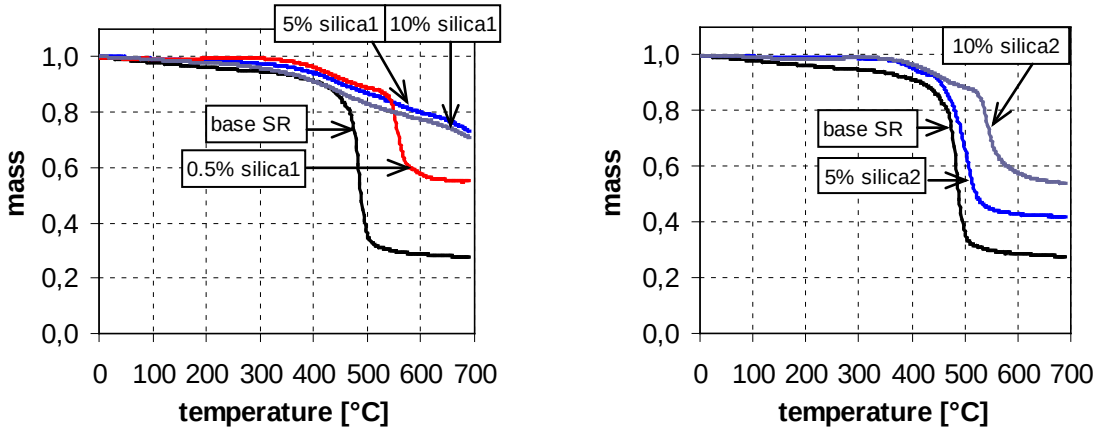

Figure 3.8.2 TGA for the base silicone rubber and silicone rubber with 0.5 wt%, 5 wt% and 10 wt% precipitated silica (left) and silicone rubber with 5 wt% and 10 wt% fumed silica (right).

Thorough investigations on possible improvements in nano-filler dispersion and its effect on tracking resistance were recently performed by Ramirez *et al* (2007), (2008), and (2009). The authors proposed to modify nano-filler particles with surfactants and showed that one of them, e.g. Triton TM X-100, appeared especially suitable for improving the dispersal in silica and alumina based SIR compositions. The investigated properties included studies of resistance to arcing by means of three different test techniques as well as evaluation of thermal and mechanical properties. A significant reduction in eroded mass was found in SIR samples containing Triton TM X-100 treated fumed silica filler in the controlled infrared laser ablation test. The study showed that resistance to heat erosion equivalent to a SIR filled with 30 wt% of micro-sized silica could be obtained with only 2.5 wt% of fumed silica treated with the surfactant. In addition, fumed silica was shown to impart greater heat ablation resistance than natural silica and alumina. The accumulation of silica at the surface forming a heat-resistant barrier preventing further erosion of the underlying SIR was proposed. This phenomenon was not reported being

observed in the alumina filled specimens. In addition composites involving combination of nano- and micro-sized silica displayed significantly improved resistance to heat ablation than composites with only one or the other filler, particularly when Triton was used to disperse the particles.

Results of investigations, on erosion resistance of silicone rubber filled with nano- and micro-alumina particles, though without any special filler treatment, were also recently reported by Venkatesulu and Thomas (2009) and showed that the performance of composite filled with 4 wt% nano-particles was comparable to that filled with 30 wt% micro-particles.

Epoxy based materials with surfaces structured with nano-particles and characterized by superhydrophobic properties (contact angle≥ 130°) were recently evaluated by Wu and Schnettler (2008) for their pollution performance in modified rotating wheel dip test, clean fog test and condensation test. While the performance became enhanced under rain or fog conditions, a decline in the resistance to form continuous moisture layer was observed under dew condition.

Epoxy composites containing nano- and micro silica fillers were also recently evaluated in a round-robin investigation arranged by CIGRE WG D1.24. Among various properties, changes imposed by corona and ozone treatment on electrical properties (surface and volume charging currents and dielectric response) of compositions filled with five different nano- and micro-filler proportions were investigated by Bin *et al.* (2004). It was found that the long-term corona-ozone exposure had obvious effect on the surface properties for all the compositions investigated and the contents of the micro- and nano-fillers played a significant role in the observed changes. On the other hand, the effects of the treatment on volume charging current, dielectric permittivity and dissipation factor (dielectric losses), all being the properties of the material bulk, did not exhibit high sensitivity to the treatment. However, a clear effect of the nano-filler addition on activation energy of the polarization phenomena could be seen.

References

Bin M, Gubanski SM, Krivda A, Schmidt LE., Hollertz R (2004) Dielectric properties and resistance to corona and ozone of epoxy compositions filled with micro- and nano-fillers. CEIDP, Virginia Beach, USA

Dengke C, Hui YJ, Xishan W, Lei L (2004) Research on characterization of RTV silicone rubber/LS (layered silicate) electrical insulation nanocomposites. ICSD, Toulouse, France: 796-799

El-Hag AH, Jayaram SH, Cherney EA (2004) Comparison between silicone rubber containing micro- and nano- size silica fillers [insulating material applications. CEIDP, Boulder, CO, USA: 385-388

El-Hag AH, Simon LC, Jayaram SH, Cherney EA (2006) Erosion resistance of nano-filled silicone rubber. Trans IEEE DEI No. 13: 122-128

Lei L, Xishan W (2002) Investigation to the influence of nanomaterial on the resistance to tracking and erosion of RTV coatings. Proc. International Conference on PowerCon, Kunming, China: 1881-1883

Lei L, Xishan W, Dengke C (2004) Corona ageing tests of RTV and RTV nanocomposite materials. ICSD, Toulouse, France: 804-807

Meyer LH, Cabral SHL, Araujo E, Cardoso G, Liesenfeld N (2006) Use of nano-silica in silicone rubber for ceramic insulators coatings in coastal areas. IEEE ISEI, Toronto, Ontario, Canada: 474-477

Ramirez I, Cherney AE, Jayaram S, Gauthier M (2007) Silicone rubber nanocomposites for outdoor insulation applications. CEIDP: 384-387

Ramirez I, Cherney EA, Jayaram S, Gauthier M (2008) Nanofilled silicone dielectrics prepared with surfactant for outdoor insulation applications. Tans IEEE DEI No. 15: 228-235

Ramirez I, Jayaram S, Cherney EA, Jayaram S, Gauthier M, Simon L (2009) Erosion resistance and mechanical properties of silicone nanocomposite insulation. Trans IEEE DEI No. 16: 52-59

Rätzke S, Kindersberger J (2005) Erosion behavior of nanofilled silicone elastomers. Proc. XIVth ISH Beijing, China: C09

Rätzke S, Kindersberger J (2009) Resistance to high Voltage Arcing and Resistance to Tracking and Erosion for Silicone/SiO2 Nanocomposites. Proc. XVIth International Symposium on High Voltage Engineering, Cape Town, South Africa: F-10

Rätzke S, Kindersberger J (2010) The Role of the Interphase on the Resistance to High-Voltage Arcing and to Tracking and Erosion of Silicone/SiO2 Nanocomposite, IEEE Trans DEI 17-2:607-614

Venkatesulu B, Thomas MJ (2009) Erosion resistance of silicone rubber nanocomposite at low filler loadings. Proc. XVIth. International Symposium on High Voltage Engineering, Cape Town, South Africa: C-48

Wu J, Schnettler A (2008) Degradation assessment of nanostructured superhydrophobic insulating surfaces using multi-stress methods. Trans IEEE DEI No. 15: 73-80

3.9. Thermal Endurance and Conductivity

Thermal endurance gives an assessment of the useful life of insulation. This was well summarized for composite dielectrics by Yingsuo, Bai, Quixing *et al.* (1999). Operating temperature of an insulation system is known to play a determinant role in its ageing. That would have been of great value for establishing the real gain for the applications of polymer nanocomposites. However, the corresponding data is scarce, and thus, the information here has been complemented by considering thermal conductivity data. Thermal conductivity remains a property the least studied. But in recent years, this property has increased in importance due to the need of high levels of conductance for instance in circuit boards. Especially in filled compositions, the thermal conductivity is required for predicting heat transfer process during moulding. Here, representative trends were established based on the available data. Thermal conductivity was also selected as a parameter because it was found to respond, on some limited range of variables, like the dielectric strength.

Motori *et al.* (2005) and Saccani *et al.* (2007) have made an interesting study relative to nanostructured isotactic polypropylene (iPP). Isothermal thermogravimetric analysis was used. The nanofiller was a layered-silicate type consisting of fluorohectorite. Many positive comments can be made from the experimental results. However, the comparison is made with respect to base polypropylene. Different compositions were prepared ranging from 0 to 6% wt. At its maximum loading, the temperature index improved considerably (by as much as 15^{o}C) and life expectancy increased. But maybe the most striking feature was that the nanostructured iPP remained with thermoplastic nature, with a substantially higher operating temperature that compares with that of XLPE, a cross-linked polyolefin. Other parameters are linked to the thermal behaviour of materials. Thermal stability and degradation studies may provide interesting insight. Though it is not the topic of the present section, the reader is referred to the overview given by Pandey *et al.* (2005) annotating the degradability of polymer nanocomposites.

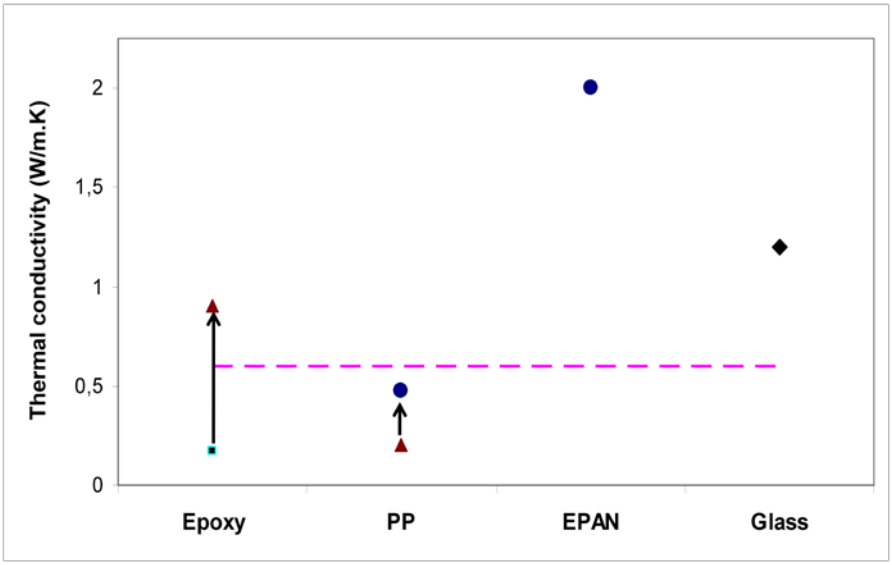

Figure 3.9.1 Thermal conductivity scaled for several polymer cases.

In order to grasp the thermal conductivity context, Fig. 3.9.1 was constructed. It illustrates that polymers, in general, have a low conductivity. Overall, a thermal conductivity not exceeding 0.6 W/m.K is found. For

thermoplastics like polyethylene, polyamide, polystyrene, and thermosets such as polyester resin, phenol resin, the boundary was chosen according to Tanaka *et al.* (2004). While we are seeking effects on conductivity due to adjunct of nano fillers in the polymer or nanostructuration, it is important to realize some increase in conductivity that can be achieved by considering other approaches.

In Figure 3.9.1, conventional base epoxy shows a typical low conductivity around 0,17 W/mK. Takezawa *et a.l* (2003) have shown that increasing the mesogen content helps in scattering phonons, and this results into an increase of the thermal conductivity. On the graph, an increase by a factor 5 is indicated. Ito *et al* (2005) pushed further by combining high-order structured epoxy and fillers of the type magnesium oxide or boron nitride, reaching thermal conductivities as high as 10 W/mK. Another approach is based on using PBT monomers, unlike commonly used epoxies. With this context of PBT in underfills, the cyclic monomer may be melted and filled with 40 wt % boron nitride. Ishida and Rimdusit (1998) have produced specimen exhibiting thermal conductivities just under 4 W/mK.

The second case in the Fig. 3.9.1 recalls the observation that the conductivity of PP can be pushed up towards that of XLPE (0.475 W/m.K at 23 ^{o}C). Finally, the third case considered is EPAN, a compound developed by AREVA that consists of a matrix of epoxy with a high load (about 76% wt.) of aluminum nitride. The final product has a thermal conductivity that reaches 2 W/Km at a temperature of 120 ^{o}C. The results were reported by Perot and James (2006).

Indeed, there is a wide range of possible thermal conductivities that may be reached by adding fillers. For that purpose, using metallic fillers (typ. 1000 times the thermal conductivity of polymers) or inorganic (typ. one order of magnitude larger than the polymer thermal conductivity) may modify easily the thermal conductivity. The book edited by Godovsky and Privalko (1995) provides a good source of information in order to gain a basic understanding of the phenomenologies involved. For instance, geometry and orientation of the filler particles were found to have a significant impact on the end results. There is no particle-particle interaction expected at least up to 30% volume fraction. Also, of interest, much information provides evidence that using inorganic fillers such as CaO, MgO and Al_2O_3 is as efficient as metals for increasing the thermal conductivity. Finally, so far, in practice, it is found that the increase in thermal conductivity is limited to 10 times that of the unfilled polymer matrix.

Other powerful fillers can be considered as an additional help due to their very high intrinsic conductivities, for instance diamond (≥ 1500 W/mK) and carbon nanotubes (3000 W/mK), e.g. Xiea *et al.* (2005).

Irwin *el al* (2003) studied polyimide. They showed the importance for the nanofiller to be pre-treated before mixing. Fillers were not identified. Adjunct of 5% wt. coated nano filler in polyimide resulted into a substantial increase in thermal conductivity as compared to that obtained with an equivalent polyimide microcomposite. At 5% content and room temperature, the conductivity reached about 0.35 W/mK, a factor 1.3 above that of the microcomposite. Increase of the thermal conductivity over the 0 to 5% range was observed to be quite linear.

In his thesis, Kotsilkova (2005) measured thermal conductivities for a series of epoxy nanocomposites containing a constant 3% volume fraction of the nano fillers. A matrix of epoxy resin was used (araldite LY556,

0.15 W/m.K)) and the nano fillers were variants of the organo-smectites, graphite/diamond and diamond. An anhydride-type hardener was used. Some observations were gained. Addition of organoclay was found to reduce the conductivity, and it was the adjunct of nanodiamond that produced the highest gain with respect to neat epoxy: 0.44 W/mK. Overall, gradability of the thermal conductivity between 0.15 and 0.44 W/mK was demonstrated.

Kochetov *et al.* (2009a) have reported increases in thermal conductivity by using nanopowder in an epoxy matrix. Both pre-treated aluminum nitride AlN and boron nitride BN were used as fillers constituting from 0 to 10% wt of the load. Over this span, the thermal conductivity was found to vary quasi linearly with the adjunct of the nano filler. The thermal conductivity determined by a THASYS system gave a value of 0.168 W/m.K for the neat epoxy. At the maximum loading of 10%, the adjunct of AlN and BN resulted into an increase of 18% and 14% in conductivity, respectively.

Kochetov *et al.* (2009b) continued this research. Other results were reported later that same year. The same trends were observed with nano fillers such as silica, alumina, and mixtures of SiO_2/Al_2O_3 and SiO_2/AlN. Linearity of the increase in thermal conductivity was observed as a function of wt% of the nano filler content. At 5 %wt., it is still the nanocomposite consisting of epoxy and aluminum nitride which exhibits the highest conductivity. Overall, the maximum increased in thermal conductivity that was produced amounted to about 10%.

So far, using low percent content of nanofiller, it was demonstrated that increasing and grading the thermal conductivity of a polymer matrix is feasible.

References

Godovsky YK, Privalko VP, Guest Eds. (1995) Thermal and electrical conductivity of polymer materials Advances in polymer science, Vol. 119, Springer-Verlag, Berlin, 130 pages

Irwin PC, Cao Y, Bansal A et al (2003) Thermal and mechanical properties of polyimide nano-composites Ann. Rep. CEIDP pp. 120-123

Ishida H and Rimdusit S (1998) Very high thermal conductivity obtained by boron nitride-filled polybenzoxazine", Thermochimica ACTA, Vol. 320, 177

Ito M, Yamanaka H, Hattori M, Takahashi Y, Kanai J, Yonekura M, Kamata M, Fukushiina K, Takahashi H, Takezawa Y (2005) Development of high thermal conductive laminates Proceedings of intemationat symposium on electrical insulating materials, June *5-9*, Kitakyushu, Japan, pp. 199-202

Kochetov R, Andritsch T, Lafont U el al (2009a) Thermal behaviour of epoxy resin filled with high thermal conductivity nanopowders, IEEE Electrical insulation conference, Montreal, QC, Canada, 31 May - 3 June, pp. 524-528

Kochetov R, Andritsch T, Lafont U, et al (2009b) Thermal conductivity of nano-filled epoxy systems, 2009 CEIDP Ann. Rep. Electrical insulation and dielectric phenomena, Virginia beach, VA, Oct.

Kotsilkova R, ref. 47, Chap.6 (2007), quoted in Thermoset nanocomposites for engineering applications Ed. R. Kotsilkova, Smithers Rapra Technology limited, United Kingdom, pp. 253-255

Motori A, Patuelli F, Saccani A et al (2005) Improving thermal endurance properties of polypropylene by nanostructuration Proceedings of 2005 CEIDP, Nasville, TN, USA, October 16-19 pp. 727-734

Pandey JK, Reddy KR, Kumar AP et al (2005) An overview on the degradability of polymer nanocomposites Polymer Degradation and Stability 88, pp. 234-250.

Perot F and James I (2006) Avancées technologiques dans les systèmes diélectriques haute tension à forte conductivité thermique REE, No 6/7, Juin/juillet, pp. 98-104

Saccani A, Motori A, Patuelli F et al (2007) Thermal endurance evaluation of isotactic poly(propylene) based nanocomposites by short-term analytical methods IEEE Trans. on diel. elec. insul., Vol. 14, No. 3, June, pp. 689-695.

Takezawa Y, Akatda M, Farren C (2003) High thermal conductive epoxy resins with controlled high order structure Proceedings of the 7th international confer ence on properties and applications of dielectric materials June 1-5 Nagoya, pp. 1146-1149

Tanaka T, Montanari GC, Mulhaupt R (2004) Polymer-nanocomposites as dielectrics and electrical insulation – perspectives for processing technologies, material characterization and future applications IEEE Trans. on Diel. and Electr. Insul., Vol. 11, No. 5, October, pp. 763-784

Xiea XL, Maia YW, Zhoub XP (2005) Dispersion and alignment of carbon nanotubes in polymer matrix: a review", Materials Science and Engineering R 49 89–112

Yingsuo Z, Yi B, Quixing X, and Zhiping Z (1999) Evaluation of thermal life for composite dielectrics IEEE Electrical Insulation Magazine November/December Vol. 15 No. 6 pp. 12-19

3.10. Flame Retardant Properties

3.10.1. Introduction

Flame retardant (FR) compounds find uses in a wide range of practical applications, most notably for wire and cable applications in confined spaces. In an enclosed environment smoke and fumes generated in the event of a fire pose a serious threat to anyone exposed to the decomposition by-products. It has been reported that 80% of fire fatalities can be attributed to smoke and gases (Lews 1989). Consequently there has been a global shift in FR materials from FR halogen materials, to FR low-halogen or hybrid and finally FR non-halogen.

Traditional halogen-free FR (HFFR) or Low Smoke Zero Halogen (LSOH) materials (ie without nano-materials), offer a number of advantages compared to FR materials:

1. Low smoke – provides improved visibility and increases the time to exit the fire area
2. Low corrosion – acid gases generated when halogenated materials decompose corrode and damage equipment during and after the fire
3. Low toxicity – less harmful emissions increase the time to exit the fire area
4. Ecology – the absence of halogens promotes ease of recycling; additionally there are no heavy metals

HFFR cables are typically used in public buildings such as airports or offices, or where protection of equipment is paramount, e.g. chemical plants or shipboard/military applications. Consequently HFFR materials are most often used for LV, telecom and fiber optic cables. Nevertheless, HFFR power cable jacketing is an increasingly important usage, either for MV industrial plants or shipboard application. Additionally, some utilities now specify HFFR jacketing for cables up to EHV levels in substation basements or cable tunnels.

3.10.2. Testing

Cone calorimetry is the most commonly used method to assess the FR properties of materials (Babrauskas 1995). The method determines the rate of heat release from materials or articles when exposed to controlled levels of radiant heating by measuring oxygen consumption. Measurements from this single method can include:

1. Time to ignition
2. Average, peak and total heat release
3. Smoke opacity
4. Total, peak and mass loss rate
5. Rate and extent of Carbon monoxide produced during combustion
6. Corrosive effect of combustion gases

Information on the thermal stability of materials can also be obtained from thermogravimetric analysis (TGA), whereby the mass of a sample is measured as it is heated in either an inert or oxidative atmosphere.

3.10.3. Standards

Given the critical uses of FR materials there is a clear need for standards. A wide variety of standards exist for characterizing the FR properties of materials; Table 3.10.1 lists some representative standards.

Table 3.10.1 Representative international and national standards commonly used to measure the characteristics of HFFR materials.

Attribute	**Standard/test**
Flammability	ASTM D2863 LOI, BS 2782 LOI, UL-94 V0, NES 715 critical temperature index, Cone calorimetry
Smoke	ASTM E662, NES 711, JCS 397
Acid gas	IEC 754-2, MIL C24643, VDE 0472; part 813
Toxicity	NES 713, Pittsburgh Protocol
Other	Fluid resistance, UV stability

3.10.4. Typical results

Conventional HFFR materials contain high levels (50-70 wt%) of mineral flame retardants, e.g. aluminum hydroxide or magnesium hydroxide. When exposed to heat these flame retardants decompose releasing water; this has two effects (i) it cools the polymer and (ii) dilutes the combustion gases locally lowering the concentration of oxygen and fuel gases. Although an effective solution, the high loadings of flame retardants make such materials difficult to process and negatively impacts properties such as mechanical strength.

The addition of nano-materials to polymers has been shown to improve flame retardancy (Beyer 2002, 2006, 2007), (Cogen, Lin et al. 2003). Clays with high length to thickness aspect ratio have been found to provide these enhancements. As discussed elsewhere within this report the preparation of the material is crucial to achieve compatibility and easy dispersion. The benefits of adding well dispersed clay include good char formation to prevent dripping, reduced peak heat release rate and increased peak decomposition temperature of the composite. For example, nano-composites of EVA can reduce the peak heat release rate by 47% and increase the peak decomposition temperature by 40 °C (Alexandre, Beyer et al. 2001), (Gilman, Kashiwagi et al. 2000). To achieve such improvements, the nano-material typically replaces 2-10 wt% of the metal hydroxide.

The clays used can be mined (e.g. montmorillonite) or synthesised, but in both cases purity is essential to limit coloration of the composite material and also to control possible degradation (Grimshaw 1980). Undesired coloration of the HFFR nano-composite is particularly important when the final product can be seen; under these circumstances synthetic clays may be favorable.

Table 3.10.2 Compositions of two nano-composites and a conventional control specimen used to generate the data discussed below.

Material	**A**	**B**	**C (control)**
EVA	45	45	45
$Mg(OH)_2$	50	50	55
Montmorillonite	5		
Synthetic clay		5	

Table 3.10.2 shows the composition of three HFFR compounds, all contained 45 wt% EVA and 55 wt% of additives, composed of either conventional FR (sample C) or a mixture of conventional FR and nano-material. Cone calorimetry data showing heat release rates are shown in Figure 3.10.1 (Cogen, Lin et al. 2003). The materials with nano-material perform better than the conventional control; peak heat release rate is reduced 37% and 48% for montmorillonite and synthetic clay respectively. Similarly the peak smoke release rate is lowered by 40% for the nano-composites (Cogen, Jow et al. 2003). Similar results have been reported for other host matrices, including polypropylene by Qin et al 2005 and polyethylene by Hasegawa and Usuki 2004.

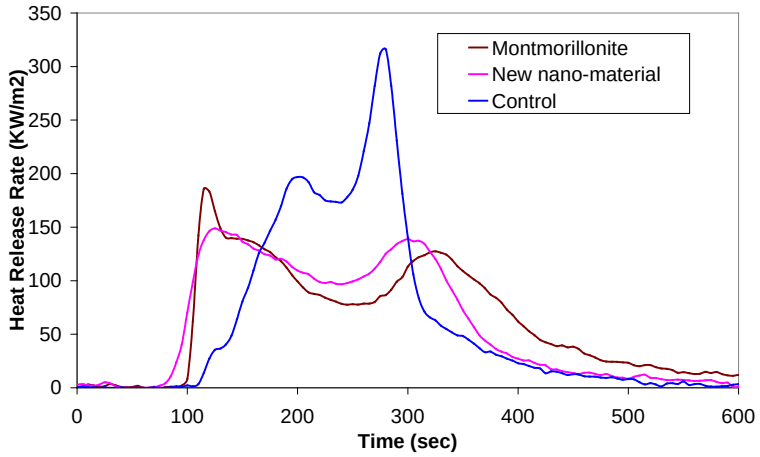

Figure 3.10.1 Heat release rate data from cone calorimetry (heat flux = 35 kW/m2), for montmorillonite nano-composite, new synthetic clay nano-composite and conventional FR control sample (from Cogen et al. Proc. 52nd IWCS, 2003, 102-107)

Clear differentiation is also apparent between the conventional and nano-enhanced materials in the resulting char layer (Figure 3.10.2). The samples with added nano-material form a more coherent char which acts as a barrier between the composite and superficial zone where combustion takes place (Cogen, Lin et al. 2003), (Beyer 2005).

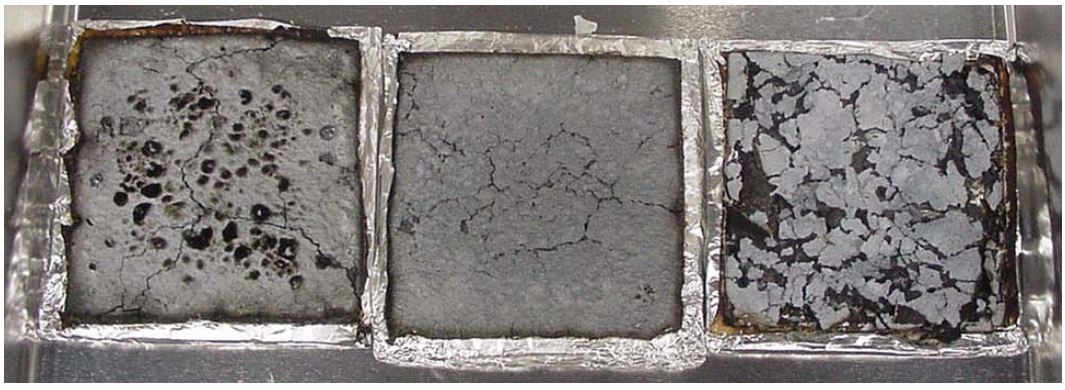

Figure 3.10.2 Samples after cone calorimetry; montmorillonite nano-composite (left), synthetic clay nano-composite (middle) and conventional filler control (right) (from Cogen et al. Proc. 52nd IWCS, 2003, 638-644)

3.10.5. Summary

A wide range of nano-composites have been examined for their FR properties, generally based on the addition of clays to traditional FR materials. It is generally agreed that well dispersed clay slows the diffuse of gases into and out of the polymer, which suppresses burning, as well as acting as a superior thermal insulator. Furthermore, the addition of nano-material can catalyze the decomposition of the polymer, although the precise behavior varies

depending on the polymer, type of clay, modifiers and compatibilizers. The net effect is the formation of a more stable char layer, often more rapidly, than with traditional FR materials.

References

Alexandre M., Beyer G, Henrist C., Cloots R., Rulmont A., Jerome R., Dubois P (2001) Macromol. Rapid. Commun, 22: 643

Babrauskas V(1995) The Development and Evolution of the Cone Calorimeter: A Review of 12 Years of Research and Standardization, pp.3-22, in Fire Standards in the International Marketplace, ASTM STP 1163, Arthur F. Grand, Ed., American Society for Testing and Materials, Philadelphia

Beyer G (2002) Proceedings of the 51st International Wire & Cable Symposium, 584-588

Beyer G (2005) J. Fire Sci 2005, 23, p75

Beyer G (2006) Polymers for Advanced Technologies 17(4): 218-225

Beyer G (2007) Nanopolymers 2007, International Conference, Berlin, Germany, June 12-13, 2007 (2007) Rapra Technology Ltd., Shrewsbury, UK

Cogen JM, Lin TS, Morgan AB, Garcés JM (2003) Proceedings of 52nd International Wire and Cable Symposium, pp. 638–644

Cogen JM, Jow J, Lin TS, Whaley P (2003) Proceedings of 52nd International Wire and Cable Symposium pp.102-107

Gilman JW, Kashiwagi T, Morgan AB, Harris RH, Brassell LD, Van Landingham M, Jackson Cl (2000) NIST Internal Report (NISTIR) 6531 July

Grimshaw RW (2000) The Chemistry and Physics of Clays and Other Ceramic Material, 4th ed, Benn, London

Hasegawa N, Usuki A (2004) J Appl Polym Sci , 93: 464

Lews CF (1989) Flammability testing: fighting fire with fire, ME, August, pp31-34

Qin H, Zhang S, Zhao C, Wu G, Yang M (2005) Polymer 46: 8386

3.11. Radiation Resistance

Articles dealing with resistance to radiation of compounds containing nanocomposites are scant. This may seem surprising when so many plastics are subjected everyday to radiation which can have a long term detrimental effect. It should be mentioned that, currently, many commercialised additives (non nano) can improve plastic material resistance to radiation.

Due to the fact that there are different types of radiation, that there are many varieties of plastics, as well as different types, shapes and concentrations of nanocomposites in addition to the diverse assessment techniques; it is not possible yet to precisely evaluate the exact effect of nanocomposites in the host material. Nevertheless, nanocomposites generally improve radiation resistance of the polymer matrix.

Here are some conclusions of published papers and articles:

- The addition of $Ti0_2$ nanocomposites to an epoxy/carbon fibre composite decreases the radiation degradation by about one half thus greatly extending the epoxy composite's lifetime (Jiang el al. 2003).

- PVDF with layered silicate nanocomposites resists much better than unfilled PVDF to high energy swift heavy ions (Tiwari et al. 2009).

- The addition of organophilic montmorillonite nanocomposites in an SBS matrix greatly improves its radiation stability (Zhang et al. 2004).

- Carbon nanotube nanocomposites were shown to reinforce the resistance of PMMA to degradation of UV and e-beam radiation (Najafi et al. 2005).

- Single walled carbon nanotubes addition to polyimide has been found to improve the tensile properties but reduce the transparency as compared to unmodified polyimide when subjected to e-beam radiation Nielsen et al. 2008).

References

Jiang L, He S, Yang D (2003) Journal of Materials Research 18:654-658.

Najafi E, Shin K (2005) Radiation resistant polymer–carbon nanotube nanocomposite thin films, Colloids and Surfaces A: Physicochem. Eng. Aspects 257 258: 333–337

Nielsen KLC (2008) The radiation degradation of a nanotube–polyimide nanocomposites", Polymer Degradation and Stability Vol. 93 Issue 1: 169-175.

Tiwari V, Kulriya P, Avasthi D, Maiti P (2009) Radiation-Resistant Behaviour of Poly(vinylidene fluoride)/Layered Silicate Nanocomposites, ACS Appl. Mater. Interfaces: pp 311-318.

Zhang W, Zeng J, Liu L, Fang Y (2004) A novel property of styrene-butadiene-styrene/clay nanocomposites: radiation resistance, J. Mater. Chem.14: 209 – 213.

3.12 Glass Transition Temperature

The glass transition temperature (Tg), or, as it is often simply referred to, the glass temperature, represents the temperature at which the physical qualities of a polymer change from those of a glass, at lower temperature, to those of a rubber (Tobolsky 1960) at higher temperature. These are determined by an assortment of non-polar and dipolar van der Waals forces between the polymer chains. Amorphous and polycrystalline thermoplastic polymers exhibit such a glass temperature, as also do thermoset polymers. With thermosets polymers, such as epoxies and polyesters, an amorphous phase is typically present within the crosslinked chemical structure which has a glass temperature that can vary over a wide temperature range and plays a role in the ductility/brittleness of the thermoset.

When nanoparticles are added to form a polymer nanocomposite, changes in this temperature offer a reflection of changes of the physical nature of the polymer in the interface region, up to the location where the polymer properties resume those of the unfilled polymer. This insight into changes in the interface region is of help in explaining some of the changes in electrical and dielectric properties of polymer nanodielectrics observed in different investigations (Reed 2010). As the concentration of nano particles is increased, we can expect that the changes will vary.

Alcoutlabi and McKenna (2005) have performed a “topical review”, covering 406 theoretical and experimental publications on the effect of nanoparticles on melting point and glass transition temperature. They present in detail the dynamic, thermodynamic and pseudo-thermodynamic measurements reported for Tg in confined geometries for both small molecules in nanopores and for ultrathin polymer films: it is found that Tg decreases, increases, remains unchanged, or even disappears depending on details of the experimental conditions or molecular simulation. They also note that different values for Tg have been observed for the same material depending on experimental conditions. They conclude that the existing theories of Tg are unable to explain the range of behaviors seen at the nanometric size scale, in part because the glass transition phenomenon itself is not fully understood.

However, Bendler and colleagues (2009) take a more positive view and present a quantitative analysis that shows that most, if not all, experimental results on the nanoconfinement of the glass transition temperature can be explained by a defect diffusion model. The model incorporates defect-defect interaction enthalpy, defect concentrations, defect lattice geometry, correlation length, and percolation fraction, to determine Tg; it provides a quantitative relationship between the percolation fraction of rigid to mobile regions and Tg. The results explain clearly confinement effects that had been difficult to understand previously.

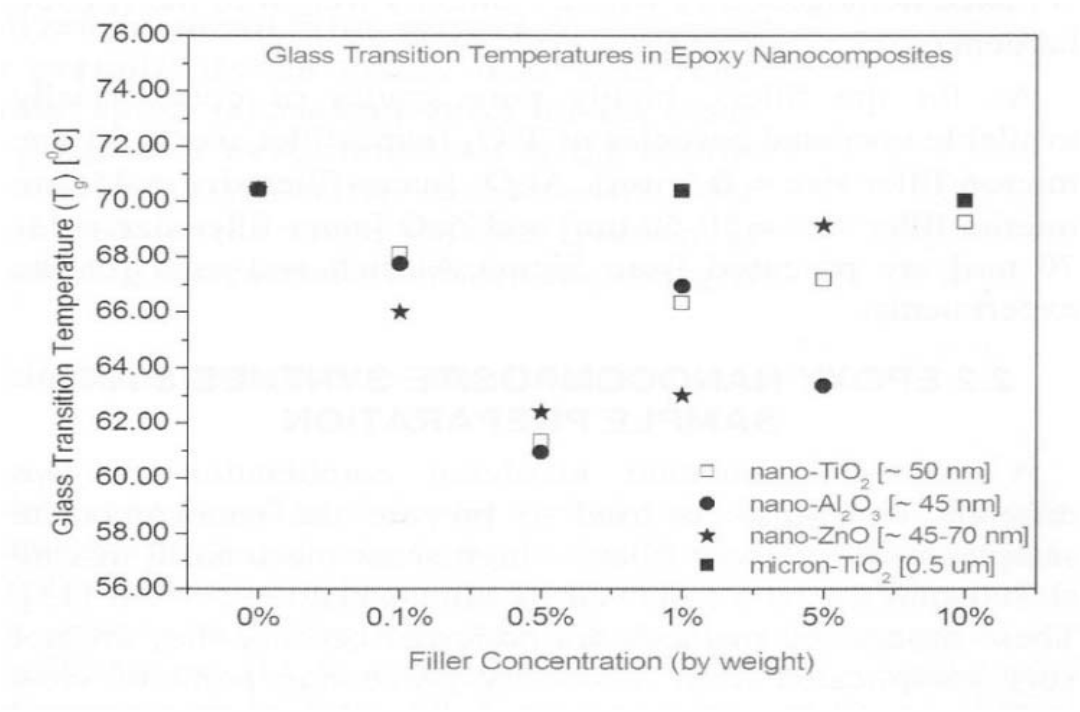

Figure 3.12.1 Tg versus filler concentration in epoxy nanocomposites (Singha 2008)

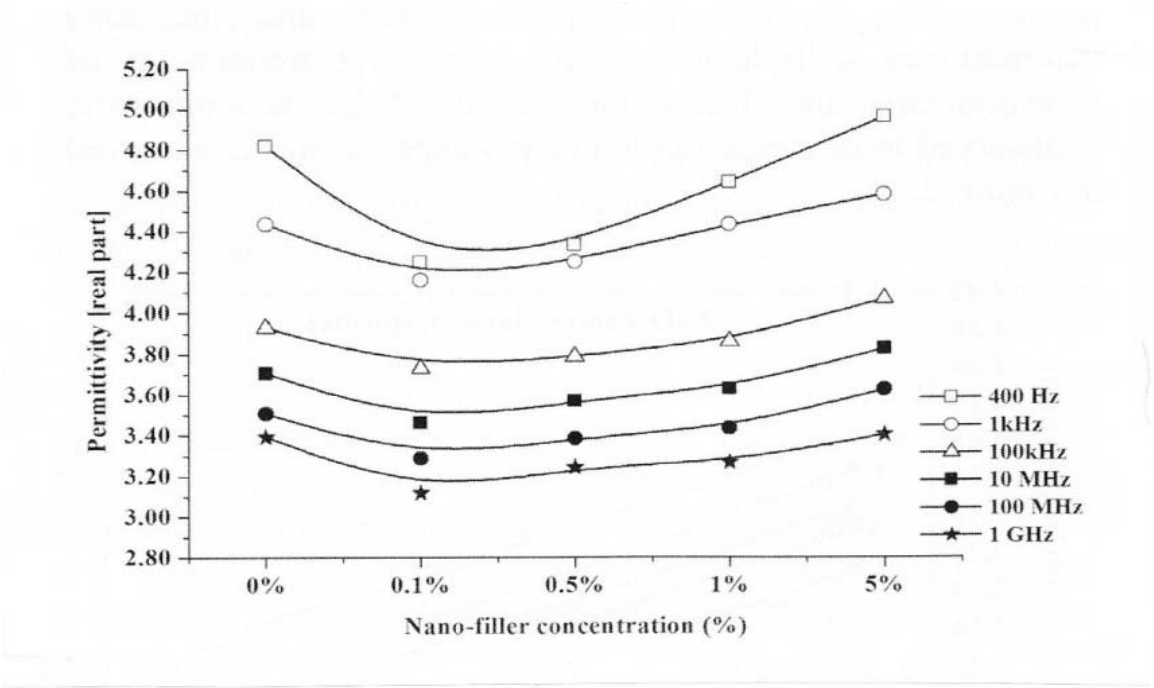

Figure 3.12.2 Permittivity versus filler concentration in ZnO-epoxy nanocomposites (Singha 2009)

Work by Singha and Thomas (2008) for different spherical inorganic nanoparticles in bisphenol-A epoxy, as a function of filler concentration, illustrates the strong, unusual sensitivity of Tg to concentration shown in Figure 3.12.1. The results illustrate why other workers, where measurements were made at only one or two concentration levels,

might have found decreases or increases in Tg, or even no change in Tg, from the value of the unfilled matrix polymer; or why seemingly contradictory results might be found by different workers.

The Tg versus concentration measurements have a similar behavior to that of real permittivity measurements versus filler concentration shown in more recent work on ZnO-epoxy nanocomposites by the same authors (Figure 3.12.2). The permittivity first drops at a concentration of 0.1%, then slowly rises as the concentration increases to 5%. It is easy to understand why permittivity will increase, due to increased amounts of the higher permittivity filler. However, it is more difficult to understand why Tg would do so, as concentration is increased above 0.1%, given the resulting increased interface volume. It will be interesting to see how the defect diffusion model is able to address these results.

References

Alcoutlabi M, McKenna GB (2005) Effects of confinement on material behavior at the nanometric size scale. J Phys: Condens Matter 17: R461-R524

Bendler JT, Fontanella JJ, Shlesinger MF et al. (2009) The defect diffusion model and the glass transition in nanoscale and bulk films. Computational and Theoretical Nanoscience 6: 1-5

Reed CW (2010) Dielectric Polymer Nanocomposites. Springer, New York, NY. chapter 4 The chemistry and physics of the interface region and functionalization. In press

Singha S, Thomas MJ (2008) Dielectric properties of epoxy nanocomposites. Trans IEEE DEI-15: 12-23

Singha S, Thomas MJ (2009) Influence of filler loading on dielectric properties of ZnO-epoxy nanocomposites. Trans IEEE DEI-16: 531-542

Tobolsky AV (1960) Properties and structure of polymers. John Wiley and Sons, Inc.

4. Safety and Security

4.1. Introduction

The use of nanoparticles in industrial products is steadily increasing. At the same time concerns about adverse effects of the nanoparticles on human health have emerged (Oberdoerster *et al* 2007, Hoet *et al* 2004, Nel *et al* 2006, Borm *et al* 2006, Reijnders 2006, Donaldson *et al* 1998, Gurr *et al* 2005). These concerns have mainly originated from long-term studies of very-fine air-borne industrial pollution in the cities and from the use of asbestos in industrial products in the past (Maynard and Aitken 2007, Oberdoerster *et al* 2005a, Maynard and Kuempel 2005, Donaldson and Tran 2004, Calderon-Garciduenas *et al* 2002, Shi et al 2001, Harrison and Yin 2000, Jung *et al* 2000).

The main purpose of the present text is to provide basic information on

- possible effect of nanoparticles on human health,
- safe working practices in laboratories and at industrial working places, and
- risk assessment of nanoparticles,

so that informed decisions about future production lines, the use and recycling of nanomaterials in power engineering can be made. It should be noted that the field of nanotoxicology is new and detailed mechanisms of nanoparticle effects on environment are not fully understood. In fact, a broader research activity in this field has just started. Although the mankind was always exposed to nanoparticles from natural sources such as volcano outbursts and forest fires, the systematic exposure of humans to man-made nanoparticles started with the invention of fire. With first industrial achievements came also first reports on susceptibility of human health to fine dust and sub-micro sized particles. These reports date as back as two thousand years ago to stone crushers in quarries, workers in coal mines and welders exposed to metallic fumes. Typical household sources of nanoparticles are pure wax candles, which can release 250 000 nano-sized particles per cubic centimeter during one evening. Smoke released by one cigar can contain more than 70 000 nano-sized particles per cubic centimeter (Afshari *et al* 2005). A recent study has shown that some laser printers can release nano-particles during the printing process (He et al 2007). Nanoparticles are also used in food, textile and cosmetics industry to improve, for example, processibility or appearance of a product (Kühling, nanoforum.org, Nohynek *et al* 2007).

4.2. Hazard and Risk Associated with the Use of Nanoparticles

Generally there are three ways of human exposure to nanoparticles:

- skin penetration,
- inhalation, and
- digestion.

Theoretically the skin can be penetrated intercellularly, transcellularly and along the hair shaft (follicle penetration). Fortunately the skin is relatively thick, consists of several layers and is shed regularly and thus penetration by ordinary (not coated with biologically compatible agents) nanoparticles is less likely (Baroli *et al* 2007, Nohynek *et al* 2007). There are many uncertainties though (Ryman-Rasmussen *et al* 2006). For example it is not clear whether nanoparticles could penetrate through wounds and cuts. In some skin conditions the thickness

of the skin can be significantly reduced and thus the risk of penetration by nanoparticles is increased. It is also difficult to assess what happens to nanoparticles deposited on skin surface via application of sunscreen or another cosmetic product containing nanoparticles during physiotherapeutic massage when the nanoparticles might pierce the skin.

There are two possible ways for nanoparticles to enter human body during inhalation. The first path, through nasal cavity and along the olfactory nerve leads directly to the brain (Oberdoerster *et al* 2004). This has been confirmed in inhalation studies of carbon nanoparticles in rats. The second path, via the alveolar-capillary barrier in the lungs allows penetration of nanoparticles into the blood stream and human body natural filters – liver and spleen (Nemmar *et al* 2002, Geiser *et al* 2005). It should be realized that human lungs have more than two thousands kilometers of airways and an area of about 150 m^2. Penetration sites for nanoparticles are thus plentiful. Since females and juveniles have thinner airways than males different deposition rates are expected for males, females and children (Jaques and Kim 2000).

During inhalation of nanoparticles part of them will also be deposited in the mouth cavity and will end up in the digestion system by swallowing them together with food. Once in the digestion system, nanoparticles can penetrate through the gastrointestinal barrier into the blood stream and end up in the liver and spleen (Jani *et al* 1992, Jani *et al* 1994). Nanoparticles from over-worn porcelain bridges were observed in the liver of patients (Gatti and Rivasi 2002). The critical point in these studies was that non-toxic materials (porcelain) caused health problems and even death of some humans. Patients suffering from inflammatory bowel diseases, such as Crohn's disease and ulcerative colitis, have abnormal intestinal permeability, which may allow for easy penetration of nanoparticles (Gatti 2004). As it is usual in such cases, sensitive parts of population will suffer most. In general, the smaller the nanoparticles, the further is the translocation in the human body and once in the human body, nanoparticles mostly create damage by generating oxidative species, which cause oxidation of human body.

The effect of nanoparticles on environment was examined in several studies. For example, it was observed that 13 nm Al_2O_3 nanoparticles inhibited root growth in plants (Yang and Watts 2005). Fullerenes in sub-lethal concentrations changed behavioral patterns of Daphnia, which in turn increased the risk of predation and increased reproductive decline (Lovern *et al* 2007). It was also observed that sub-lethal doses of fullerenes led to bio-accumulation in Daphnia with lethal consequences for Daphnia. Several types of nanoparticles (MgO, TiO_2, fullerenes and most notably Ag) were found to be bactericidal (Stoimenov *et al* 2002, Lee *et al* 2003). The concerns of wastewater treatment plants related to penalties for release of toxic waste harmful to aquatic organisms led to regulation of antibacterial nanosilver in the USA with a re-call of products such as washing machines or clothes using or containing nanosilver. Further claims were that nanosilver is highly toxic even in low concentrations and it accumulates in clams. There are several hypotheses to explain antibacterial working of nanoparticles. Since bacteria and spores are usually negatively charged because of the presence of carboxyl groups, they are electro-statically attracted to positively charged nanoparticles. Since many types of nanoparticles have sharp edges these by a simple act of abrasion cut through the walls of bacteria and thus physically destroy them (Stoimenov *et al* 2002).

It should be born in mind that most of the toxicological studies focused on a single type of nanoparticles. It is very likely that in natural environment, where many types of nanoparticles are present, various synergy effects

will take place. For example, the first type of nanoparticles would cut open the skin and the second type of nanoparticles, different for example in chemical composition, shape and surface charge from the first type of nanoparticles, would then cause damage to the human body.

At the present time there are several hundreds products containing nanoparticles available on the market but a few of them were tested for long-term effects on human body or environment.

4.3. Safety measures and risk assessment related to nanoparticles in power industry

Four areas of human exposure to nanoparticles have to be addressed when adopting safety measures in power engineering industry (Dreher 2004):

• production of power equipment. It is preferred to work with liquid suspensions, pastes or granules rather than dry powders, and fully closed rather than open manufacturing systems should be used.

• storage and transportation of nano-sized powders and liquid suspensions containing nanoparticles. The most common danger present spills, vapor leaks and fire during accidents.

• operation of equipment. Nanoparticles can be released into environment via mechanical abrasion, ablation (surface discharges, flashovers) or from equipment fires.

• end of equipment lifetime. Ecotoxicity of nanoparticles and sudden catalytic reaction with a risk of explosion in incinerators have to be considered during recycling and waste disposal of power equipment. Preparation of ionic solutions instead of solid nanoparticles and creation of microagglomerates may address these challenges.

It should be borne in mind that toxicity of materials depends on the magnitude and duration of exposure. Manufacturers of toxic materials follow several basic rules which can also be used for work with nanoparticles and nanomaterials. These are:

• minimize the number of people working with nanoparticles,
• minimize the time spent in environment with nanoparticles,
• maximize protection (wear nano-proof certified clothes and masks, use glove boxes),
• perform a toxicology study for a given nanomaterial by a renowned toxicological institute
• prepare material data sheets.

It is important to prevent formation of dust and aerosols in the workplace. A small underpressure in the working area is recommended to prevent escape of nanoparticles to other working areas. Ventilation systems are to be equipped with nanocertified filters to prevent outflow of nanoparticles to nature. Cleaning of the working place should be performed by moping up or extraction systems (special vacuum cleaners) but never with blowers.

In absence of clear rules some manufacturers perform measurements of nanoparticles in the ambient air in their facilities on a voluntary base. These measurements are usually carried out by certified health and safety authorities. It is important to realize that the number of nanoparticles in air may vary with the time of nanoparticle production and location in a factory.

Toxicology studies are usually expensive (from 50 kUSD to 5 000 kUSD, depending on the depth of such a study) and take several years but this cost is insignificant compared with the penalties paid by companies in asbestos victims trials where it was not unusual to pay several hundred millions US dollars per company.

A typical toxicological study should include (Oberdoerster *et al* 2005b, Tsuji *et al* 2006):

• detailed particle characterization.

This usually means measurements of spatially resolved chemical composition (coating, bulk), size distribution, agglomeration state with statement on deagglomeration tendencies, shape (spherical, irregular, rods, sharp edges), crystal structure, surface area, surface chemistry, surface charge, porosity, fiber flexibility, solubility, biopersistance, protein adsorption, and many others.

• exposure to at least three doses.

Long-term low-level exposure experiments are important because of possible accumulation of nanoparticles in human body.

• data interpretation against mass, surface area and number of nanoparticles.
• nano versus micro control study.

It is recommended that independent toxicological institutes perform such studies.

Since the field of nanotoxicology is relatively new and regulation is either entirely lacking or is in preparation there is a risk that small companies, which lack human and financial resources, would introduce products harmful to humans and ecosystem to financially benefit from the present lack of regulation without long term legal consequences (Schulte and Salamanca-Buentello 2007). Introduction of basic rules from the health and safety authorities is therefore necessary.

Insurance companies are only gradually becoming aware of potential risks related to nanoparticles and consequently their policies may not fully reflect the state of the art in the field of nanorisk assessment. However, the first certifiable nanorisk management and monitoring system has already been developed by an independent company [Innovation Society].

Many issues are still open. For example, labeling of products containing nanoparticles with the “Nano-inside” label. Some renowned companies, especially in the cosmetics industry, openly say that if nanolabelling would be required by legislative they would remove their products from the market. On the other hand, there are companies proudly using and displaying the word “nano” on their products as a marketing tool to increase sales even when the product does not contain any nanoparticles (nanoforum.org 2006).

Although the field of risk assessment related to short- and long-term human and environment exposure to nanoparticles is new, the awareness and first steps towards responsible use of nanoparticles has been made by governmental and also non-governmental organizations (OECD, ISO TC 229, CEN TC 352, NIOSH 2007, Dupont 2007, nanosafe, Meili *et al* 2007, VCI 2008, Aitken *et al* 2004, Riediger 2003). As a matter of fact, the pre-cautionary principle for new technologies is a part of the European Union Maastricht treaty (von Schomberg 2009). More detailed international and national regulation schemes will certainly follow and hopefully provide further guidance on how to use the nanotechnology in a safe and responsible way.

References

Afshari A, Matson U, Ekberg LE (2005) Characterisation of indoor sources of fine and ultrafine particles: a study conducted in a full-scale chamber, Indoor Air 15: 141-150

Aitken RJ, Creely KS, Tran CL (2004) Nanoparticles: An occupational hygiene review – Research Report 274, Institute of Occupational Medicine, United Kingdom

Baroli B, Ennas MG, Loffredo F, Isola M, Pinna R, Lopez-Quintela MA (2007) Penetration of metallic nanoparticles in human full-thickness skin, Journal of

Investigative Dermatology 127:1701-1712
Borm PJA, Robbins D, Haubold S, Kuhlbusch T, Fissan H, Donaldson K, Schins R, Stone V, Kreyling W, Lademann J, Krutmann J, Warheit D, Oberdoerster E (2006) The potential risks of nanomaterials: a review carried out for European Center for Exotoxicology and Toxicology of Chemicals, Particle and Fibre Toxicology 3: 11-46
Calderon-Garciduenas L, Azzarelli B, Acuna H, Garcia R, Gambling TM, Osnaya N, Monroy S, Del Rosario Tizapantzl M, Carson JL, Villarreal-Calderon A, Rewcastle B (2002) Air pollution and brain damage, Toxicologic pathology 30: 373-389
CEN TC 352 – European Committee for Standardisation Technical Committee 352 Nanotechnologies, Principles for the oversight of nanotechnologies and nanomaterials, Document N65
Donaldson K, Li XY, MacNee W (1998) Ultrafine (nanometer) particle mediated lung injury, Journal of Aerosol Science 29-5/6: 553-560
Donaldson K, Tran LC (2004) An introduction to the short-term toxicology of respirable industrial fibres, Mutation Research 553:5-9
Dreher KL (2004) Toxicological highlight - Health and environmental impact of nanotechnology: Toxicological assessment of manufactured nanoparticles, Toxicological Sciences 77: 3-5
Dupont (2007) Nano risk framework
Gatti AM, Rivasi F (2002) Biocompatibility of micro- and nanoparticles. Part I: in liver and kidney, Biomaterials 23: 2381-2387
Gatti AM (2004) Biocompatibility of micro- and nanoparticles in the colon. Part II, Biomaterials 25: 385-392
Geiser M, Rothen-Rutishauser B, Kapp N, Schuerch S, Kreyling W, Schulz H, Semmler M, Hof VI, Heyder J, Gehr P (2005) Ultrafine particles cross cellular membranes by nonphagocytic mechanisms in lungs and in cultured cells, Environmental Health Perspectives 113-11:1555-1560
Gurr JR, Wang ASS, Chen CH, Jan KY (2005) Ultrafine titanium dioxide particles in the absence of photoactivation can induce oxidative damage to human bronchial epithelial cells, Toxicology 213: 66-73
Harrison RM, Yin J (2000) Particulate matter in the atmosphere: which particle properties are important for its effects on health?, The Science of the Total Environment 249: 85-101
He C, Morawska L, Taplin L (2007) Particle emission characteristics of office printers, Environmental Science and Technology 41: 6039-6045
Hoet PHM, Brueske-Hohlfeld I, Salata OV (2004) Nanoparticles – known and unknown health risks, Journal of Nanobiotechnology 2: 12-27
Innovation Society Ltd - www.inovationgesellschaft.ch
ISO TC 229 – International Organisation for Standardisation Technical Committee 229 Nanotechnologies
Jaques PA, Kim CS (2000) Measurement of total lung deposition of inhaled ultrafine particles in healthy men and women, Inhalation Toxicology 12: 715-731
Jani PU, Florence AT, McCarthy DE (1992) Further histological evidence of the gastrointestinal absorption of polystyrene nanospheres in the rat, International Journal of Pharmaceutics 84:245-252
Jani PU, McCarthy DE, Florence AT (1994) Titanium dioxide (rutile) particle uptake from the rat GI tract and translocation to systemic organs after oral administration, International Journal of Pharmaceutics 105:157-168
Jung M, Davis WP, Taatjes DJ, Chrug A, Mossman BT (2000) Asbestos and cigarette smoke cause increased DNA strand breaks and necrosis in bronchiolar epithelial cells in vivo, Free Radical Biology and Medicine 28-8:1295-1299
Kühling, W, Aus dem Labor auf den Teller – Die Nutzung der Nanotechnologie im Lebensmittelsektor, Bund für Umwelt und Natutschutz
Lee HJ, Yeo SY, Jeong SH (2003) Antibacterial effect of nanosized silver colloidal solution on textile fabrics, Journal of Materials Science 38: 2199-2204
Lovern SB, Strickler JR, Klaper R (2007) Behavioral and physiological changes in Daphnia magna when exposed to nanoparticle suspensions (titanium dioxide, nano-C_{60} and $C_{60}HxC_{70}Hx$), Environmental Science and Technology 41-12:4465-4470
Maynard AD, Kuempel ED (2005) Airborne nanostructured particles and occupational health, Journal of Nanoparticle Research 7: 587-614
Maynard AD, Aitken RV (2007) Assessing exposure to airborne nanomaterials: current abilities and future requirements, Nanotoxicology 1-1:26-41
Meili C, Widmer M, Husmann F, Gehr P, Blank F, Riediker M, Schmid K, Start W (2007) Synthetische nanomaterialen: Riskobeurteilung und Risikomanagement – Grundlagenbericht zum Aktionsplan, Bundesamt fuer Umwelt und Bundesamt fuer Gesundheit, Switzerland
nanoforum.org (2006) Nanotechnology in consumer products
nanosafe – Safe production and use of nanomaterials – www.nanosafe.org
Nel A, Xia T, Maendler L, Li N (2006) Toxic potential of materials at the nanolevel, Science 311: 622-627
Nemmar A, Hoet PHM, Vanquickenborne B, Dinsdale D, Thomeer M, Hoylaerts MF, Vanbilloen H, Mortelamns L, Nemery B (2002) Passage on inhaled particles into the blood circulation in humans, Circulation 105:411-414
NIOSH (2007) Progress toward safe nanotechnology in the workplace, Department of Health and Human Services, Centers for disease control and prevention,
National Institute for Occupational Safety and Health, USA
Nohynek, G, Lademann J., Ribaud C, Roberts M.S. (2007) Grey goo on the skin? Nanotechnology, cosmetic and sunscreen safety, Critical Reviews in Toxicology, 37: 251-277
Oberdoerster G, Sharp Z, Atudorei V, Elder A, Gelein R, Kreyling W, Cox C (2004) Translocation of inhaled ultrafine particles to the brain, Inhalation Toxicology 16:437-445
Oberdoerster G, Oberdoerster E, Oberdoerster J (2005a) Nanotoxicology: an emerging discipline evolving from studies of ultrafine particles, Environmental Health Perspectives 113: 823-839
Oberdoerster G, Maynard A, Donaldson K, Castranova V, Fitzpatrick J, Ausman K, Carter J, Kan B, Kreyling W, Lai D, Olin S, Monteiro-Riviere N, Warheit D, Yang H (2005b) Principles for characterizing the potential human health effects from exposure to nanomaterials: elements of screening strategy, Particle and Fibre Toxicology 2: 8-43
Oberdoerster G, Stone V, Donaldson K (2007) Toxicology of nanoparticles: a historical perspective, Nanotoxicology, 1-1: 2-25
OECD – OECD database on research into the safety of manufactured nanomaterials – www.oecd.org/env/nanosafety/database
Reijnders L (2006) Cleaner nanotechnology and hazard reduction of manufactured nanoparticles, Journal of Cleaner Production 14: 124-133
Riediger G (2003) Ultrafeine Aerosole an Arbeitsplaetzen – BIA Report 7/2003, Berufsgenossenschaftliches Institut fuer Arbeitschutz, Germany
Ryman-Rasmussen JP, Riviere JE, Monteiro-Riviere NA (2006) Penetration of intact skin by quantum dots with diverse physicochemical properties, Toxicological Sciences 91-1:159-165
Schomberg, von R. (2009) Challenges for governance of nanotechnologies and the European Code of conduct for responsible nanoscience and nanotechnology research, Framing nano governance platform, National Conference, Bern, Switzerland
Schulte PA, Salamanca-Buentello F (2007) Ethical and scientific issues of nanotechnology in the workplace, Environmental Health Perspectives 115-1:5-12
Shi JP, Evans DE, Khan AA, Harrison RM (2001) Sources and concentrations of nanoparticles (<10 nm diameter) in the urban atmosphere, Atmospheric Environment 35: 1193-1202
Stoimenov PK, Klinger RL, Marchin GL, Klabunde KJ (2002) Metal oxide nanoparticles as bactericidal agents, Langmuir 18: 6679-6686
Tsuji JS, Maynard AD, Howard PC, James JT, Lam CW, Warheit DB, Santamaria AB (2006) Research strategies for safety evaluation of nanomaterials, Part IV: Risk assessment of nanoparticles, Toxicological Sciences 89-1: 42-50
VCI – Verband der Chemischen Industrie (2008) Responsible production and use of nanomaterials
Yang L, Watts DJ (2005) Particle surface characteristics may play an important role in phyto-toxicity of alumina particles, Toxicology Letters 158:122-132

5. Prospect of Industrial Applications

Insulation materials play an important role in heavy electric apparatuses and cables, and the properties of them sometimes dominate the designing of apparatuses and cables. The insulation materials commonly contain micro-scale inorganic fillers to obtain indispensable properties for electric apparatuses and cables. Recently, nanocomposites, which are composed of nano-scale fillers and polymers, attract much attention in the insulation material field, because many studies have shown that the nanocomposites have advantages compared to conventional materials. Moreover, industrial applications are becoming primary interest in the nanocomposite research. Main contribution of this chapter is to show perspective of industrial applications in the nanocomposites.

5.1. Switchgears

5.1.1. Development of Environmentally-conscious Switchgear

Sulfur hexafluroride (SF_6) gas has excellent chemical stability, insulation and interruption properties. The SF_6 gas insulation system has contributed to high-voltage and downsize of the switchgears. However, the greenhouse effect of SF_6 gas is approximately 24,000 times as large as CO_2 gas (Houghton et al. 1996). SF_6 gas was designated as a greenhouse gas in the 1997 Kyoto protocol on global warming.

Electric power industry is the largest consumer of the SF_6 gas. The effect of the SF_6 gas on an increase of ambient temperature was estimated in Figure 5.1.1(IEEJ 1999). However, the SF_6 gas emissions into the atmosphere are strictly controlled at present. The gas insulated switchgears are still expected to continue to be the mainstream apparatuses for the future. On the other hand, the electric power industry is positively working to reduce SF_6 gas use. For example, the environmentally-conscious switchgear with compressed dry-air insulation system has already been developed as shown in Figure 5.1.2(Matsui et al. 2005). Moreover, development of CO_2 gas insulation(Uchii at al. 2004) and solid insulation system(Shimizu et al .2003) has been conducted as alternative insulation systems.

5.1.2. Solid Insulated Switchgear with Nanocomposites

The solid insulation systems have attracted attention because of its downsizing of switchgears as well as its SF_6 gas free system. Solid insulation systems need the materials with thermal, mechanical and insulation properties that are superior to those of conventional materials. An effective approach to meeting the demand for high performance materials has focused on polymer nanocomposites. Many studies have shown that addition of a few weight-percentages of nano-scale fillers improves the dielectric and insulation properties in the nanocomposites (Tanaka et al. 2004). Therefore, the nanocomposites are leading candidates for realizing solid insulation systems.

In the solid insulation system, high-voltage components of the switchgear (e.g. metal conductor and vacuum interrupter) are molded with epoxy-based insulation material as shown in Figure 5.1.3(Imai 2006). A large difference between the thermal expansion coefficients causes exfoliation at component/insulation material interfaces due to thermal-cycling. Therefore, the epoxy-based insulation material is commonly filled with a large amount of micro-scale fillers (e.g. silica or alumina) to achieve the same low thermal expansion as the components.

However, the nanocomposites have much larger thermal expansion coefficients than those of the components, because they have only a few weight-percentages of nano-scale fillers. Thus, nano- and micro-filler mixed composite (NMMC), which has a few weight-percentages of nano-filler and approximately 60 weight-percentages of micro-silica fillers in epoxy resin, has been developed in recent years.

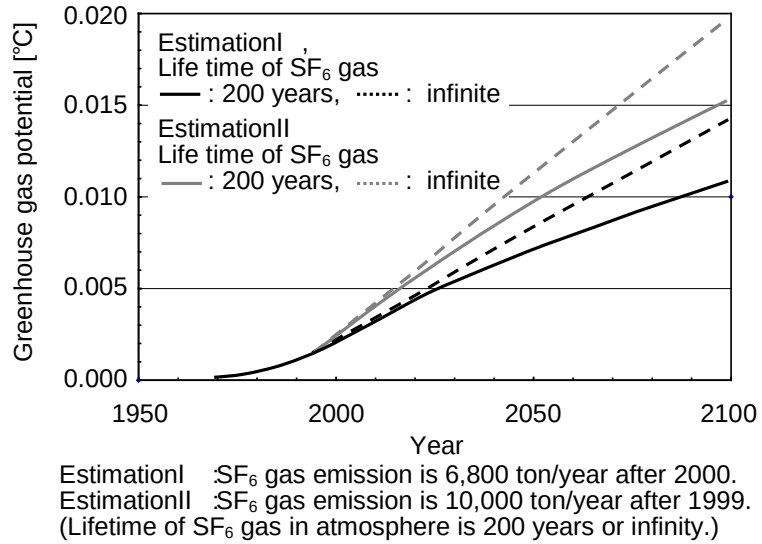

Figure 5.1.1 Estimation of greenhouse potential due to SF_6 gas in the world. (IEEJ 1999)

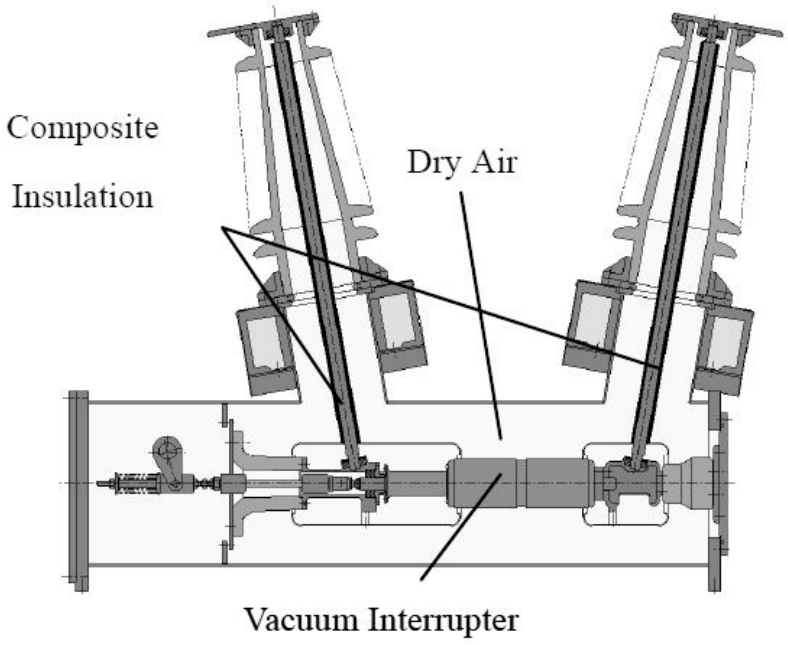

Figure 5.1.2 Cross-section of 72/84kV environmentally-conscious switchgear using compressed dry-air insulation system.(Matsui et al. 2005)

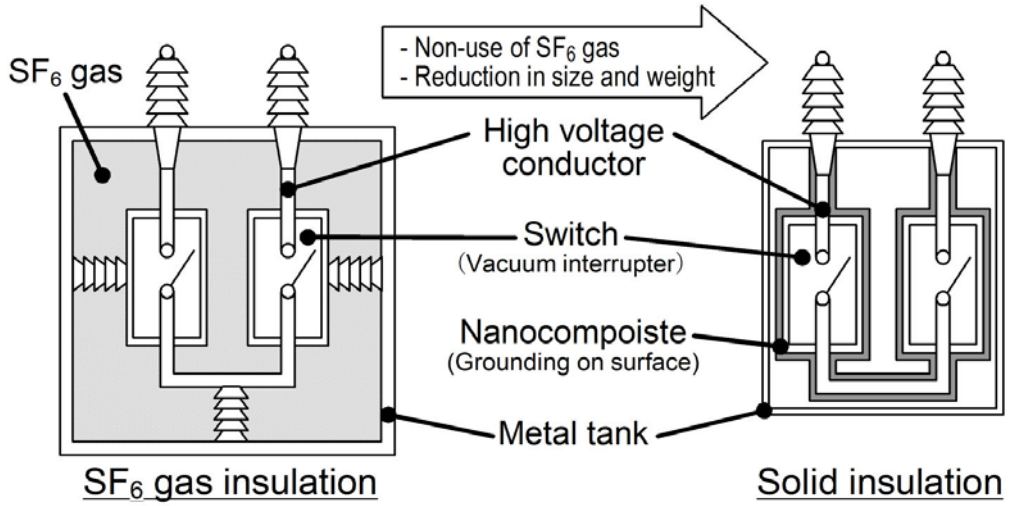

Figure 5.1.3 Environmentally-conscious switchgear using solid insulation system.
(Imai 2006)

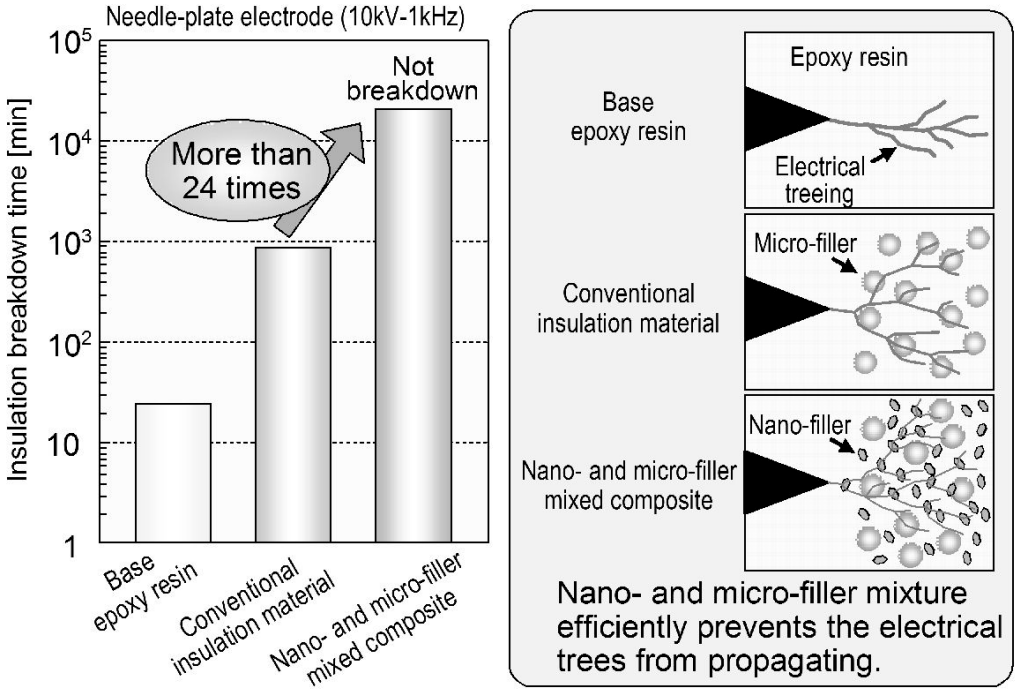

Figure 5.1.4 Improvement of Insulation breakdown time in nano- and micro-filler mixed composite.
(Imai 2006)

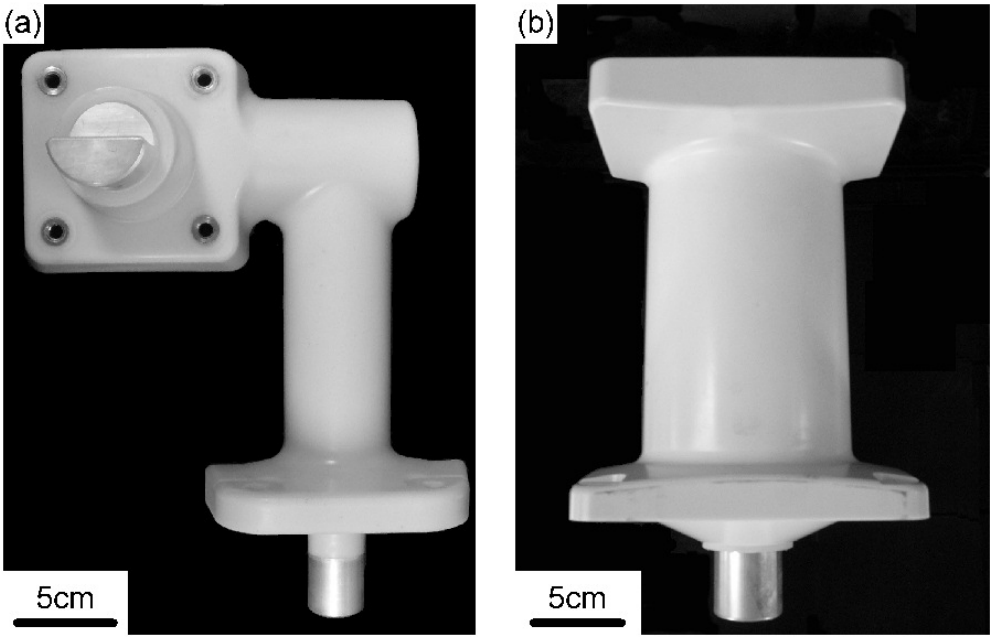

Figure 5.1.5 Full-scale trial models molded with nano- and micro-filler mixed composite,

(a) Molded connecting conductor, (b) Molded vacuum interrupter.(Imai et al. 2008)

The NMMC has the same low thermal expansion as the components. Moreover, the NMMC has more than 24 times longer insulation breakdown time that that of conventional insulation material (approximately 60 weight-percentages of micro-silica fillers loading in epoxy resin) as shown in Figure 5.1.4(Imai 2006). The nano-fillers in the NMMC increase the frequency of encountering between electrical treeing and fillers more than the conventional insulation material. It is assumed that an increase in encountering frequency by nano- and micro-filler mixture efficiently prevents the trees from propagating. The result is that the insulation breakdown time is improved in the NMMC.

In addition, full-scale trail models, which are an aluminum conductor and a vacuum interrupter molded with the NMMC, were reported as shown in Figure 5.1.5(Imai et al. 2008). Next work will be to evaluate the NMMC in the full-scale trial models.

References

Houghton JT, Meira Filho LG, Callander BA et al. (1996) Climate Change 1995, Intergovernmental Panel on Climate Change (IPCC), Cambridge University Press 22

Imai T (2006) Nanocomposite insulation materials for environmentally- conscious heavy electric apparatuses, Toshiba Review 61-12:60-61 (in Japanese)

Imai T, Komiya G, Murayama K et al. (2008) Improving Epoxy-based Insulating Materials with Nano-fillers toward Practical Application, Proceeding of IEEE International Symposium on Electrical Insulation (ISEI):201-204

Matsui Y, Saitoh H, Nagatake K, et al.(2005) Development of Eco-Friendly 72/84kV Vacuum Circuit Breakers, Proceeding of International Symposium on Electrical Insulating Materials (ISEIM):679-682

Shimizu T, Kinoshita S, Makishima S et al. (2003) Material and Simulation Technology for Solid Insulated Switchgear, IEEE 7th Intern. Conf. Properties and Application of Dielectric Materials (ICPADM) S22-5:1194-1197

Tanaka T, Montanari GC, Mülhaupt R (2004) Polymer Nanocomposites as Dielectrics and Electrical Insulation-perspectives for Processing Technologies, Material Characterization and Future Applications, IEEE Trans. Dielectr. Electr. Insul. 11-5:763-784

The Institute of Electrical Engineers of Japan (IEEJ) (1999) Investigation R&D Committee, The 1999 Annual Meeting Record S3 (in Japanese)

Uchii T, Hoshina Y, Miyazaki at al. (2004) Development of 72kV Class Environmentally-Benign CO_2 Gas Circuit Breaker Model, IEEJ Trans. PE, Vol.124, No.3:476-484 (in Japanese)

5.2. High Voltage DC Power Cables

5.2.1. Advantages of DC Power Transmission and Transition of High Voltage DC Power Cable

DC power transmission has many advantages as listed below.

1) Compact facilities of the electric transmission and low construction cost

2) Enlargement of the transmission capacity based on the high stability compared to the AC power transmission

3) Easy interconnection of power systems unaffected by the deference of system rating

4) Interconnection of power systems without the increment of short-circuit capacity of AC system

5) Quick control of the power flow and easy operation

6) Ability of full power transmission up to the temperature limitation

Since the operation start-up in 1954 of the world's first project, -100kV long distance dc power transmission between the mainland and Gotland of Sweden using submarine cable, many project of the dc power transmission are carried out, and the capacity growth has been promoted as shown in Figure 5.2.1 (IEEJ 1999).

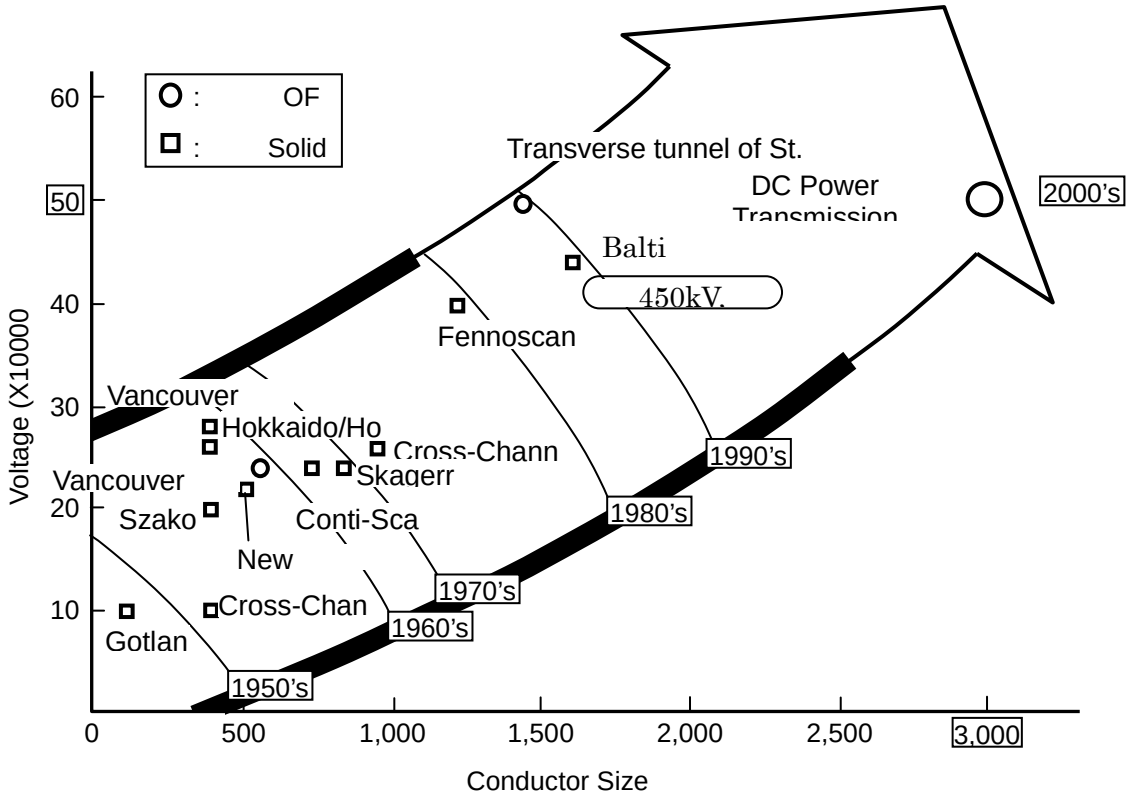

Figure 5.2.1 Capacity growth of dc power cable (IEEJ 1999)

Although the oil-impregnated paper cables (oil-impregnated paper solid cable, GF cable, OF cable) were used as the existing high voltage dc power cable, the cross-linked polyethylene (XLPE) cable was studied for the advantages of the low environmental risk of the oil-spill and the reduction of the oiling equipments.

To apply the XLPE cable as the ultra high voltage dc cable, there are many problems as shown bellow.

1) Low dc breakdown strength under high-temperature, and the large dependence of breakdown strength for the thickness

2) Large breakdown strength deterioration for the reversal of polarity and/or the superimposition of the dc voltage or the reverse polarity lightning impulse voltage.

As the space charges formed in the bulk of XLPE have a big influence to these problems, some improvement methods as shown bellow are investigated.

1) Use of the additives / fillers

- XLPE filled with the polar inorganic filler (Maekawa 1991) (Terashima et al. 1998) (Maekawa et al. 2002)
- XLPE filled with the conducting inorganic filler (Ogata et al. 1990)

2) Reformulation of the polymer

- Polar group introduced XLPE (Terashima et al. 1997)
- Denatured HDPE (Suzuki et al.1992)

The development of 500kV DC XLPE cable using the nano-compositised XLPE with the polar inorganic filler is introduced bellow.

5.2.2. Application of nano-composite to the dc cables

The improvement of the dc insulation property was attempted by mixing the inorganic micro-filler. [(2)] While the dc insulation property was improved for this attempt, the lightning impulse voltage became lower than the usual ac XLPE cables.

The various improvements, as the filler miniaturization from micro to nano-size, lead to the present nano-composite material improved the lightning impulse resistance. The 500kV dc submarine XLPE cable listed in Table 5.2.1 was developed (Maekawa et al. 2002) by using this XLPE nano-composite with considering the influence of the space charge (Terashima et al. 1999). Figure 5.2.2 shows the developed 500kV dc submarine cable (Maekawa et al. 2002). Here the cable has the lead sheath and the steel wire arming. The operation voltage and the size of this cable are highest in the world as the solid insulated dc power cable.

The cable-joint is also developed using the developed nano-composite material. The test cable line involving the joint was evaluated by the tensile test which simulated the mechanical influence of the submarine construction, the test of the initial performance and the test of long-term performance. Here the dc voltage withstand test, the lightning impulse voltage withstand test and the lightning impulse voltage breakdown test were carried out as the initial performance test. The long-term voltage energization test, the dc and reverse polarity lightning impulse voltage withstand test, the dc voltage withstand test, the lightning impulse voltage withstand test and the lightning impulse voltage breakdown test were carried out as the long-term performance test. The results of these tests as shown in Table 5.2.2 and 5.2.3 prove that the developed 500kV dc submarine XLPE cable has the enough insulation properties for the dc and lightning impulse voltage in the actual use (Maekawa et al. 2002).

Table 5.2.1 Specification of dc 500kV submarine XLPE cable

Items		Unit	Value
Conductor	Nominal Size	mm^2	3000
	Specification	-	5 Divide Compressed Circularity
	Outer Diameter	mm	67.0
Inner Semiconducting Layer	Thickness	ca mm	2.5
Insulator	Nominal Thickness	mm	23.0
Outer Semiconducting Layer	Thickness	ca mm	1.0
Water Prevention	Thickness	ca mm	1.0
Lead Sheath	Thickness	mm	4.5
PE Corrosion Proof Layer	Thickness	mm	6.0
	Outer Diameter	ca mm	143.0
Inner PP Yarn	Thickness	ca mm	2.0
Steel Wire Arming	Wire Diameter	mm	8.0
	Number of Wire	-	56
Outer PP Yarn	Thickness	ca mm	4.5
Cable	Outer Diameter		172
	Mass in air	ca kg/km	83.900
	Mass in water	ca kg/km	60.700

Source: (Maekawa et al. 2002)

Figure 5.2.2 500kV dc submarine XLPE cable (Maekawa et al. 2002)

Table 5.2.2 Initial property test results of full-scale cable

Items	Condition	Result
Tensile Test	15t x 3 times	Normal
DC Voltage Withstand Test	-1,200kV 6h (90℃)	Good
Lightning Impulse Voltage Withstand Test	-1,355kV 3 times (90℃)	Good
Lightning Impulse Voltage Breakdown Test	-1,400kV～ (90℃) -50kV step / 3 times	-2,050kV Breakdown at cable part

Source: (Maekawa et al. 2002)

Table 5.2.3 Long-term property test results of full-scale cable

Items	Condition	Result
Tensile Test	20t x 3 times	Normal
Long-term Voltage Energization Test	700kV x 101 days (H/C, with reversal of polarity)	Good
Residual Performance Test	Conductor Temp. 90℃	
DC and Reverse Polarity Lightning Impulse Voltage Withstand Test	Pre-Energization +/-500kV Overload Cycles	Good
DC Voltage Withstand Test	+/- 500kV 3h	Good
Lightning Impulse Voltage Withstand Test	+/-1,250kV 3 times	Good
Lightning Impulse Voltage Breakdown Test	-1,250kV ～ -50kV step / 3 times	-1,950kV Breakdown at cable part

Source: (Maekawa et al. 2002)

A 45 kilometers submarine cable project is planned for connecting Hokkaido Island and Honshu Main Land in a turn-key basis by Electric Power Development Co., Ltd. DC ±250kV XLPE cable shall be applied for this project. The application of XLPE cable for DC transmission is the first project in Japan and, 250kV is the highest voltage for DC XLPE cable in the world for commercial use. Moreover, this cable allows the polarity reverse operation, and this is also first in the world. J-Power Systems Corporation is concentrating its resources on this project aiming start of operation in 2011 (J-Power Systems 2009). It is probable that nanocomposite XLPE insulation will be utilized for this project. It is partly based on the experimental results as demonstrated in a literature (Murata et al. 2005).

Reference

IEEJ (1999) Technological Trend and Future Problem of DC Power Cable, IEEJ Technical Report, No.745

J-Power Systems (2009) http://www.jpowers.co.jp/pr/090427_2/090427_2_e.pdf

Maekawa Y, Yamaguchi A, Ikeda C, Sekii, Hara M (1991) Research and Development of DC XLPE Cables, Proceeding of Jicable 91, B.9.3: 562-569

Maekawa Y, Yamanaka T, Kimura T, Murata Y, Katakai, Matsunaga O (2002) DC 500kV Submarine XLPE Cable, Hitachi Cable Densen, No.21: 65-72

Murata Y, Murakami Y, Nemoto M, Sekiguchi1 Y, Inoue1 Y, Kanaoka M, Hozumi N, Nagao M (2005) Effects of Nano-sized MgO-filler on Electrical Phenomena under DC Voltage Application in LDPE, Annual Rpt. IEEE-CEIDP 2C-4: 158-161.

Ogata S, Maekawa Y, Terashima K, Yoshida S, Yamanouchi H, Yokoyama S (1990) Electric Properties of DC XLPE Cable, Fujikura Technical Review, No.79: 32-39

Suzuki K, Niwa T, Takahashi T, Miyata H (1992) Development of Polymer Insulating Material for DC Power cable (II), IEEJ Trans. PE, 112-10: 914-920

Terashima K, Kawakami S, Muto S, Ichiyanagi N (1997) Fundamental Development of DC Solid Insulated Cable", Annual Meeting Record of IEEJ, No.7: 203 -204

Terashima K, Suzuki H, Hara M, Watanabe K (1998) Research and Development of +/- 250kV DC XLPE Cable, IEEE Trans. on Power Delivery, 13-1: 7-16

Terashima K, Murata Y, Muto S, Uozumi T, Yoshida M (1999) Study of Design Method of XLPE Cable for DC Voltage, IEEJ Trans. PE, 119-2: 212-222

5.3. Enameled Wires

5.3.1. Degradation of Enameled Wire Due to Inverter-surge

From the benefits of the high energy efficiency and the easy maintenance, the variable speed control of the electric motor using the inverter has been increased significantly. Accompanied with the prevalence of motors controlled by the inverter, the problem of surge voltage arising from the inverter has become intensified.

The high frequency components of the inverter switching pulse voltage lead to the over-voltages due to the impedance of the cable between the inverter and the motor as shown in Figure 5.3.1 (Imai et al. 2007). The over-voltages, which are called "inverter-surge", induce partial discharges (PDs) between adjacent enameled wires, and the PDs erode the coating of enameled wire as shown in Figure 5.3.2 (Imai et al. 2007). In particular, thin enamel film coated on the wire conductor has been easily degraded by the PDs in low voltage motors with random winding coils. As a result, the life of the motor is shortened by increasing aging rates.

Consequently inverter-fed motors demand the enameled wires with high-resistance to the PDs. Developments of the enameled wires using nanocomposite materials have been conducted (Imai et al. 2007)(Kikuchi 2004)(Kikuchi et al. 2006)(Ozaki et al. 2005).

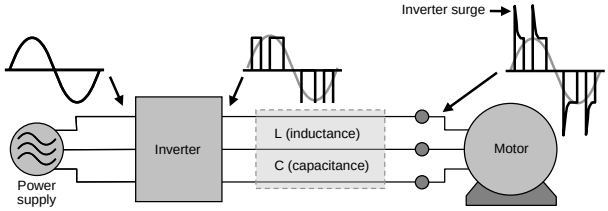

Figure 5.3.1 Induced over-voltages in Inverter-fed motors.

(Imai et al. 2007)

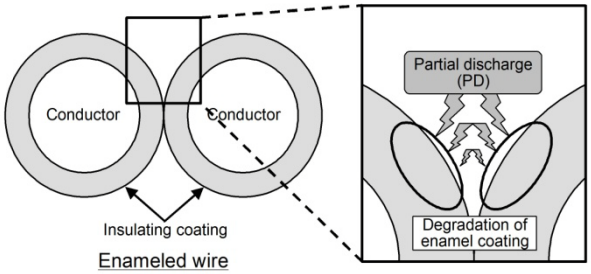

Figure 5.3.2 Degradation of enameled wire due to partial discharges.

(Imai et al. 2007)

5.3.2. Inverter-surge Resistant Wire with Nanocomposite Coating

Nanocompsoite enameled wire, which has excellent resistance to the PDs, was developed by Hitachi Magnet Wire Corporation(Kikuchi 2004)(Kikuchi et al. 2006). The enameled wire is composed of inner coating with polyester-imide/silica nanocomposite and outer coating with polyamide- imide as shown in Figure 5.3.3.

Insulation breakdown time of the nanocomposite enameled wire under 10kHz sinusoidal voltages is shown in Figure 5.3.4. The nanocomposite enameled wire has longer insulation breakdown time than that of the conventional enameled wire.

In the inner coating of the nanocomposite enameled wire, silica nano-fillers are formed by the sol-gel (in-situ) method, and transmission electron microscope (TEM) observation demonstrates that silica nano-fillers are dispersed homogeneously. Silica nano-fillers have PD resistance superior to polymer materials. Therefore, the silica nano-fillers in the coating prevent PD erosion efficiently, and the nanocomposite enameled wire has excellent resistance to the PDs compared to the conventional enameled wire. In particular, at low voltage such as 1.13kV, the nanocomposite enameled wire shows more than 1,000 times longer breakdown time than that of the conventional enameled wire.

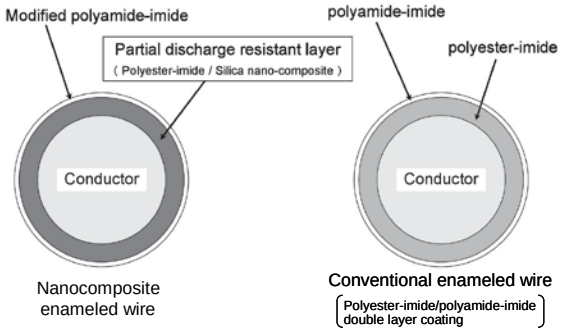

Figure 5.3.3 Cross section structure of nanocomposite enameled wire.

(Kikuchi et al. 2006)

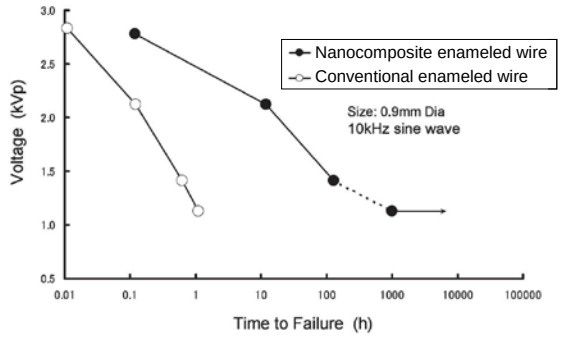

Figure 5.3.4 Comparison of insulation breakdown time of nanocomposite and conventional enameled wires.

(Kikuchi et al. 2006)

Toshiba Corporation and Unimac Ltd. also developed the nanocomposite enameled wire with nano-clay dispersed coating(Imai et al. 2007) (Ozaki et al. 2005). Cross-section after polymer removing of coating by plasma etching technique was observed by scanning electron microscope (SEM). The SEM micrograph shows that the nanocomposite coating comprises a densely-packed structure with nano-clays, as shown in Figure 5.3.5. Moreover, the nano-clays seem to be arranged in parallel to the conductor surface due to the manufacturing process of the enameled wire.

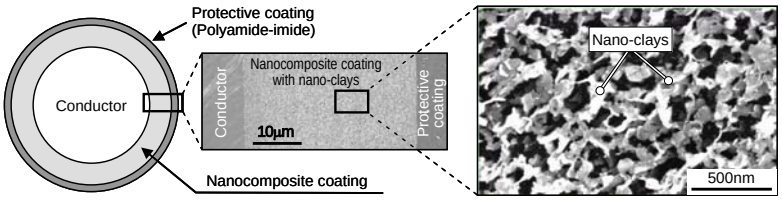

Figure 5.3.5 SEM micrograph of nanocomposite coating.

(Imai et al. 2007)

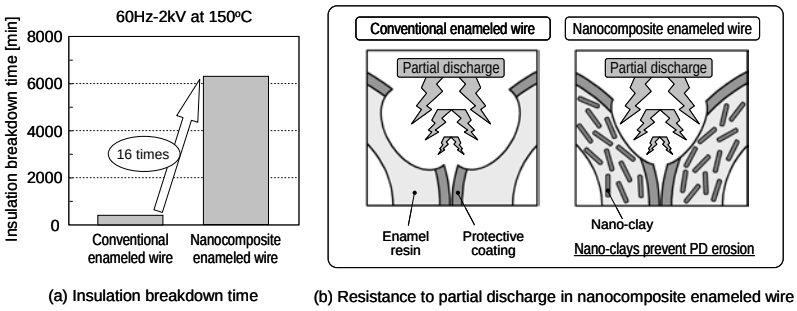

Figure 5.3.6 Comparison of insulation breakdown time between nanocomposite and conventional enameled wire.

(Imai et al. 2007)

Flexibility is one of the important properties for the enameled wire, because the enameled wire is usually used in random winding coil. To evaluate the flexibility of the wire, the crack number of the wire surface was measured when it was wound up 100 turns around itself. The nanocompsoite enameled wire had no cracks as same as the conventional enameled wire, which indicates that the nanocomposite enameled wire has sufficient flexibility.

Furthermore, Figure 5.3.6-(a) compares the insulation breakdown time between the nanocomposite and conventional enameled wire under 60Hz-2kV at 150^{o}C. The twisted specimen of the nanocomposite enameled wire has 16 times longer insulation breakdown time than that of the conventional enameled wire. The nano-clyas in the coating prevent PD erosion efficiently. In particular, the plate-shaped and oriented nano-clays seem to enable the nanocomposite enameled wire to have excellent resistance to PDs as shown in Figure 5.3.6-(b).

References

Imai T, Sawa F, Ozaki T et al (2007) Expected Materials for the Future 7-7:6-13 (in Japanese)

Kikuchi H (2004) Inverter Surge Resistance Enameled Wire Applied Nano-composite Insulating Material" , The Papers of Technical Meeting on Dielectrics and Electrical Insulation, IEE Japan DEI-04-77:29-34 (in Japanese)

Kikuchi H, Asano K (2006) Development of Organic/inorganic Nano-composite Enameled Wire, IEEJ Trans. PE, 126-4:460-465 (in Japanese)

Ozaki T, Imai T, Sawa F et al (2005) Partial Discharge Resistant Enameled Wire, Proceeding of International Symposium on Electrical Insulating Materials (ISEIM):184-187

5.4. Rotating Machines

5.4.1. Low Voltage Rotating Machines with Random Coil

Some polymer nanocomposites has been commercialized in the field of the rotating machines such as motors and generators. Some examples are followings.

Recently, in the low voltage rotating machines with random coil, the risk of the partial discharge (PD) by inverter surge is arising. IEC is planning the new international testing standard to manage the reliability of the insulation in the inverter-fed motors. According to its specifications, no partial discharge throughout their service life is the only criterion in using conventional enamel wire. This standard will be approved.

On the other hand, some surge-resistant enameled wires derived from the nanocomposite material technology are commercialized. This nanocomposite based surge-resistant wires exhibit superior PD resistant properties to conventional wires. In the F type insulation, the three products of polyester-imide (PEI) based surge-resistant wire, KMKED (Kikuchi et al. 2008), UMW-T(Ozaki et al. 2005) and VOLTRON^{TM} , have been commercialized.

As shown In Figure 5.4.1, the results of voltage endurance life test of the four types of enamel wires were reported by University of Hyogo and TOSHIBA MITSUBISHI-ELECTRIC INDUSTRIAL SYSTEMS CORPORATION. The tested wires are UMW-T (A), KMKED (B) and two conventional enamel wires(C), (D) (Uozumi et al. 2007). Their respective diameters are almost the same. To simulate the mechanical stress of wires in motor manufacturing process, twisted pair specimens were made with 10% elongation. Applied frequency was 1 kHz. The nanocomposite surge-resistant wires ((A) or (B)) exhibit excellent voltage endurance life which is sixty times longer than conventional wire ((C) or (D)) at 10 % probability of failure.

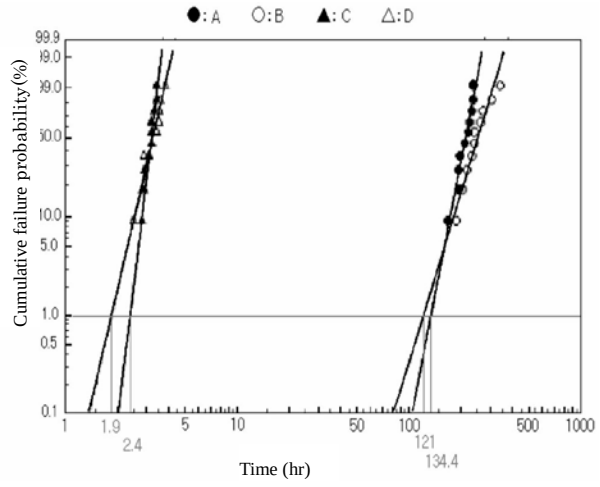

Figure 5.4.1 Voltage endurance test results of KMKED and UMW-T surge-resistant voltage wire. (Time (hr) vs Probability of Failure (%)) (Uozumi et al. 2007)

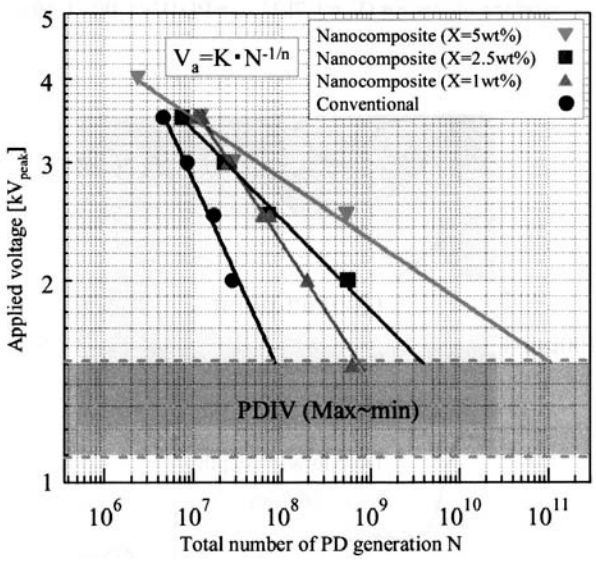

Figure 5.4.2 V-N curveture of the nanocomposite wire.
(Nakamura et al. 2008)

The research group of Nagoya University and Toshiba Corporation is studying about the effect of the filler content and inverter surge voltage on the life of PEI nanocomposite surge-resistant wire. They concluded that the life of nano wire at PD inception voltage (PDIV) is one thousand times longer than that of conventional wire as shown in Figure 5.4.2 (Yoshimitsu et al. 2007)

VOLTRON™ is the PEI nanocomposite wire developed by DuPont. The comparison among four type wires, one conventional wire and three surge-resistant wires is shown in Figure 5.4.3. For each specimen, the right bar shows the result with 10% mechanical elongation and the left bar means without any mechanical stress. All specimens were applied 16kHz inverter voltage at 155℃ in air. This result indicates that VOLTRON has much higher reliability than conventional or recent surge-resistant wire under the mechanical stress.

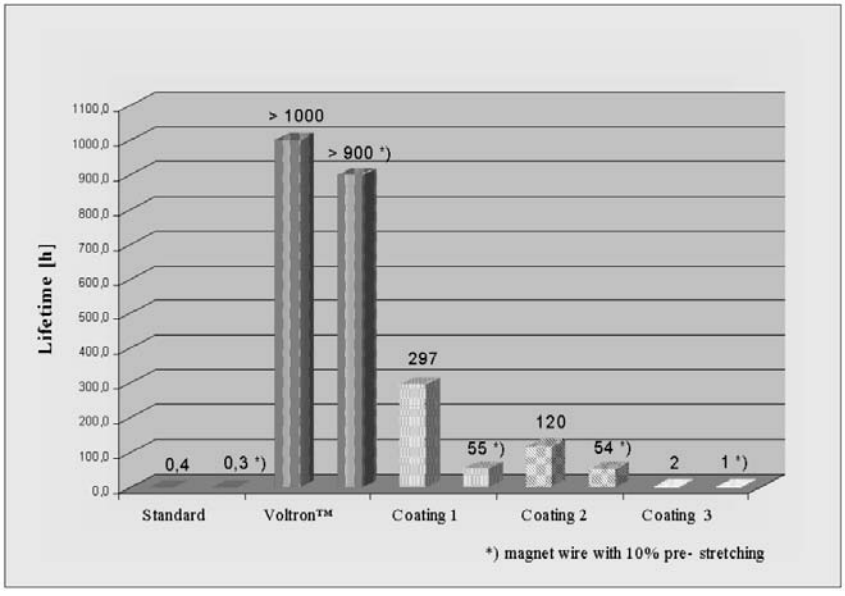

Figure 5.4.3 Lifetime of the VOLTRON wire. (Boehm 2007)

5.4.2. IEC standards and the applicability of the nanocomposite wire to the commercial machines

As described above, it could be possible that the rotating machines with surge-resistant nanocomposite wire can be operated without electrical failure during their service life. This aspect has been discussed in the JEMA WG-`Insulation of rotating machines` and this WG made a comment on the IEC standard that the point of designing and manufucturing rotaing machines in PD detection level should be open to futher discussion. Up to now, the revised provision including the above sentence was presented from JEMA to IEC, and it is being discussed in international level. If the revised provision is adopted, manufacturers can design and manufucture inverter-fed motors with random coil in PD (generated from inverter surge) inception level under the condition of using nanocomposite wire.

5.4.3 .High Voltage Rotating Machines with Formed Coil

In the case of high voltage and high capacity rotating machines with formed coil, inverter-fed drive is increasing. It is pointed out that the turn-to-turn insulation, main wall insulation and partial discharge protection layer are degraded specially in the formed coil when drove in inverter-fed mode. The application of nanocomposite to these materials will be expected because it increases performance and reliability of products. In the aspect of thermal conductivity, if high thermal conductive insulation material is produced by nanocomposite technology, it will be widely used because of realizing compact machine or simple structure of cooling system.

5.4.4. Future Expectation for Nanocomposite Material

The promising aspects of nanocomposite material, which are the possibility to manufacturing the inverter-fed motors with random coil above PDIV level and the improvement of thermal conductivity, were shown previously.

References

Boehm FR, Nagel K, Schindler H (2007) Voltron™ - A New Generation of Wire Enamel for the Production of Magnet Wires with Outstanding Corona Resistance, Dupont Catalog.

Kikuchi H, Asano K (2006) Development of Organic/inorganic Nano-composite Enameled Wire, IEEJ Trans. PE 126-4:460-465 (in Japanese)

Nakamura Y, Inano H, Hayakawa N et al. (2008) Deterioration Resistant Mechanism against Partial Discharge under Inverter Surge Voltage in Nano-composite Enameled Wire, The Papers of Technical Meeting on Dielectrics and Electrical Insulation, IEE Japan, DEI-08-17:81-86 (in Japanese)

Ozaki T, Imai T, Sawa F et al. (2005) Partial Discharge Resistant Enameled Wire, Proceeding of ISEIM: 184-187.

Uozumi Y, Kikuchi Y, Fukumoto N et al. (2007) Dielectric Life and Partial Discharge Characteristics of Surge Resistant Enameled Wire Applied, Nano-composite Insulating Material, The Papers of Technical Meeting on Dielectrics and Electrical Insulation, IEE Japan, DEI-07-64:51-57 (in Japanese).

Yoshimitsu T, Wakimoto Y, Kobayashi H et al. (2007) Examination about the Actual Application of the Serge Resistant Wire, Proceeding of the 38th Symposium on Electrical Insulating Materials D3: 95-99 (in Japanese).

5.5. Capacitors / Condensers

Since the introduction around 50 years ago, of thin biaxially-oriented polypropylene (BOPP) film, made either by extrusion (drawn and tentered) or by the expanding bubble process, to replace thin cellulosic paper, BOPP has increasingly provided a preferred dielectric for hv power capacitors (using foil + film w/wo cellulosic layer + impregnant liquid), for lv industrial capacitors (using metalized BOPP w/wo non-swelling impregnant liquid), and for high-energy density capacitors spanning both lv and hv designs with a wide variety of operational requirements. Above the upper use temperature of BOPP (~100C), or for other specialty applications, such as medical, military, or space applications, polymer films other than BOPP find selective use.

With all of these applications, the high breakdown strength afforded by BOPP in the thickness range from 2 to 12μm during required factory testing and long time service is critical to the success of polypropylene (PP), although low losses and higher use temperatures are among other important requirements. Many improvements in resin quality and film manufacture have led to progressive increases in operating stresses for the resulting capacitors. It is therefore of major interest to see whether the use of nanodielectrics can improve the stresses achieved with BOPP films, and whether the addition of nanoparticles such as those found to significantly improve voltage endurance in XLPE (Roy 2008), can lead to improvement in the breakdown of BOPP films or to alternative polymer films to replace BOPP.

A key factor in achieving high breakdown strength with BOPP film, shown initially by Eustance and Solberg in the mid 1960s, then confirmed by Gao et al. (1990), was shown to be the formation of lamellar crystallites during biaxial orientation of the film; which it was concluded led to a scattering of the electrons involved in breakdown. This has spawned the use of proprietary inorganic and organic nucleating agents and careful control of PP molecular weight and branching to promote planar crystallization, while preserving melt strength to insure a pinhole-free BOPP film, even down to thicknesses as low as 2μm. This information should prove helpful to the quest of using nanodielectrics for capacitors.

Though proprietary efforts by polymer film and capacitor manufacturers are likely taking place, to-date there have been no published reports of the successful commercialization of nanodielectric capacitors to replace capacitors using BOPP. However, two publications, with quite different approaches, illustrate the range of R&D that is underway. In one case, polyhedral oligomeric silsesquioxane (POSS) nanoparticles were dispersed in capacitor-grade PP, and ac and lightening impulse breakdown measurements performed. In the other, nanometric alternating layers of polycarbonate (PC) polymer and a copolymer of polyvinylidene fluoride and hexafluoropropylene (coPVDF) were used to address a high-energy-density capacitor requirement of 10 J/cc or higher.

In the work by Takala and colleagues (2008), on octamethyl and isooctyl POSS particles dispersed in capacitor grade isotactic PP, at concentrations of 1 to 10 wt %, increases in both 50Hz and 1.2/50 μs impulse breakdown were observed: for octamethyl at 3 wt%, an increase in ac breakdown of 22% was found, and at 10 wt%, an increase in impulse breakdown of 13%. For isooctyl POSS, the increases were less. Permittivity, tan δ, and resistivity were weakly affected by inclusion of the nanoparticles. The authors conclude that “better dielectric strength can be achieved with POSS nanocomposites”. We note that the measurements were made at room temperature, on relatively thick samples (500-700μm, compared with typical capacitor grade PP of thickness 5-10μm); nor were the samples biaxially-oriented. Hence, we look forward to seeing the impact of POSS with experiments on more representative samples over a

temperature range of relevance to commercial capacitors.

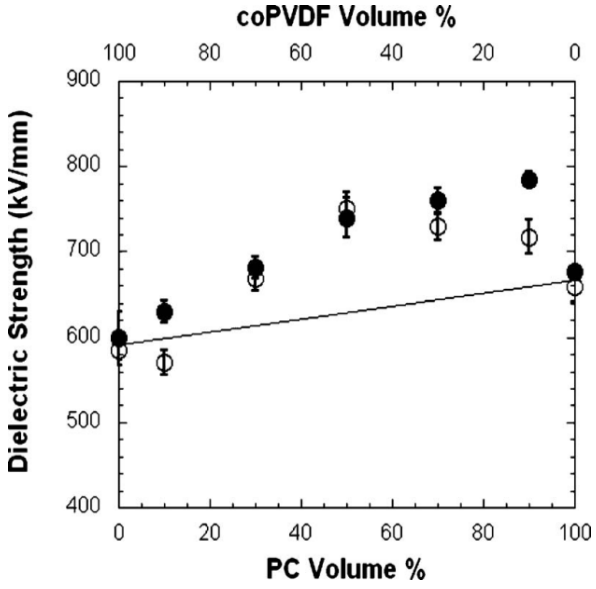

Figure 5.5.1 Average dielectric strength of 32-layer (solid circles) and 256-layer (open circles) PC/coPVDF films. The solid line represents the expected Eb (Wolak et al. 2008) .

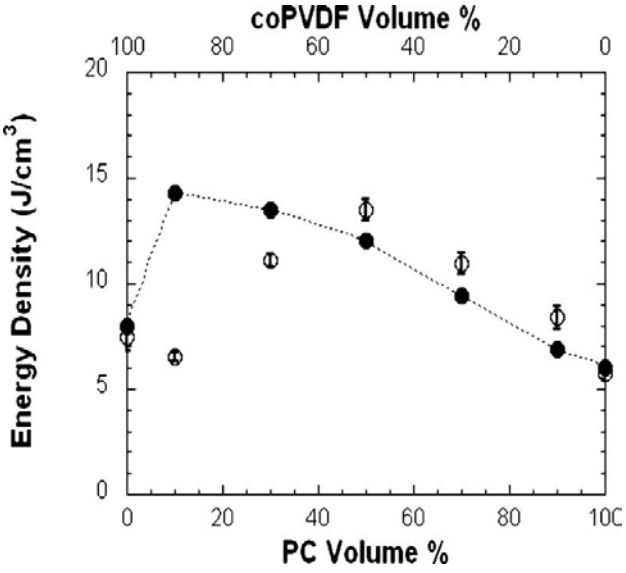

Figure 5.5.2 Maximum projected (filled circles) and measured (open circles) energy density of 256-layer PC/coPVDF films. The projected value for the coPVDF control film was average.

In the work by Wolak and colleagues (2008), 32- and 256-layer films, made with alternating PC and coPVDF nanolayers, were evaluated for their potential for high-energy-density capacitor application. Component volume concentrations (PC/coPVDF), controlled by relative layer thicknesses, were 10/90, 30/70, 50/50, 70/30, and 90/10. Small area, uniform field ac breakdown (500V/s) and permittivity and other dielectric properties were measured. Key breakdown measurements are shown in Figure 5.5.1 and the computed energy density is shown in Figure 5.5.2. Significant improvements in breakdown relative to the individual polymers are evident; and energy densities as high as 14 J/cc, which is about 60% higher than the component polymers, are seen with the 50/50 composition. The authors conclude that the high breakdown strengths result from “barrier effects of the layers”.

References

Gao LY, Tu DM, Zhou SC, et al. (1990) The influence of morphology on the electrical breakdown strength of polypropylene film. Trans IEEE EI 25: 535-540

Roy M, Nelson JK, Reed CW et al. (2005) Polymer nanocomposite dielectrics: the role of the interface. Trans. IEEE DEI 12: 629-643

Takala M, Karttunen M, Salovarra P, et al. (2008) Dielectric properties of nanostructured polypropylene-polyhedral oligomeric silsesquioxane compounds. Trans. IEEE DEI 15: 40-51

Wolak M, Pan M-J, Wan A, et al. (2008) Dielectric response of structured multilayered polymer films fabricated by forced assembly. Appl Phys Lett 92: 113301-03

5.6. All Solid Insulated Substations

5.6.1. Proposal of all solid insulated substations

Electricity is one of the essential energy sources for modern human life and it is consumed mainly in the urban area with still increasing demand. It is however getting hard to acquire the place for the substation and so on. Recent economy forces utility companies to reduce initial and operating cost such as construction, inspection and maintenance are required as well as extension of inspection period and replacement period. Moreover the electric power equipment have been required to be more environmentally benign, for instance, reduction of usage of SF6 gas due to its high GWP (global warming potential) (Shibuya et. al 2000).

One of possible solutions is to apply solid insulating materials instead of SF6 gas because solid insulation has an extremely high performance in electrical insulating property, which may reduce the size of power equipment. Solid insulated power equipment has advantages in flame-retardant properties, environmental benignity and so on, compared with the oil and SF6 gas insulated equipment. From these viewpoints, All Solid Insulated Substation has been proposed as a next-generation substation. The conceptual image of the all solid insulated substation is shown in Figure 5.6.1.

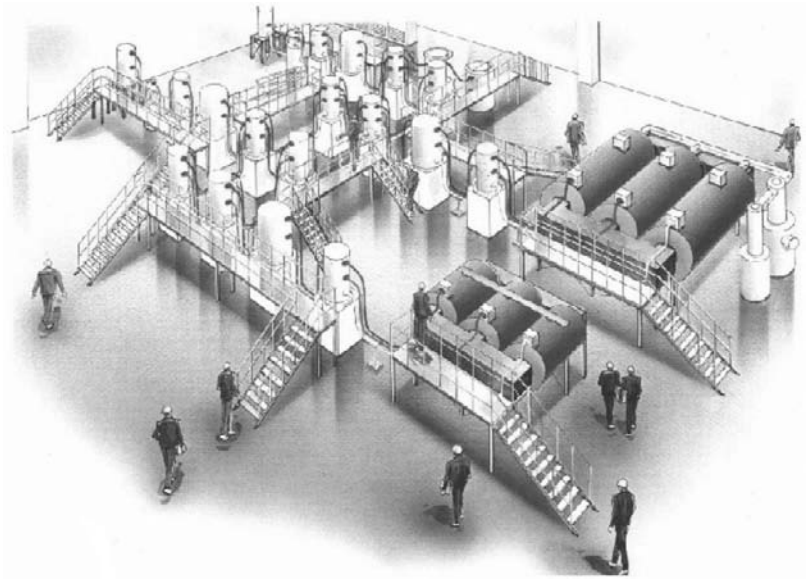

Figure 5.6.1 The concept of Underground All Solid Insulated Substation.(Shibuya et. al 2000)

5.6.2. New insulating material with nano-composites for all solids insulated substations

One of the most important element technologies for establishing all solid insulated substations is to develop an all solid insulated power transformer with new insulating materials having high thermal conductivity as well as insulation and mechanical performances. With high thermal conductivity insulation, compact all solid transformer design can be achieved and this compactness is essential in molding process. In other words, too thick insulation design cannot be allowed for

production of an all solid insulated high voltage transformer.

AlN(aluminum nitride) composite material can be possible candidate for this new design material because it has higher thermal conductivity then conventional epoxy resin compounds with almost the same electrical and mechanical properties. Figure 5.6.2 shows several candidate material properties in terms of design criteria of a 275 kV/66 kV 300 MVA power transformer as an example (Mizutani Y et. al 2002). Micro composite material (Material A in the figure) is 42.5 vol% of crashed AlN with 15 mm in average particle size and 2.2 [W/m/K] which is ten times higher thermal conductivity of unfilled epoxy resin (Material D). Material C in the figure is 35 vol% of spherical AlN. Material B is 40 vol% of micro and nano AlN particle. This material improves the design tolerance as shown in the figure.

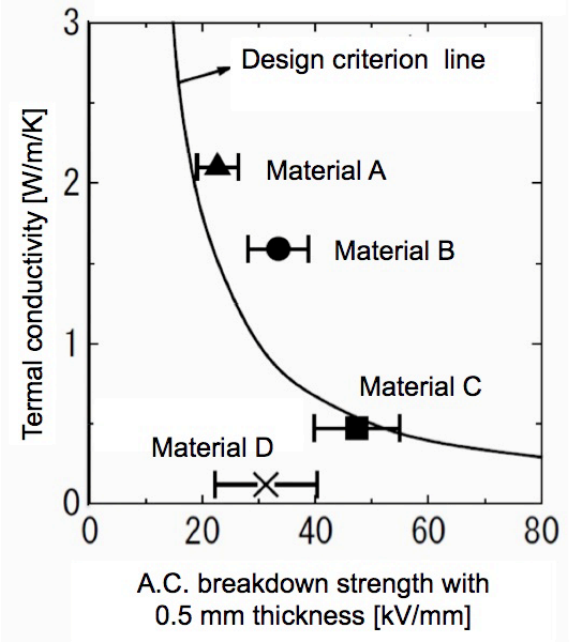

Figure 5.6.2 Designable relationship between thermal and electrical property of the insulating materials (Mizutani Y et. al 2002)

The concept srtucture of micro-nano composite particle is shown in Figure 5.6.3 with a SEM photograph(Iwata M et. Al 2006). A novel method of synthesizing AlN composite particles using transferred type DC nitrogen arc plasma has been developed. The shape of the synthesized particles, the diameter of micro-particles and the volume fraction of micro-particles in the synthesized composite particles were controlled simply by varying the travelling time of the raw AlN angular particles in the arc plasma. The travelling time was controlled by varying the plasma length and the plasma gas flow rate. The diameter of the nano-particles in the synthesized composite particles was controlled simply by varying the travelling time of the raw AlN particles in the arc plasma, and varying the temperature and the vapor density in the nano-particle synthesis space. The temperature and the vapor density were controlled by varying the flow rate of reacting/quenching ammonia gas. The AlN content in the synthesized composite particles was higher than 99%. TEM observation clarified that many small particles (nano-particles, less than 100 nm) adhered uniformly to the surface of the synthesized particle. It was considered that these

nano-particles were synthesized from the vapor formed by raw particles. This micro-nano compsite particle reduces the viscosity of filled epoxy resin and therefore the production of bulky moulding may be achieved.

Thought this new type micro-nano composite particle can be a possible solution for establishing the all solid insulated transformer, consequently all solid insulated substation, futher sutdy shoul be made in terms of application of this maerial to all solid insulated transformers thought real production processes. And also long time stability of the filled epoxy resins as well as degradation mechanisms of the filled epoxy resins under high thermal and high electric stresses should be studied.

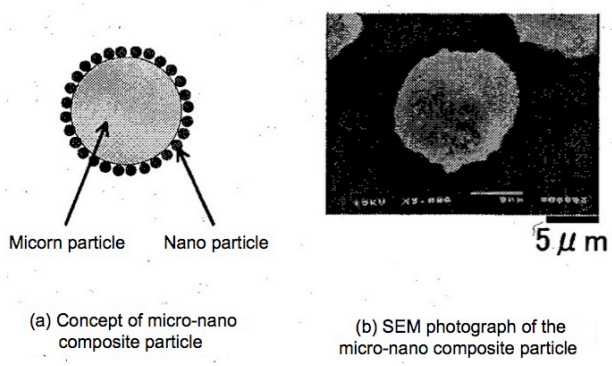

Figure 5.6.3 Concept and SEM photograph of micro-nano composite particle for the new insulating materials (Iwata M et. Al 2006)

References

Iwata M, Furukawa S, Mizutani Y et al. (2006) Development of components of all solid insulated substation Part4, Research Report of CRIEPI, H05008
Mizutani Y, Iwata M, Okamoto T et al. (2002) Development of components of all solid insulated substation Part2, Research Report of CRIEPI, W02024
Shibuya M, Okamoto T, Kuzuma Y et al. (2000) All solid insulated substation, Research Report of CRIEPI, W00047

5.7 Outdoor Insulation

5.7.1 Material for outdoor insulation

Power system equipments that have the most important factor in outdoor insulation are cable termination, polymer insulator, and bussing for transmission and distribution. Main insulation materials for these equipments are epoxy resins, EPDM, ethylene vinyl acetate copolymer (EVA) and silicone rubbers (IEEJ 2006). This part reports about the application of nano-material in silicone rubber of polymer insulator. Partial discharge and arcing on the surface of polymer insulator are generated by electrical stress under the condition of outdoor environment (rain, mist, UV and pollution) (IEEJ 2006).

5.7.2 Application of nano-composite material for polymer insulator

The nano-composites show some superior properties by adding small amounts of nano-fillers (<10 wt %). It is reported that the arc and erosion resistance of silicone rubbers with 5-10wt% nano-particle of silica are increased as much as that of silicone rubbers with 50wt% micro-silica(Ei-Hag et al. 2006). However, nano-particles are likely to concentrate in process of mixture. It is important to mix them homogeneously.

Ramirez measured the erosion resistance of silicone rubbers by changing an additive amount of interfacial active agent(X-100) to produce uniform mixture (Ramier et al. 2008). The properties of nano-composites of silicone are showed in Table 5.7.1. They evaluated the erosion resistance by measuring wear amount of samples. The major cause of erosion by arcing is the thermal decomposition of polymer and so dry band arc is simulated by irradiation of infrared laser. The relationship between the amounts of additives and erosion of the silicone rubbers with 2.5wt% fume-silica is shown in Figure 5.7.1. The amount of erosion with the increase of additive is decreased and it saturates by the addition of 20 pph nano-silica. The property is enhanced greatly by mixing micro-particles and nano-particles. The results of verification are shown in Figure 5.7.2.

Table 5.7.1 Properties of nano-particles added in silicone rubbers (Ramier et al. 2008)

Nanofiller	Average particle size (nm)	Surface area (m^2/gram) (BET)	Density (g/mL) @25 °C
Fumed Silica	7	390±40	2.2
Natural Silica	10	590-690	2.2-2.6
Alumina	2-4	350-720	4

In order to remove adsorbed moisture, fume-silica was burned before using. The amount of erosion showed minimum value by combination of 40wt% micro-particles, 2.5wt% burned nano-particles and 20 pph of Triton agents. In Ramirer's paper, as shown below, useful research results about silicone nano-composites are reported.

1) An essential condition of realizing superior property is the uniformly distribution of nano-particles.
2) A dispersing agent is effective to facilitate dispersion of nano-particles.
3) It is effective in improving properties to remove the moisture adsorbed on the surface of nano-particles.
4) The effect of nano-particle additives is increased by mixing micro-particles,.

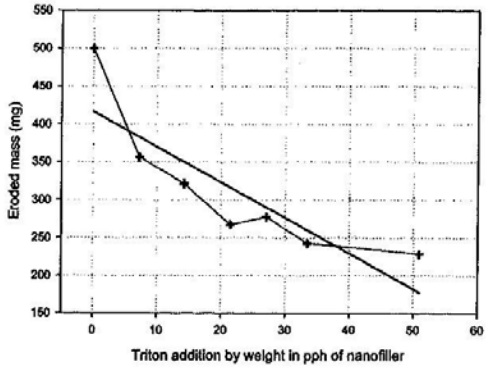

Figure 5.7.1 Relationship of the additive amount of TRITON and the amount of erosion in silicone rubbers with 2.5wt% fumed silica (colloid silica) (Ramier et al. 2008)

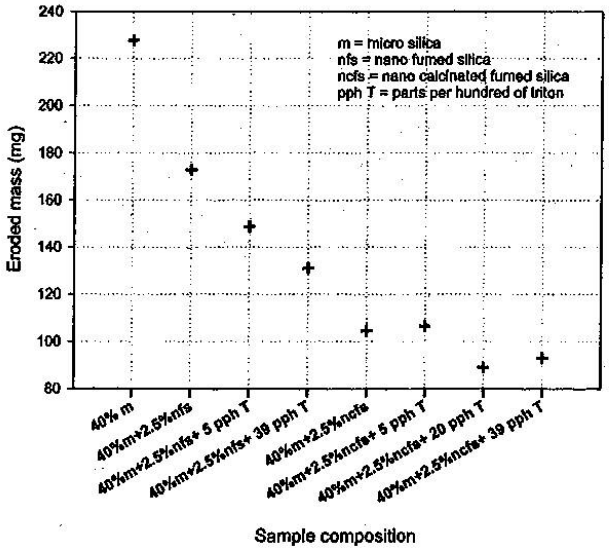

Figure 5.7.2 Relationship of the additive amount of TRITON and the amount of erosion in silicone rubbers with 2.5wt% fumed silica (colloid silica). (Ramier et al. 2008)

L. H. Meyer began exposure test of two types of glass insulator coated with RTV silicone rubber filled with nano- and micro particles in coastal areas. In 45 days test, the addition of nano-particles reduced the leakage current and the amount of salt deposited on the surface of glass insulators (Meyer et. al. 2008).

References

Ei-Hag AH, Simon LC, Jayaram SH et al. (2006) Erosion Resistance of Nano-filled Silicone Rubber, IEEE Tarns. Dielectr. Electr. Insul. 13:122-128

IEEJ (2006) Evaluation of insulation interface and reforming technology, IEEJ Investigation Committee Report No.948 (in Japanese)

IEEJ (2006) Discharge properties and degradation phenomenon on surfaces of materials for polymer insulator, IEEJ (The Institute of Electrical Engineers of Japan) Investigation Committee Report No.948 (in Japanese)

Meyer LH, Cabarl SHL, Cardoso GE (2008) Use of Nanosilica in Silicone Rubber Coatings for Ceramic Insulators in Coastal Areas-Field Results, IEEE Inter. Symp. Electr. Insul. (ISEI): 676-679

Ramier I, Cherny ED, Jayaram SH et al. (2008) Nano-filled Silicone Dielectrics Prepared with Surfactant for Outdoor Insulation Applications, IEEE Trans. Dielectr. Electr. Insul., 15:228-235

5.8 Power Electronics

Recent industrial and consumers' power electronics requires high density integration and high voltage assembly. Not only voltage (V) but also electric field stress (kV/mm) will tend to increase, resulting in the necessity of appropriate electrical insulation design that has ever been neglected. Therefore much attention is paid to compact power conditioners for various purposes such as automatic voltage regulators, photovoltaic systems, and electric vehicle automotives. IGBT (Insulated Gate Bipolar Transistors) and future SiC (Silicon Carbide) GTO **(Gate Turn-off** Thyristors) are some of the examples whose electrical insulation should be improved.

Figure 5.8.1 Potential Applications of Nanocomposite PWB (Printed Wiring Board) to General Purpose Inversters

Courtesy of Fiji Electric Co

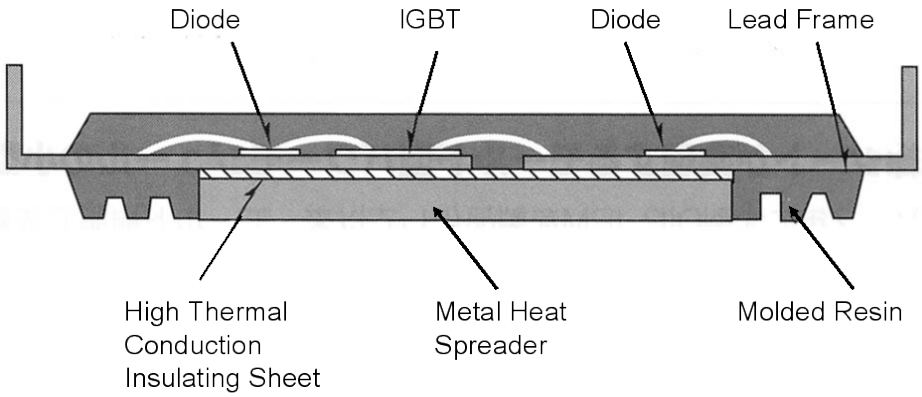

Figure 5.8.2 Structure of Metal Base PWB (Printed Wiring Board)

Figure 5.8.2 shows an example of metal base PWBs. This includes a high thermal conduction insulating sheet. Ceramics are used for that purpose at present, but they are brittle and expensive. Research and development are

now taking place to replace this kind of materials by epoxy resins that are considered to be mechanically tough and rather inexpensive. Epoxy resins are thermally less conductive in nature, and fortunately become more conductive, if micro ceramic fillers are filled. But dielectric breakdown strength will decrease due to inclusion of such micro fillers. To compensate this lowering, it is now considered to a good way to nanostructure the microcomposites. Some evidence was obtained as shown in Figure 5.8.3. It indicates the advantage of nano-structured microcomposites over plain microcomposites.

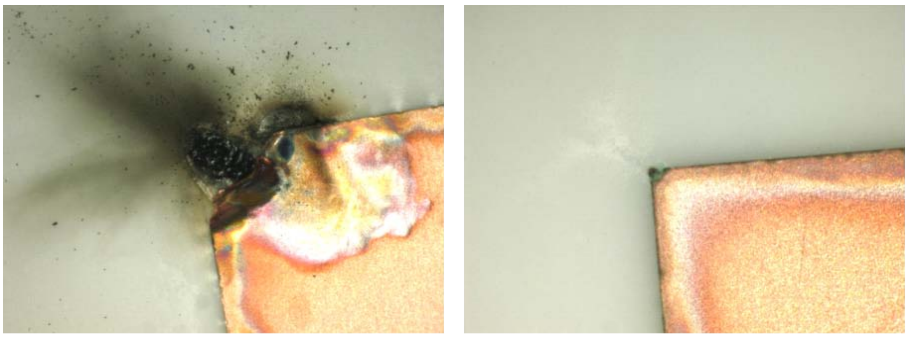

Figure 5.8.3 Comparison of dielectric breakdown strength between a plain microcomposite and a nano-structured microcomposite (Li et al. 2009)

High integration PWBs and three dimensionally assembled structures require narrow spacing between lead wires and electrodes and wires, resulting in the induction of high electric filed to facilitate both surface and bulk electrochemical migration from metal wires and electrodes. Space charge accumulation will take place at high field regions under normal and abnormal conditions to cause material degradation. Nano filler addition is considered to be a good way to prevent such phenomena.

References

Li Z, Tanaka T, Okamoto K et al. (2009) Role of Nano-Filler on Partial Discharge Resistance and Dielectric Breakdown Strength of Micro-Al_2O_3/Epoxy Composites Proc. ICPADM H-6: 753-756.

Appendix: Case Study

Various Characteristics of MgO/LDPE Nanocomposite for High Field Insulation

Source: 2008 Group Meeting Paper D1.301

Summary

Polymeric electrical insulating materials are widely used in various power equipments and cables. Additives and fillers are often adopted to polymeric materials for improving insulating and mechanical properties. Recently, nano-fillers are attracting attentions of many researchers and engineers, since they seem to bring higher potentials for advancement of electrical insulating properties as nanocomposites. This paper reports evaluation results of various insulating properties of a MgO/LDPE nanocomposite, jointly carried out by several organizations, aiming at development of an electrical insulating material for higher DC electric field.

The DC breakdown strength and the volume resistivity increased with the addition of MgO nano-fillers. The thermally stimulated depolarization current (TSDC) peak that spreads over a wide temperature range was observed in all the MgO/LDPE nanocomposites. Furthermore, by adopting a partial heating method, the wide TSDC peak was resolved into several component peaks and it turned out that one of the peaks was attributed to MgO nano-filler, from which it is suggested that a new trap is generated in the nanocomposites. And it was observed from space charge measurement that addition of MgO nano-fillers suppressed packet-like charges in the nanocomposite. The relative permittivity once decreased slightly by addition of MgO nano-fillers and then increased by more addition of them. The electrical treeing inception voltage increased with increasing MgO nano-filler content and it is also recognized that the tree propagation in the MgO/LDPE nanocomposite was suppressed significantly by the addition of MgO nano-fillers. The partial discharge erosion depth of the MgO/LDPE nanocomposite also becomes smaller than that of base LDPE. It is summarized that addition of a small amount of nano-fillers brought excellent insulating performances of the MgO/LDPE nanocomposite.

The MgO/LDPE nanocomposite exhibits promising electrical insulating properties to cope with severe requirements and is expected as a new generation of electrical insulating materials for higher electric field application, especially for DC voltages.

Keywords

Nanocomposite, Polyethylene, Magnesium Oxide, Breakdown Strength, Volume Resistivity, Thermally Stimulated Depolarization Current, Space Charge, Relative Permittivity, Electrical Treeing, Partial Discharge Resistance

A.1 Introduction

Polymer insulating materials are widely used in many pieces of power equipments and cables. Additive agents and fillers are often used for improving insulating and mechanical properties (Kärner HC 1993) (Watanabe E et al. 1996). Especially, adjunction of inorganic fillers into XLPE insulation brings excellent electrical properties under DC voltage application, and DC power cable for operating voltage up to 500 kV had been developed by adopting the inorganic fillers added XLPE insulation (Maekawa Y et al. 1994) (Maekawa Y et al. 2001). These fillers used in the development were already nano-sized, but it was not recognized that they were in the field of nano-technology at that time. Recently, nano-technology is attracting attentions of many reseachers and engineers in the field of dielectrics and electrical insulations, and recent researches of nanocomposite are still being encouraged (Lewis TJ 1994) (Tanaka T et al. 2004).

A nanocomposite material is composed of nano-fillers, which diameter is as short as a few tens to a few hundreds of nanometers, and a polymer as a matrix. As the superficial area of the interface between the fillers and the matrix is enormously larger than that of conventional microcomposite materials, some improvements of insulating performances are expected to be brought to realization using such materials. Therefore, the various insulating properties of the MgO/LDPE nanocomposite were evaluated for applications to electrical insulating materials for higher electric field. In this paper, DC breakdown strength, volume resistivity, thermally stimulated depolarization current, space charge distribution, relative permittivity, electrical treeing phenomena and partial discharge resistance of the MgO/LDPE nanocomposite were measured by several research organizations in Japan.

A.2 Materials Used for Experiments

MgO/LDPE nanocomposites were prepared from raw LDPE and magnesium oxide of several ten nm, which concentrations were 0, 0.2, 0.5, 1, 2, 5 and 10phr, using a blowing method. (phr : per hundred parts of resin. For example, 1 phr nanocomposite consists of 1 part of filler and 100 parts of LDPE.) Furthermore, 0 phr nanocomposite which is used as a reference means LDPE without MgO nano-fillers. All specimens subjected to the experiments were cut from the blown films made of the same batch. The uniformity of dispersion of MgO nano-filler in the MgO/LDPE nanocomposite was evaluated with a transmission electron microscope (TEM). Figure A-1 shows a TEM photograph of a 5 phr nanocomposite sample. The lamella structure can be identified in the photograph in white striped patterns. From another point of view, polka-dot shapes which are much darker in brightness than the surrounding area can also be noticed. They were proved as MgO by energy dispersive X-ray fluorescence analyses (EDX) (Murata Y et al. 2005). Thus, it is confirmed that MgO nano-fillers are uniformly dispersed.

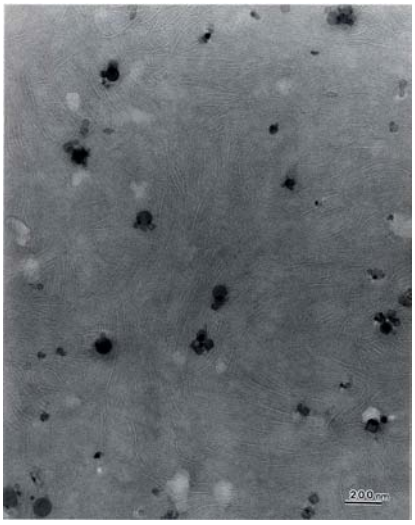

Figure A-1 TEM photograph of MgO/LDPE nanocomposite material in which MgO nano-filler content is 5 phr.

A.3 DC Breakdown Strength and Volume Resistivity

Figure A-2 shows the influence of the MgO nano-filler content on DC breakdown strength measured with McKeown type electrode at 303 K (Masuda S et al. 2007). The sample was subjected to a ramp voltage with increase rate of 500 V/s. The error bar and the solid sign are standard deviation and the average of 10-15 samples,

respectively. DC breakdown strength of the sample with MgO nano-filler increased compared with that without MgO nano-filler. Above the MgO nano-filler content of 0.2 phr, the DC breakdown strength of the sample with MgO nano-filler also shows saturated value. Figure A-3 shows the temperature dependence of DC breakdown strength. DC breakdown strength of the sample with MgO nano-filler content of 1 phr is also higher than that of 0 phr at 363 K although the DC breakdown strengths of the samples with or without MgO nano-filler decreased with increasing temperature.

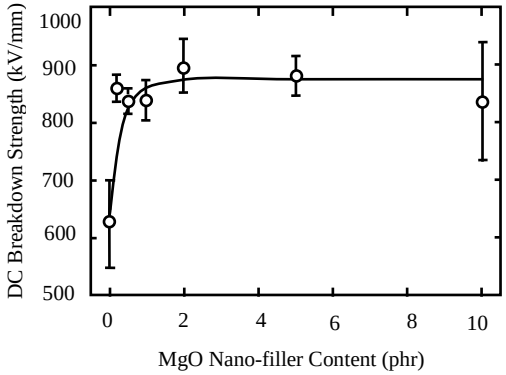

Figure A-2 Influence of the MgO nano-filler content on DC breakdown strength at 303 K.

Figure A-4 shows the influence of the MgO nano-filler content on the volume resistivity under the field application of 40 or 80 kV/mm at 303 K (Masuda S et al. 2007). The volume resistivity of the sample with MgO nano-filler by the adding a few of MgO nano-filler increased compared with that without MgO nano-filler under the each field.

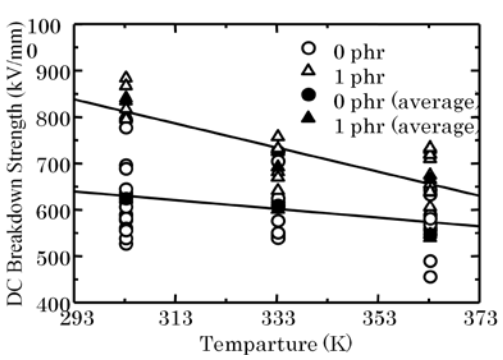

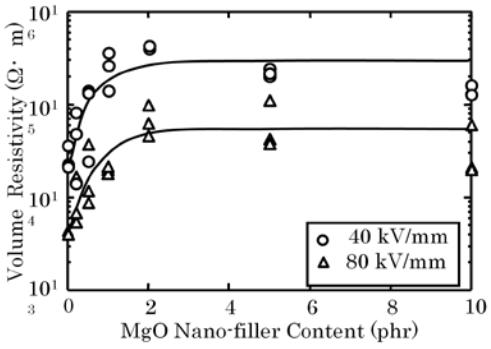

Figure A-3 Temperature dependence of DC breakdown strength. **Figure A-4** Influence of the MgO nano-filler content on volume resistivity at 303 K.

These characteristics of the volume resistivity are strikingly similar to that of the DC breakdown strength as shown in Fig. A-2. From these results and the space charge measurement, it is suggested that the MgO nano-filler may trap the charge in the vicinity of the electrode under the high field, and may suppresse conduction current by reducing the local field at the electrode. Since the electron avalanche is considered to be scattered by MgO nano-filler, the DC breakdown strength of the sample with MgO nano-filler increase than that without MgO nano-filler. However, the saturation of the DC breakdown strength of the sample with MgO nano-filler content of more than 0.2 phr is difficult to be interpreted only by the electron avalanche breakdown process. Considering that thermal breakdown is one of the possible process for the DC breakdown in LDPE (Nagao M et al. 1990) as well as that the DC breakdown strength and the volume resistivity shows similar dependence on MgO nano-filler content, thermal process might be the preferable process at this moment.

A.4 Thermally Stimulated Depolarization Currents

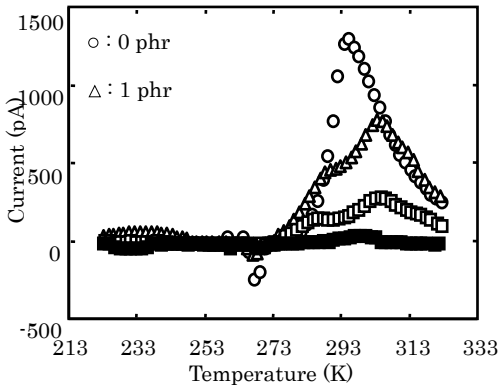

Figure A-5 Thermally stimulated depolarization current (TSDC) spectra of the nanocomposites.

Figure A-5 shows the thermally stimulated depolarization current (TSDC) spectra of four MgO/LDPE nanocomposite samples with different filler contents observed by increasing the sample temperature from 173 K to 348 K at a rate of 10 K/min after the samples had been poled by applying DC field of 150 kV/mm at 348 K for 30 minutes (Ishimoto K et al. 2007). A TSDC peak that spreads over a wide temperature range from 273 to 333 K was observed in all the samples. Furthermore, by adopting a partial heating method, the wide TSDC peak was resolved into several component peaks. Among them, the peak at around 285 K was found not to appear in the base

LDPE. By analyzing its initial rising portion, the 285 K peak was assumed to have a fairly deep energy depth of about 2 eV. These results indicate that charge carriers tend to be captured more strongly by the addition of MgO nano-filler. If these captured charge carriers induce homocharge layers in the vicinity of the electrodes, further formation of space charge would be suppressed. This seems to explain the fact that the amount of space charge is smaller in the nanocomposite with a proper addition of MgO nano-filler than in the base LDPE (Kärner HC 1993) (Murakami Y et al. 2006) (Takada T et al. 2007).

A.5 Space Charge

Figure A-6 shows the time dependent space charge distribution under applied field of 250 kV/mm at room temperature (Kärner HC 1993). As shown in Fig.6 (a), the packet-like charge is clearly observed. The packet-like positive charge seems to be still moving and increasing even at 1 hour after voltage on. Anyway, when the DC high electric field is applied to a sample without MgO nano-filler, a huge packet-like charge appears and it makes the local electric field increase. In the case of the sample with MgO nano-filler of 0.2 phr, while it is not clear in Fig. A-6 (b), repetitious behavior was obtained several times in the long time scale observation. The repetitions of packet-like charge injection were also observed in some experiments on XLPE (Hozumi N et al. 1998) (Matsui K et al. 1994). However, any clear explanation has not been given to such phenomena yet. While the proposed model suggests the behavior of the positive packet-like charge well, the model is based on a simple assumption of an injection of only positive charge from the anode. However, for such repetitious behavior shown in Fig. A-6 (b), the existence of the negative charge must be concerned. In other words, since the simultaneous negative and positive charge injection makes some complicated condition such as their overlapping or interference, it is hard to give some clear explanation for the phenomena. On the other hand, no remarkable packet-like charge is observed in the sample with MgO nano-filler of 1 phr as shown in Fig. A-6 (c). Almost the same result is obtained in observation of the space charge profiles in the sample with MgO nano-filler content of 0.5 phr. However , it seems that small amount of positive charge is observed at a vicinity of the cathode electrode. It is difficult to recognize the movement of the positive charge from Fig. A-6 (c), however, by careful observation, we can find that a very small packet-like charge moves from the anode to the cathode quickly. However, since the amount of charge is very small , the electric field doesn't seem to be affected by the positive charge. Therefore, it can be said that no remarkable packet-charge generates in the sample with MgO nano-filler content of more than 0.5 phr under the applied electric field up to 250 kV/mm.

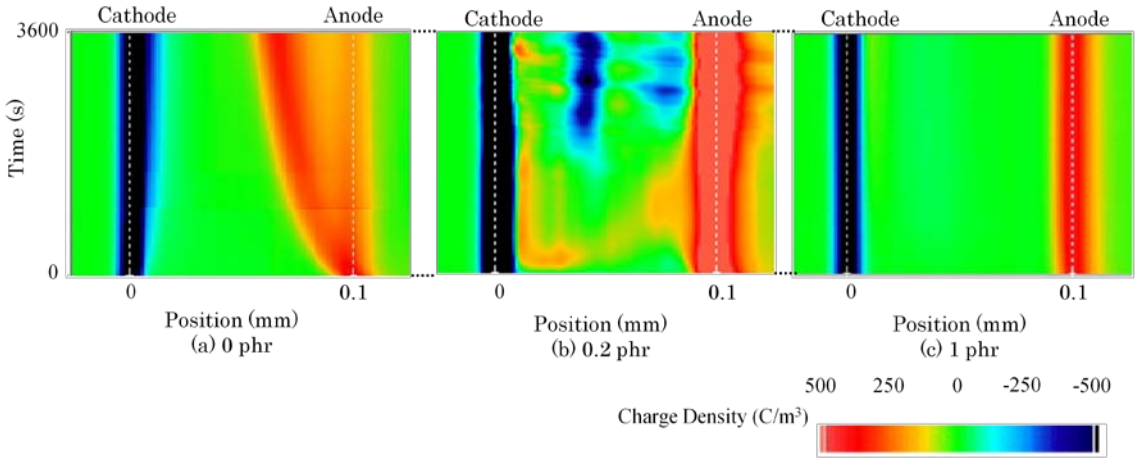

Figure A-6 Time dependent space charge behavior under applied field of 250 kV/mm at room temperature.

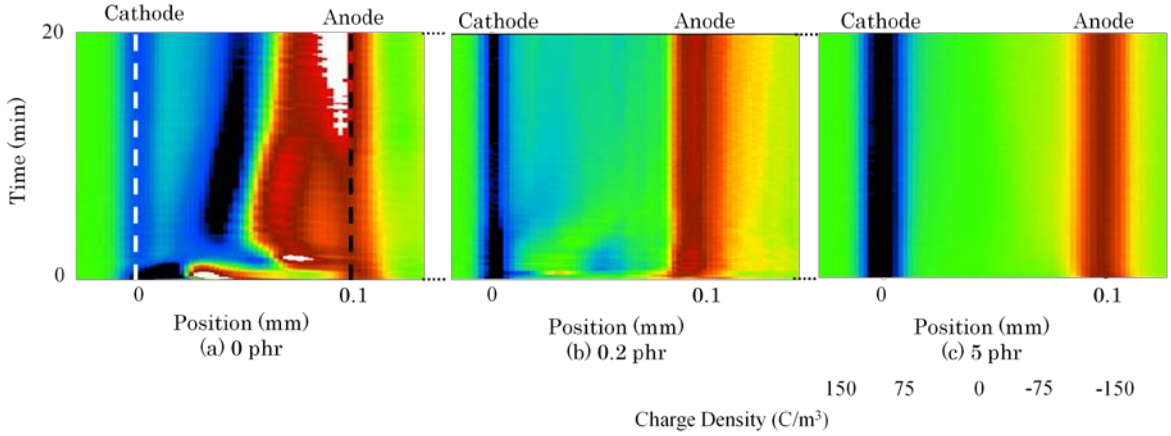

Figure A-7 Time dependent space charge behavior under 150 kV/mm at 333 K

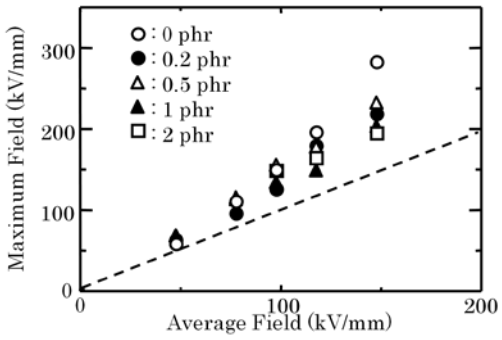

Figure A-8 Maximum electric field enhanced by the injected charge at 333 K.

Figure A-7 shows the time dependent space charge behavior in (a) 0 phr, (b) 0.2 phr and (c) 5 phr under applied electric field of 150 kV/mm at 333 K (Maezawa T et al. 2007). As shown in Fig. A-7 (a), at 333 K, the positive packet-like charge moves quickly towards the cathode side, and the negative charge injection becomes dominant after that. It is also observed a complicated charge behavior led by the positive packet-like charge movement in the sample with MgO nano-filler content of 0.2 phr as shown in Fig. A-7 (b). On the other hand, almost no remarkable charge injection is observed in the sample with MgO nano-filler content of 5 phr as shown in Fig. A-7 (c). Judging from these results comparing with the results observed at room temperature shown in Fig. A-6, the

positive charge movement becomes faster it seems to lead the negative charge injection at higher temperature. However, even at higher temperature, any remarkable positive charge injection is not observed in the sample with MgO content of 5 phr. Figure A-8 shows the maximum electric field enhanced by the injected charge at 333 K. As shown in Fig. A-8, the electric field enhancement is suppressed by increasing the MgO nano-filler content in the nanocomposite.

A.6 Relative Permittivity

Figure A-9 shows the relative permittivity measured at 30 Hz as a function of temperature using the samples with an upper and a lower evaporated circular Au electrode which effective diameter is 25mm (Kikuma T et al. 2006). As the sample temperature becomes higher, the permittivity lowers monotonously in all the samples including those with MgO nano-filler up to 10 phr. As for the MgO nano-filler content dependence, the sample with the MgO nano-filler content of 1 phr has smaller permittivity values than the one without nano-filler as shown in Fig. A-9, although the difference is small. This result might appear doubtful, when the fact that the relative permittivity of MgO (=9.7 (Lide DR 1993)) is much higher than that of LDPE (=2.3) is taken into account. The permittivity then increases according to the order of MgO nano-filler content of 5 and 10 phr. This trend is always the case regardless of the measurement frequency. A similar tendency was also confirmed by a different research group with different measurement apparatus (Tanaka T et al. 2006). Namely, the permittivity also showed the lowest at 1 phr addition and it increased with a further increase in the filler content for a similar set of four samples taken from a different lot measured by an LCR meter (Tanaka T et al. 2006). Therefore, it is reasonable to assume that the result shown in Fig. A-9 is reliable. It has been reported for many nanocomposites that permittivity is decreased by the addition of fillers despite a higher permittivity of the fillers (Fuse N et al. 2004) (Fothergill JC et al. 2004). There is a possibility that the low permittivity is an indication of a good nanocomposite (Tanaka T 2005). In this context, this property of MgO/LDPE nanocomposite as shown in Fig. A-9 is corresponding to that of other nanocomposites.

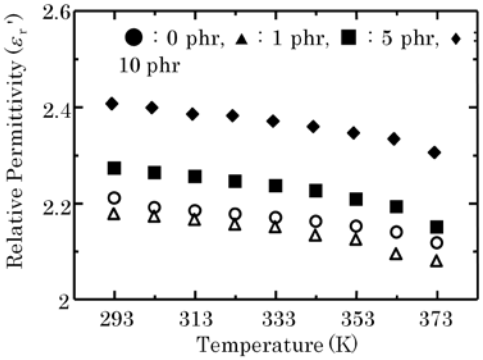

Figure A-9 Relative permittivity measured at 30 Hz as a function of temperature.

A. 7 Electrical Treeing

The tree inception voltage and the relative time of tree propagation up to breakdown as sketched in Fig.A-10 were measured at room temperature using a newly developed leaf-like sample with 0.2 mm in thickness (Kurnianto R et al. 2007). Figure A-11 shows Weibull plots of inception voltage in various contents of MgO nano-filler. The tree inception voltage increased with increasing MgO nano-filler content in LDPE. This statistical analysis shows that 63.2% of tree inception voltges were 4.44, 4.60, 4.95 and 5.66 kV_{rms} in the 0, 1, 5 and 10 phrs of MgO nano-filler content, respectively. The existence of MgO nano-fillers in LDPE would increase the electron affinity that finally made the electron easily be trapped in around MgO nano-filler surface in the vicinity of the needle electrode tip. Then electron avalanche would be difficult to occur and this will consequently increase the tree inception voltage. Another alternative suggestion might be explained as follows.

From the TEM photograph, the diameter and grain spacing of MgO nano-filler were about a few hundreds nm and about 500 nm, respectively. As the tree propagated away along 0.01 mm distance, the electrons would collide with the MgO nano-fillers, this would restrain the electron avalanche then it would take a longer time for tree to propagate comparing with the sample without MgO nano-filler. The more filler content in LDPE, the more obstruction would be generated and then finally would lead to the higher tree inception voltage. Table A-1 shows the 63.2 % values evaluated form Weibull plots of time to bridge counter electrode, time to treeing breakdown and time-lag to breakdown. It is also recognized that these treeing properties in LDPE with MgO nano-filler were superior to that without MgO nano-filler.

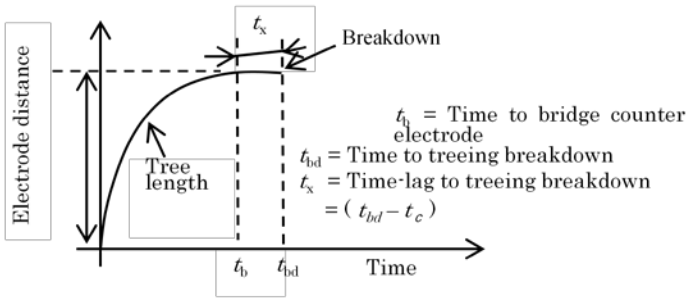

Figure A-10 Graphical image of electrical treeing from initiation to breakdown.

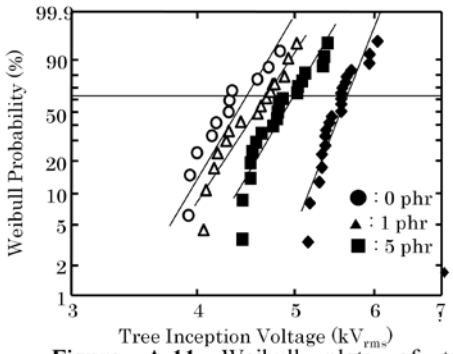

Figure A-11 Weibull plots of tree inception voltage in various contents of MgO nano-filler.

Table A-1 The 63.2 % values evaluated form Weibull plots of time to bridge counter electrode, time to treeing breakdown and time-lag to breakdown.

	MgO nano-filler Content (phr)			
	0	1	5	10
Time to bridge counter electrode t_b (min)	3.84	5.13	8.15	10.51
Time to treeing breakdown t_{bd} (min)	5.27	7.11	10.32	14.57
Time-lag to breakdown, t_x (min)	0.78	1.51	2.23	4.39

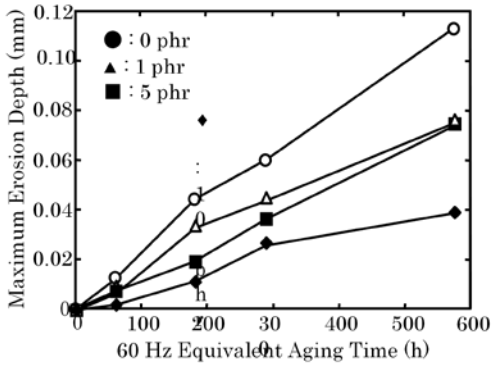

Figure A-12 Dependence of the maximum erosion depth on 60 Hz equivalent aging time.

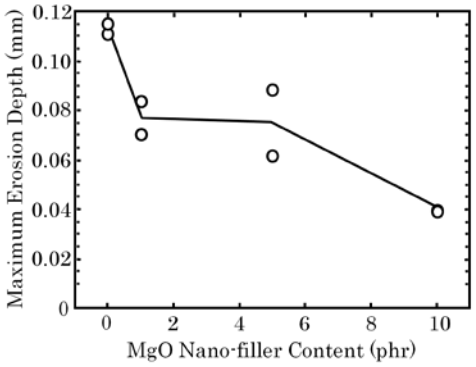

Figure A-13 Dependence of PD erosion depth on MgO nano-filler loading at 576 h aging time.

A.8 Partial Discharge Resistance

The partial discharge (PD) erosion depth on the sample surface was measured after the partial discharge aging using needle-plane electrode under the voltage of 4 kV with 720 Hz at room temperature (Tanaka T et al. 2006). The samples tested were of rectangular sheet with 1 mm thickness. Figure A-12 shows the dependence of the maximum erosion depth on 60 Hz equivalent aging time (The sample was subjected to PD's up to 48 hours.). It is recognized that the erosion increases, as aging time increases from zero to 576 hours. There is data scatter in

short time range. This is considered to be caused by original surface roughness. From the data obtained at aging time of 576 hours, it can be presumed that the erosion depth tends to decrease, as MgO nano-filler content increases. Erosion depth for the sample without MgO nano-filler is 1.5 times and 2.8 times deeper than that with MgO nano-filler content of 1 and 5 phr, and that with MgO nano-filler content of 10 phr, respectively. As the inverse term of erosion depth corresponds to the degree of PD resistance, it can be concluded that MgO/LDPE nanocomposites are several times larger PD resistive than base LDPE. Depth of erosion caused by PD depends on MgO nano-filler content as shown in Fig. A-13. It decreases with the increase of MgO nano-filler content, as described above. In addition, it is worthwhile to mention that big improvement is observed, when only 1 phr of MgO nano-filler is added.

A.9 Conclusion

The electric apparatus are recently being downsized in order to reduce power transmission costs, and the request to insulating materials to meet the severe insulating conditions is increased more and more. As mentioned above, MgO/LDPE nanocomposite exhibits the promising electrical insulating properties to cope these severe requirements and is expected as new generation electrical insulating materials for higher electric field application, especially for DC insulating material fields.

References

Fothergill JC, Nelson JK, Fu M (2004) Dielectric Properties of Epoxy Nanocomposites Containing TiO_2, Al_2O_3, and ZnO Fillers, 2004 Annual Rept. CEIDP : pp. 406-409.

Fuse N, Kozako M, Tanaka T, Murase S, Ohki Y (2004) Possible Mechanism of Superior Partial-Discharge Resistance of Polyamide Nanocomposites 2004 Annual Rept. CEIDP : pp. 322-325.

Hayase Y, Aoyama H, Matsui K, Tanaka Y, Takeda T, Murata Y (2006) Space Charge Formation in LDPE/MgO Nano-composite Film under Ultra-high DC Electric Stress, IEEJ Trans.FM, 126-11: 1084-1089.

Hozumi N, Takeda T, Suzuki H, Okamoto T (1998) Space Charge Behavior in XLPE Cable Insulation under 0.2-1.2 MV/cm dc Field, IEEE Trans. DEI 5-1: 86-90.

Ishimoto K, Tanaka T, Sekiguchi Y, Murata Y, Ohki Y (2007) Effects of Measuring Parameters on Thermally Stimulated Current in Low-Density Polyethylene/MgO Nanocomposite, Proc. the 38th symposium on Electrical and Electronic Insulating Materials and Applications in Systems, No.F-4: pp.147-150 (in Japanese).

Kärner HC (1993) Microscopic and Macroscopic Interface Investigation in Solid Polymeric Systems, Proc. Joint Conf. 1993 International Workshop on Electrical Insulation 25th Symposium on Electrical Insulation Materials : pp37-42

Kikuma T, Fuse N, Tanaka T, Murata Y, Ohki Y (2006) Filler-content Dependence of Dielectric Properties of Low-Density Polyethylene/MgO Nanocomposites, IEEJ Trans. FM, 126-11 : 1072-1077.

Kurnianto R, Murakami Y, Hozumi N, Nagao M (2007) Treeing Breakdown in Inorganic-filler/LDPE Nano-composite Material, IEEJ Trans. FM, 127-1: 29-34.

Lide DR, Ed. (1993) CRC Handbook of Chemistry and Physics, 74th Edition CRC Press: p.12.

Lewis TJ (1994) Nanometric Dielectics, IEEE Trans.1-5: 812-823.

Maekawa Y, Yamaguci A, Sekii Y, Hara M, Marumo M (1994) Development of DC Cable for Extra-high Voltage Use, IEEJ Trans. 114-B-6:633-641.

Maekawa Y, Watanabe C, Asano M, Murata Y, Katakai S, Shimada M (2001) Development of 500 kV XLPE Insulated DC Cable, IEEJ Trans. 121-B-3: 390-398(in Japanese).

Maezawa T, Taima J, Hayase Y, Tanaka Y, Takada T, Sekiguchi Y, Murata Y (2007) Space Charge Formation in LDPE/MgO Nano-composite under High Electric Field at High Temperature, 2007Annnual Rept. CEIDP : pp.271-273.

Masuda S, Okuzumi S, Krunianto R, Murakami Y, Nagao M, Murata Y, Sekiguchi Y (2007) DC Conduction and Electrical Breakdown of MgO/LDPE Nanocomposite, 2007Annnual Rept CEIDP : pp.290-294.

Matsui K, Tanaka Y, Takada T, Maeno T (1994) Space Charge Observation in Various Types of Polyethylene under Ultra-high DC Electric Field, 2004 IEEE ICD: pp.201-204.

Murata Y, Sekiguchi Y, Inoue Y, Kanaoka M (2005) Investigation of Electrical phenomena of Inorganic-filler/LDPE Nanocomposite Material Proc.2005 ISEIM : pp.650-653.

Murakami Y, Nemoto M, Kurnianto R, Hozumi H, Nagao M, Murata Y (2006) Space Charge Characteristic of Nano-composite Film of MgO/LDPE under DC Electric Field, IEEJ Trans.FM, 126-11:1078-1083.

Nagao M, Kimura T, Mizuno Y, Kosaki M, Ieda M (1990) Detection of Joule Heating before Dielectric Breakdown in Polyethylene Films, IEEE Trans. EI, 25-4: 715-722.

Tanaka T, Montanari GC, and Mülhaupt R (2004) Polymer Nanocomposites as Dielectrics and Electrical Insulation-perspectives Processing Technologies, IEEE Trans. DEI, 11-5: 763-784.

Tanaka T (2005) Dielectric Nanocomposites with Insulating Properties, (IEEE Trans. DEI, 12-5: 914-928

Tanaka T, Nose A, Ohki Y, Murata Y (2006) PD Resistance Evaluation of LDPE/MgO Nanocomposite by a Rod-to-Plane Electrode System, Proc. 8th ICPADM: pp. 319-322.

Takada T, Hayase Y, Tanaka Y (2007) Space Charge Trapping in Electrical Potential Well Caused by Permanent and Induced Dipoles, 2007Annnual Rept. CEIDP : pp. 417-420.

Watanabe E, Takeda Y, Yoshizawa M , Moriya T, Nakajima M (1996) The Effect of Filler Particle Size on Ultrasonic Image of Electrical Breakdown Region in Fille-Added Insulating Materials (1996 Annnual Report Conference on Electrical Insulation and Dielectric Phenomena): pp.697-700.

List of CIGRE WG D1.24 Members

Tanaka, T. (Waseda Univ., Japan), Covenor
Fréchette, M. (IREQ, Canada), Secretary
Krivda, A. (ABB, Switzerland), Secretary

Members
Ansorge, S. (Pfisterer Sefag AG, Switzerand)
Bulinski , A. (NRC of Canada, Canada)
Bayon, L. (NEXANS, France)
Castellon, J. (Univ. Montpellier 2, France)
Densley, J. (IEEE-DEIS, Canada)
Gorur, R. S. (Univ. Arizona State, USA)
Gröppel, P. (Siemens Corporate R&T, Germany)
Gubanski, S. M. (Chalmers UT, Sweden)
Henriksen, M. (DTU, Denmark)
Hillborg, H. (ABB, Sweden)
Holboell, J. (TU Denmark, Denmark)
Janssen, H. (Dow Corning Silicones, Germany)
Kindersberger, J. (TUM, Germany)
Lee, B. W. (Univ. Hanyang, Korea)
Mattmann, J-P. (Nexans, Switzerland)
Montanari, G. C. (U Bologna, Italy)
Morshuis, P. (Delft TU, the Netherlands)
Nagao, N. (Toyohashi UT, Japan)
Paajanen, M. (VTT TRC Finland)
Pelissou, S. (IREQ, Canada)
Perego, G. (Prysmian S.p.A, Italy) CIGRE B1 Liaison
Reed, C. W. (Consultant, USA)
Sedding, H. (Kinectrics, Canada) CIGRE A1 Liaison
Shimizu, T. (Toshiba, Japan)
Sutton, S. (Dow, UK) CIGRE B3 Liaison
Tanaka, Y. (Tokyo City Univ., Japan)
Tuomo, M. (Tervakoski Films Group, Finland)
Vaga, N. (Federal Grid Co., Russia)
Vaughan, A. (Univ. Southampton, UK)
Winter, H-J. (Wacker-Chemie, Germany)

Liaisons
Mehta, S.P. CIGRE A2 (Waukesha Electric Systems, USA)
Shirasaka, Y. CIGRE A1 (Japan AE Power Systems, Japan)